A.I. Alikhanyan National Science Laboratory

(Yerevan Physics Institute)

LILIT V. BARKHUDARYAN

STUDY OF THE DIVERSITY OF TYPE Ia SUPERNOVA PROGENITORS

Thesis

for acquiring the degree of candidate of physico-mathematical sciences

in division 01.03.02. "Astrophysics, radio astronomy"

Supervisor: Dr. Artur A. Hakobyan

YEREVAN – 2023

Contents

List of Figures

List of Tables

List of Publications

This PhD thesis is based on the following *Refereed Publications:*

1. Hakobyan A.A., **Barkhudaryan L.V.**, Karapetyan A.G., Mamon G.A., Kunth D., Adibekyan V., Aramyan L.S., Petrosian A.R., Turatto M., *"Supernovae and their host galaxies – V. The vertical distribution of supernovae in disc galaxies"*, Monthly Notices of the Royal Astronomical Society, 2017, Volume 471, Issue 2, pp. 1390-1400.

2. **Barkhudaryan L.V.**, Hakobyan A.A., Karapetyan A.G., Mamon G.A., Kunth D., Adibekyan V., Turatto M., *"Supernovae and their host galaxies – VI. Normal Type Ia and 91bg-like supernovae in ellipticals"*, Monthly Notices of the Royal Astronomical Society, 2019, Volume 490, Issue 1, pp. 718-732.

3. Hakobyan A.A., **Barkhudaryan L.V.**, Karapetyan A.G., Gevorgyan M.H., Mamon G.A., Kunth D., Adibekyan V., Turatto M., *"Supernovae and their host galaxies – VII. The diversity of Type Ia supernova progenitors"*, Monthly Notices of the Royal Astronomical Society, 2020, Volume 499, Issue 1, pp. 1424-1440.

4. **Barkhudaryan L.V.**, *"Constraining Type Ia supernovae through their heights in edge-on galaxies"*, Monthly Notices of the Royal Astronomical Society: Letters, 2023, Volume 520, Issue 1, pp. L21-L27.

List of Abbreviations

AD	Anderson–Darling
AGB	asymptotic giant branch
ASC	Asiago Supernova Catalogue
CC	core–collapse
CDF	cumulative distribution function
CO	carbon–oxygen
DD	double–degenerate
DR	Data Release
DTD	delay time distribution
He	helium
KS	Kolmogorov–Smirnov
LC	light curve
LOSS	Lick Observatory Supernova Search
MC	Monte Carlo
MLE	maximum likelihood estimation
MS	main–sequence
MW	Milky Way
PA	position angle
Pan-STARRS	Panoramic Survey Telescope and Rapid Response System
PDF	probability density function
RGB	red giant branch
SD	single–degenerate
SDSS	Sloan Digital Sky Survey
SED	spectral energy distribution
SFR	star formation rate
SN	Supernova
WD	white dwarf

Introduction

The detailed understanding of the spatial distribution of Supernovae (SNe) in galaxies provides important links between the nature of SNe progenitor stars and host galactic stellar populations [1–8]. These links make it possible to constrain crucial physical parameters of various SN progenitors, such as their masses [9, 10], ages [11, 12], and metallicities [13, 14]. Despite numerous excellent studies, the progenitor nature and explosion channels of SNe have been the subject of controversy for decades (see [15], for a review).

Based on modern understanding, SNe are divided into two general categories: core-collapse (CC) and Type Ia (thermonuclear) SNe. CC SNe are the colossal explosions that mark the violent deaths of young massive stars [16–18],[1] while SNe Ia are believed to be the evolutionary endpoint, accompanied by the thermonuclear explosion, of carbon-oxygen (CO) white dwarf (WD) stars in interacting close binary systems (see [19, 20], for comprehensive reviews about thermonuclear SNe). These events play a key role in understanding the evolution of binary stellar systems [21], the chemical enrichment of galaxies [22], and the nature of accelerating expansion of the Universe [23, 24].

It is now clear that Type Ia SNe are not a homogeneous population of WD explosions, as they display a variety of photometric and spectroscopic properties [25, 26]. In the local Universe, in comparison with moderately uniform normal SNe Ia [27], about one third of all SNe Ia events have peculiar characteristics [28, 29]. The most common subclasses of peculiar SNe Ia are: *i)* 91T-like events [30, 31], which are overluminous at the B-band maximum (~ 0.6 mag more

[1] According to the spectral features in visible light, CC SNe are classified into three basic classes [32]: hydrogen lines are visible in the spectra of Type II SNe, but in Types Ib and Ic SNe; helium lines are seen in the spectra of SNe Ib, but in SNe Ic. Subclass IIn SNe are dominated by narrow emission lines, while subclass IIb SNe have transitional spectra closer to SNe II at early times, then evolving to SNe Ib.

luminous than normal SNe Ia) and have slow-declining light curves (LCs), with distinctive pre-peak spectra dominated by Fe III lines, *ii)* 91bg-like SNe [33–35], which are subluminous events ($\sim$ 2 mag less luminous than normal ones) and have fast-declining LCs, with post-maximum spectra dominated by unusually strong O I and Ti II lines, and *iii)* low luminosity (more than 2 mag fainter than normal SNe Ia) and faster declining 02cx-like SNe (also called SNe Iax, [36, 37]), with early spectra resembling those of 91T-like events. There is also a tiny percentage of other peculiar SNe Ia, including the faint but slowly declining 02es-like SNe, so called Ca-rich transients, the extremely luminous 06gz-like (also called super-Chandrasekhar) SNe, and other SNe Ia with spectra showing evidence of interaction with the circumstellar medium (see [25] for a review on the extremes of SNe Ia).

The upper panel of Fig. 1 displays examples of spectral profiles for SNe Ia. The upper spectrum presents normal SN 2011fe acquired 2.9 days prior to reaching its peak B-band magnitude. Notably, the dominant characteristic of the spectrum consists of absorption lines stemming from intermediate-mass elements. Supplementary absorption features arise from iron-group elements, with a more comprehensive elucidation provided in [38]. The middle spectrum, representative for the SN 1991T-like subclass, demonstrates a spectral resemblance to post-peak normal events [39], but shows very distinctive features at earlier epoch. Members of the SN 1991bg-like classification (bottom spectrum [33]) exhibit a comparable likeness, albeit presenting a distinctive broad absorption trough (attributed to blends of Fe-group elements [40]), spanning the spectral range of 4000Å to 4500Å at the peak phase.

The bottom panel of Fig. 1 shows LC examples of different subclasses of SNe Ia. Within the panel situated on the left-hand side, the solid curves illustrate the observed R-band LCs from the database of [41]. At the same time, the dash-dotted line is the smoothed LC of SN 1991T [42] and the dashed line mentioned as “91bg” is the same for SN 1999by [43], which have absolute peak magnitude at –19.5 and –17.5 mag, correspondingly. Spanning between these two extreme curves is an interpolated set of 21 LCs, employed for the fitting procedure on the individual objects presented in the panels on the right-hand side.

In general, the behaviour of the LCs of SN Ia depends on the mass of synthesized radioactive

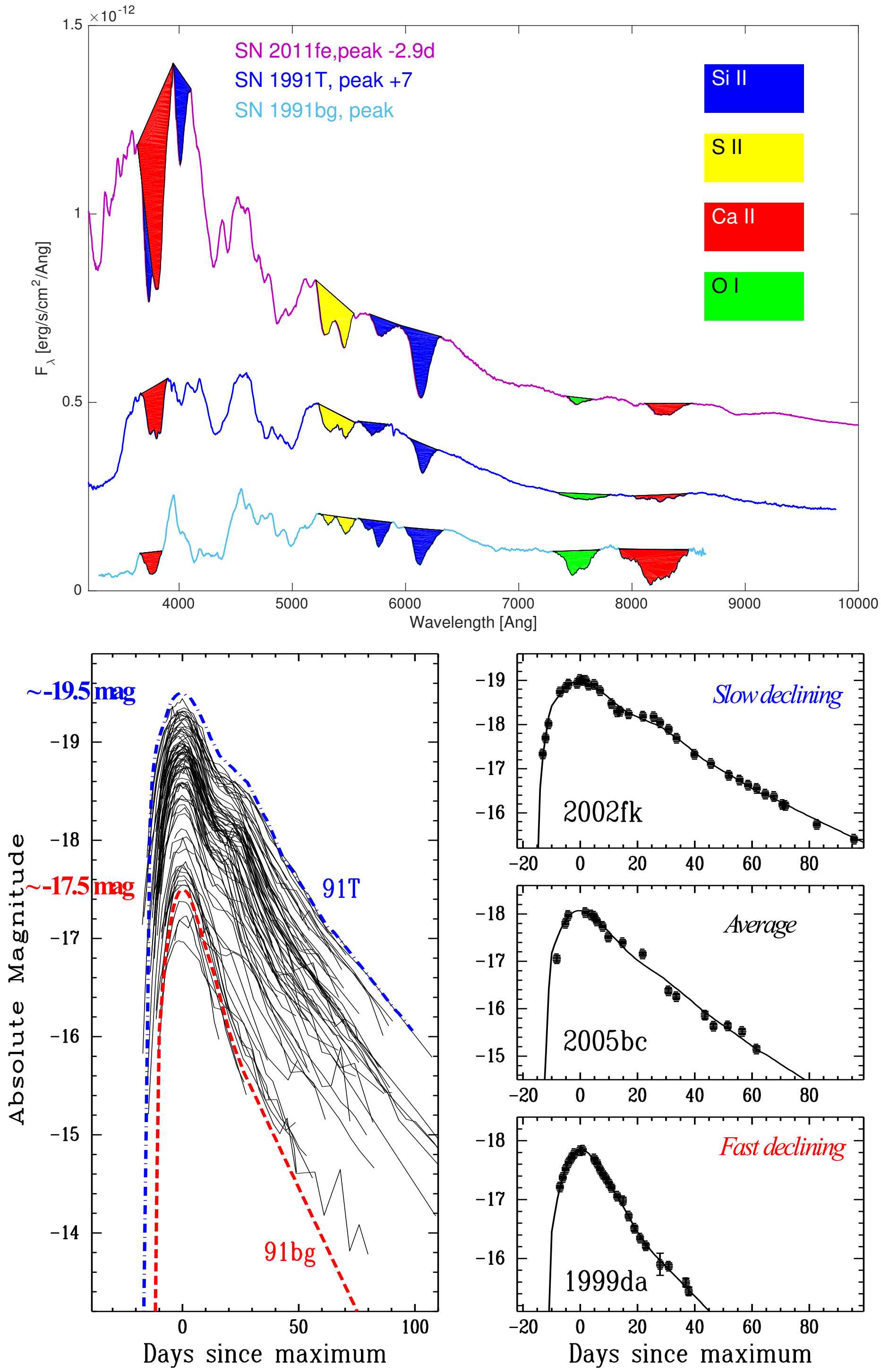

Figure 1: *Upper panel:* examples of spectra for different subclasses of SNe Ia. The panel is reproduced from [44]. *Bottom panel:* LC examples for the SN Ia subclasses (adopted from [28] and modified).

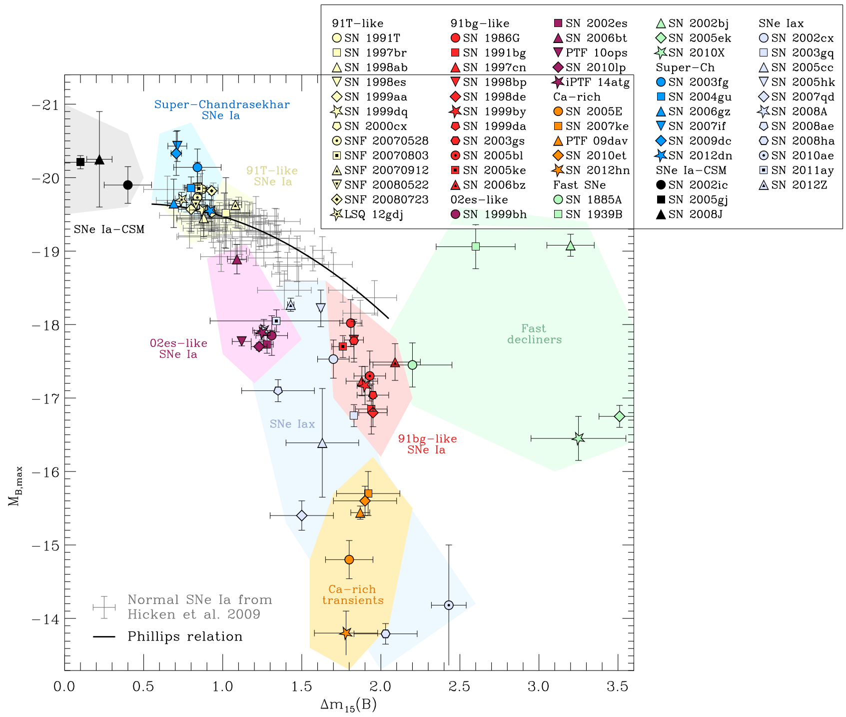

Figure 2: Graphical representation of the relationship between the peak B-band magnitudes of SNe Ia and their LC decline rates, emphasizing the discernible variations in photometric characteristics across the SNe Ia subclasses. The figure is taken from [25].

^{56}Ni, the kinetic energy of the explosion, and the opacity of the ejecta [45, 46]. Importantly, Type Ia SNe show a key relation between their luminosity at the B-band maximum and their LC decline rate Δm_{15} (i.e. magnitude difference between the maximum and 15 days after). This is known as the width-luminosity relation (often called the *Phillips relation* [47]: faster declining SNe Ia are fainter) that played an enormous role in standardization of SNe Ia and their use in cosmology as the best distance indicators. However, the width-luminosity relation is well established for normal SNe Ia, while peculiar events deviate, sometimes very strongly, from that relation [25, 48]. Fig. 2 illustrates the peak absolute B-band magnitude against the LC decline rate, quantified as the $\Delta m_{15}(B)$ [47]. Distinct classes of SNe Ia are delineated using varying color schemes. A significant number of the events manifest distinct segregation from the normal SNe Ia within this spatial representation, underscoring their inherent uniqueness based on the attributes of their LCs. An exception arises with 91T-like SNe, which display an intersection with the more gradual range of the distribution characterizing normal SNe Ia.

Notably, the distinctive characteristics of 91T-like SNe predominantly stem from spectroscopic qualities. Note that the Δm_{15} and colours of SNe Ia are also related: the faster declining events correspond to the intrinsically redder SNe [49]. For more details, see a review [25] on the extremes of SNe Ia.

Theoretically, there are many possibilities in the proposed progenitor channels for Type Ia SNe that are still under debate [50,51], however they are generally categorized into the following main classes; the *single-degenerate* (SD) and *double-degenerate* (DD) channels, both of which probably occur in nature [52]. In the SD channel [53], a degenerate WD grows in mass through accretion from a non-degenerate companion, consequently causing an explosion when the WD mass reaches the Chandrasekhar mass limit ($M_{\rm Ch} \approx 1.4 M_{\odot}$). The non-degenerate companion can be a main-sequence (MS)/subgiant star, or a red giant, or a helium (He) star [54]. In the DD channel [55, 56], an explosion occurs when two degenerate WDs coalescence or interact through accretion with each other in a binary system, after having been brought together due to the loss of orbital angular momentum via the emission of gravitational waves. Fig. 3 diagrammatically illustrates various evolutionary channels of binary stars to the subsequent explosion of Type Ia SNe.

A promising and important addition is the explosion model of sub-Chandrasekhar mass ($M_{\rm Ch} < 1.4 M_{\odot}$) WD. The explosion mechanism is realized in the double detonation of a sub-$M_{\rm Ch}$ WD, in which accreted helium shell detonation initiates second detonation in the core of CO WD [57–59]. More luminous SNe Ia that have slower declining LCs (smaller Δm_{15} values) are produced by the explosion of more massive sub-$M_{\rm Ch}$ WD, because the luminosity of SN Ia is related to the mass of ^{56}Ni synthesized during the WD explosion [60], which in turn is related to the mass of the WD (e.g. [61, 62] for a variety of specific explosion models). On the other hand, more massive WD would come from more massive MSs stars, which have shorter lifetime than the progenitors of less massive WDs. In addition, due to the gravitational wave emission, massive WDs in the binary system would interact in a shorter timescale. Thus, it should follow that the LC decline rate Δm_{15} of SN Ia is correlated with the age of the SN progenitor system [58, 63].

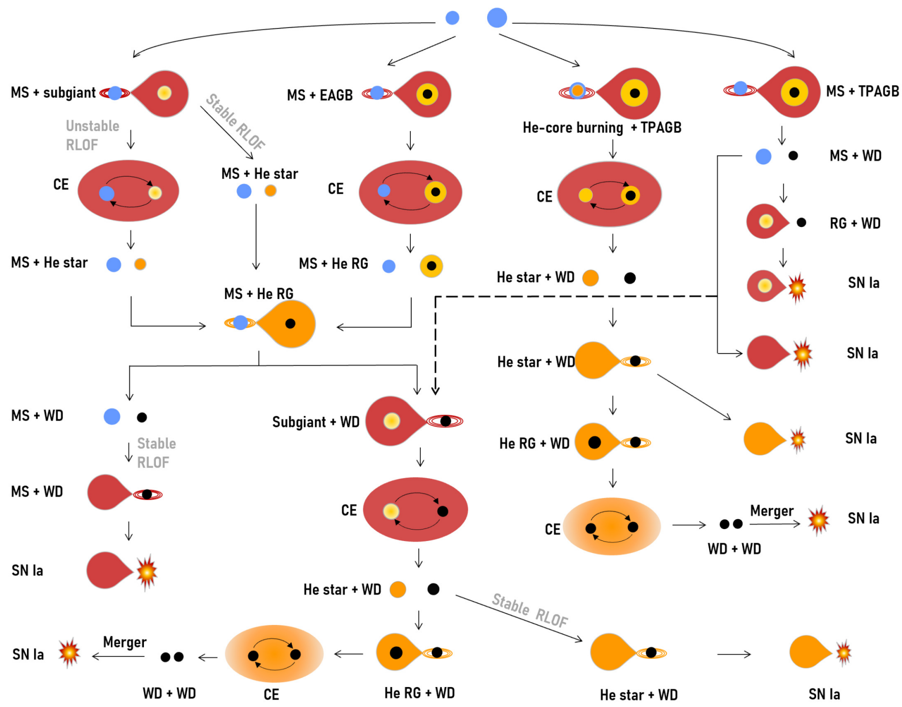

Figure 3: Diagrammatic representation of binary evolutionary channels for Type Ia SNe within the SD and DD scenarios. It should be noted that the evolutionary pathways presented herein are not complete (figure is taken from [64]).

When considering only the most populated subclasses of SNe Ia, i.e. normal, 91T- and 91bg-like events, the lower mass of the host galaxy (the later morphological type or higher the specific star formation rate [SFR]), the brighter and slower the SNe Ia that are exploded, on average [28,65–70]. Fig. 4 shows the comparison of SNe Ia host galaxy morphological classifications with the $\Delta m_{15}(B)$ parameter. Only SNe Ia with accurately established host galaxy classifications are represented in the figure. Open circles denote SNe Ia with spectroscopic peculiarities. SNe are positioned in relation to their corresponding t-type (aligned with the right axis), while the left axis serves a purely illustrative purpose. 91T-like SNe occur in star-forming host galaxies, while such an object has never been discovered in elliptical galaxies [28, 67, 68], where the stellar population almost always consists of old stars. 91bg-like events prefer host galaxies with elliptical and lenticular morphologies (E–S0), sometimes they explode also in early-type spirals [28, 67]. Normal SNe Ia are discovered in host galaxies with any morphologies from ellipticals to late-type spirals [28]. Theoretically, this is because the progenitor age distribution at the current epoch should have a bimodal shape, with the first peak being below or close to

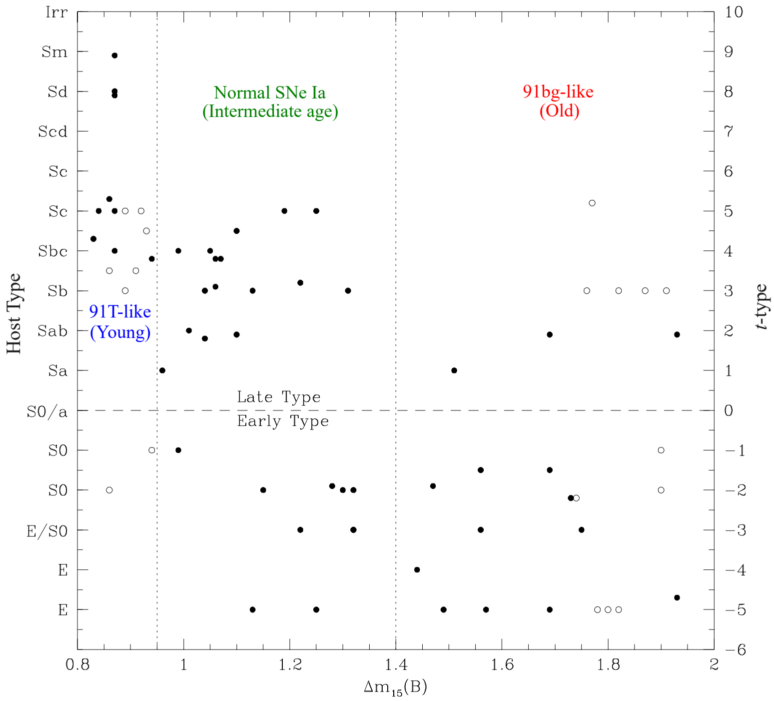

Figure 4: Comparison of Type Ia SNe host galaxy morphological classifications with the $\Delta m_{15}(B)$ parameters (figure comes from [67]).

1 Gyr and corresponding to the young/prompt SNe Ia, and the second peak being at about several Gyr and including old/delayed events [71].

In the literature, there are many efforts in studying the links between the spectral as well as LC properties of SNe Ia and the global as well as local properties at SN explosion sites of their host galaxies, such as mass, colour, SFR, metallicity, and age of the stellar population [1, 68, 69, 72–81]. In short, these studies showed that more luminous and slower declining SNe Ia explode, on average, in galaxies with later morphological type, lower mass, higher specific SFR, and younger stellar population age (for SN local environment as well). In [82], recently claimed a significant correlation between the SN Ia luminosity (or LC decline rate) and the stellar population age of its host, at a 99.5% confidence level. They suggested that the previously reported correlations with host morphology, mass, and SFR are originated from the difference in population age (see also [71, 79, 83]). However, SN Ia samples in these studies consist only of spectroscopically normal events with known LC properties, or sometimes include only a tiny portion of peculiar SNe Ia. Therefore, the relations between LC properties of peculiar SNe Ia and the characteristics of their host galaxies have not been explored in such detail as it was done for normal SNe Ia.

Moreover, in such studies, SNe Ia host galaxies with various morphological properties, e.g. old ellipticals with spherically-distributed stellar content, lenticulars with an old stellar population in a huge spherical bulge plus a prominent exponential disc, and spirals with old bulge and young star forming disc components are simultaneously included in the samples. In this case, it is difficult to precisely analyse the spatial distribution of SNe, and associate them with a concrete stellar component (bulge or thick/thin discs, old or intermediate/young) in the hosts due to different or unknown projection effects [84,85]. In addition, E–S0 and spiral host galaxies have had different evolutionary paths through major/minor galaxy-galaxy interaction [86–88], and therefore, this important aspect should be clearly distinguished.

Usually, the spatial distribution of SNe in S0–Sm galaxies is studied with the reasonable assumption that all CC SNe and the vast majority of SNe Ia belong to the disc, rather than the bulge population [1, 89, 90]. Moreover, the distributions of SNe in the disc are studied assuming that the disc is infinitely thin [3, 90]. The height distribution of SNe from the disc plane is mostly neglected when studying the host galaxies with low inclinations (close to face-on orientation) assuming that the exponential scale length of the radial distribution is dozens of times larger in comparison with the exponential scale height of SNe [91].

Direct measurements of the heights of SNe and estimates of the scales of their vertical distributions in host galaxies with high inclination (close to edge-on orientation) were performed only in a small number of cases [92–94]. Mainly due to the small number statistics of SNe and inhomogeneous data of their host galaxies, the comparisons of vertical distributions of the different types of SNe resulted in statistically insignificant differences. Therefore, while the detailed study of the vertical distributions in edge-on galaxies has allowed to constrain ages, masses and other physical parameters of their components [95–97], the lack of analogous studies on the distribution of various SN subclasses has prevented the determination of their parent populations via the direct comparison with the nearby extragalacric discs and the thick/thin discs of the Milky Way (MW) galaxy [98–100].

The main purpose of this PhD thesis is to investigate the vertical distributions of the subclasses of SNe Ia in their edge-on host galactic discs and check the potential correlation between SNe Ia LC decline rates and their heights, which may provide an indication that both parameters are appropriate stellar population age indicators. As well as to properly identify the diversity of SNe Ia, and better constrain the progenitor nature and explosion channels through a comprehensive study of the SN Ia LC decline rates and global properties of their host galaxies (e.g. morphology, stellar mass, colour, and age of stellar population). An additional objective is to investigate the galactocentric distributions of various subclasses of Type Ia SNe within elliptical host galaxies.

The thesis consists of four Chapters. Chapter 1 presents an analysis and modeling of the height distributions of the main SNe classes from the plane of their edge-on S0–Sd host galaxies. Chapter 2 performs an analyses of the vertical distributions and link the SN heights to the LC decline rates Δm_{15} of normal SNe Ia, 91T-, and 91bg-like events. Chapter 3 presents an analysis of the LC decline rates (Δm_{15}) of normal and peculiar SNe Ia and global parameters of their host galaxies. Chapter 4 performs an analysis of the galactocentric distributions of normal SNe Ia and peculiar 91bg-like events, as well as study the global parameters of their elliptical hosts. The General Conclusions provide a brief overview of the inferred key findings.

A considerable portion of this study represents *innovative exploration*, and the resultant findings are *entirely novel*. These outcomes constitute the essence of the thesis defense.

Chapter 1

The vertical distribution of SNe in disc galaxies

1.1 Introduction

Detailed studies of the vertical distributions in edge-on galaxies have allowed us to constrain the ages, masses, and other physical parameters of their components, the lack of comparable studies on the distribution of various SN types has prevented us from determining their parent populations through direct comparison with nearby extragalacric discs and the thick/thin discs of the MW galaxy.

The purpose of this Chapter is to address these questions properly through an investigation of the vertical distributions of the main classes of SNe in a nearby sample of 102 SNe and their well-defined edge-on S0–Sd host galaxies from the Sloan Digital Sky Survey-III (SDSS-III; [101]).

To conform to values used in the data base [102], a cosmological model with $\Omega_{\mathrm{m}} = 0.27$, $\Omega_{\Lambda} = 0.73$, and $H_0 = 73\,\mathrm{km\,s^{-1}\,Mpc^{-1}}$ Hubble constant [103] are adopted in this study.

1.2 Sample selection and reduction

For this Chapter, we composed our sample by cross-matching the coordinates of classified Ia, Ibc[1], and II SNe from the Asiago Supernova Catalogue[2] (ASC; [104]) with the footprint of SDSS Data Release (DR) 12 [101]. All SNe are required to have equatorial coordinates. We use SDSS DR12 and the approaches presented in [102] to identify the host galaxies and classify their morphological types. It is worth noting that morphological classification of nearly edge-on galaxies is largely based on the visible size of bulge relative to the disc because other morphological properties, such as the shape of spiral arms or presence of the bar, are generally obscured or invisible. The morphologies of galaxies are restricted to S0–Sd types, since we are interested in studying the vertical distribution of SNe in host stellar discs. A small number of Sdm–Sm host galaxies are not selected, because they show no clear discs.

From the signs of galaxy–galaxy interactions, we classify the morphological disturbances of the hosts in the SDSS DR12 following the techniques described in detail in [105]. We then exclude from this analysis any galaxy disc exhibiting strong disturbances: interacting, merging, and post-merging/remnant.

Using the techniques presented in [102], we measure the apparent magnitudes and the geometry of host galaxies.[3] In the SDSS g-band, we first construct isophotes, and then centred at the each galaxy centroid position an elliptical aperture visually fitted to the 25 mag arcsec^{-2} isophote. We measure the apparent magnitudes, major axes (D_{25}), position angles (PA) of the major axes, and elongations (a/b) of galaxies using these apertures. In this analysis, we correct the magnitudes and D_{25} for Galactic and host galaxy internal extinction [102].

[1] 'Stripped-envelope' SNe of Types Ib and Ic, including the mixed Ib/c with uncertain subclassification, are denoted as SNe Ibc.

[2] We use the updated version of the catalogue, which includes SNe exploded before 2015 January 1.

[3] Instead using the data from [102], which is based on the SDSS DR8, for homogeneity we re/measure the magnitudes and the geometry of all host galaxies, with additional new SN hosts included, based only on DR12.

1.2.1 Inclination

The main difficulty in measuring the vertical distribution of SNe above the host stellar discs is that we have no way of knowing where along the line of sight the SNe lie. This means that reliable measurements can only be done in discs which are highly inclined, i.e., closer to an edge-on orientation (e.g. $85^\circ \leqslant i \leqslant 90^\circ$). In contrast to galaxies with lower inclination, the matter is complicated by the difficulty of making an accurate determination of the inclination angle. For these galaxies, the inclination cannot be measured simply from the major and minor axes because the presence of a central bulge places a limit on the axis-ratio even for a perfectly edge-on galaxy.

This problem with the bulge has been solved by using the axial ratio of the exponential disc fits in the g-band provided by the SDSS (from the model with $r^{1/4}$ bulge and exponential disc), i.e., `expAB_g`. Indeed, real stellar discs are not flat with negligible thicknesses, but have some intrinsic width, and a proper measurement of the inclination depends on this intrinsic ratio of the vertical and horizontal axes of the disc, known as q. Therefore, we calculate the inclinations of SNe host galaxies following the formula

$$\cos^2 i = \frac{(\texttt{expAB\_g})^2 - q^2}{1 - q^2} \ , \tag{1.1}$$

where i is the inclination angle in degrees between the polar axis and the line of sight and q is the intrinsic axis-ratio of galaxies viewed edge-on. According to [106],

$$q = \mathrm{dex}[-(0.43 + 0.053\, t)] \tag{1.2}$$

for $-1 \leq t \leq 7$, where t is the morphological type code. Using equations (1.1) and (1.2), we restrict the inclinations of host galaxies to $85^\circ \leqslant i \leqslant 90^\circ$.

All the selected SNe host galaxies are visually inspected because sometimes bright stars projected nearby, strong dust layers, bright nuclear/bulge emission, large angular sizes, etc. do not allow the SDSS automatic algorithm to correctly determine the parameters of galaxies, in

Table 1.1: Numbers of SNe as a function of morphological types of edge-on S0–Sd host galaxies.

	S0	S0/a	Sa	Sab	Sb	Sbc	Sc	Scd	Sd	All
Ia	6	3	2	5	9	5	16	4	3	53
Ibc	0	0	0	0	2	0	1	3	3	9
II	0	1	1	1	11	6	12	5	3	40
All	6	4	3	6	22	11	29	12	9	102

Notes. Among SNe II, four are of Type IIb (two in Sb and two in Scd galaxies). Due to the uncertainties in the progenitor nature of Type IIn SNe, and often their misclassification [9, 107], we remove them from the sample.

particular the axis-ratio `expAB_g`. The host discs with a clearly seen dust layer, or without signs of non-edge-on spiral arms, are selected as true edge-on galaxies. In other words, we exclude the discs whose galactic plane is not aligned along the major axis of their fitted elliptical apertures (e.g. warped edge-on discs, see [108]). As a result, we select 106 SNe in edge-on host galaxies.

In S0–Sd galaxies, all CC SNe and the vast majority of Type Ia SNe belong to the disc, rather than the bulge component [84]. Therefore, for the selected 106 SNe in this restricted sample of edge-on galaxies, we perform a visual inspection of the SNe positions on the SDSS images to identify the SNe from the bulge population of host galaxies. The result is that three Type Ia (1990G, 1993aj, and 2003ge) and one Type Ib/c (2005E) SNe may belong to the bulge because of their location. The three SNe Ia are clearly outside the host discs, located far in the bulge population. The Type Ib/c SN is also located far from the host galaxy disc but it is a peculiar, calcium-rich SN whose nature is still under debate and may have a different progenitor from typical CC [109]. All these four SNe are excluded from the sample.

After these restrictions, we are left with a sample of 102 SNe within 100 host galaxies. The mean distance of this sample is 100 ± 8 Mpc, the median distance and standard deviation are 78 Mpc and 84 Mpc, respectively. The mean D_{25} of our host galaxies is 108 ± 10 arcsec with the smallest value of 22 arcsec. Table 1.1 displays the distribution of all SNe types among the various considered morphological types of host galaxies. Fig. 1.1 shows images of typical examples of edge-on host galaxies with marked positions of SNe.

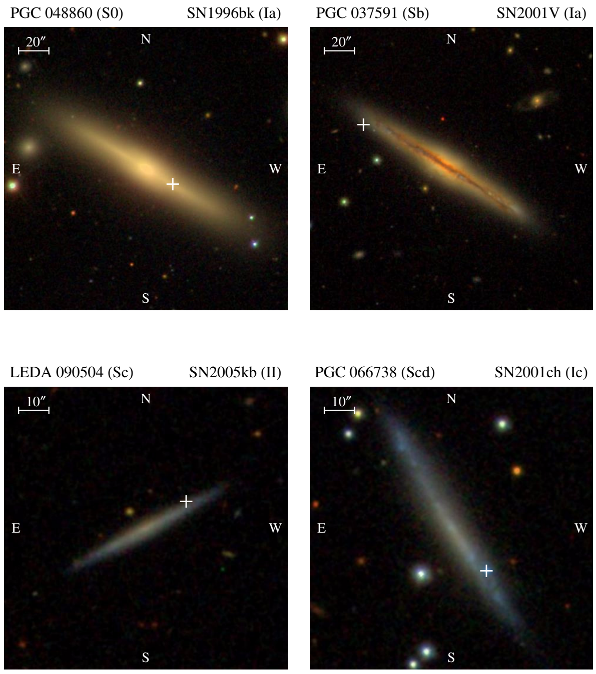

Figure 1.1: SDSS images representing examples of edge-on SNe host galaxies. The objects' identifiers with host morphologies and SN types (in parentheses) are listed at the top. The positions of SNe (marked by cross sign) are also shown.

1.2.2 Measurements of the heights of SNe

The heights of SNe above host galactic plane might be calculated by using the simple formulas presented in [3] with available SNe offsets from host galaxy nuclei and PA of the galaxies (see also [84]). However, as demonstrated in [102], SN catalogs report different offsets with different levels of accuracy. Individual offsets are based on the determination of the positions of the host galaxy nuclei, which might be uncertain and depend on many factors (e.g. colour of image, plate saturation, galaxy peculiarity, incorrect SDSS fiber targeting of the galaxy nucleus, etc.). For more details, the reader is referred to [102].

For this study, using the SN coordinates and its edge-on host galaxy image in the SDSS g-band, we measure the perpendicular distance, i.e., the height, from the major axis of the fitted elliptical aperture of each galaxy to the position of SN. At the same time, using the coordinates of the host galaxy nucleus, we also measure the projected galactocentric radius of SN along the same major axis. Fig. 1.2 schematically illustrates the geometrical location of an SN within an edge-on disc, where V is the height (in arcsec) and U is the projected galactocentric radius (in

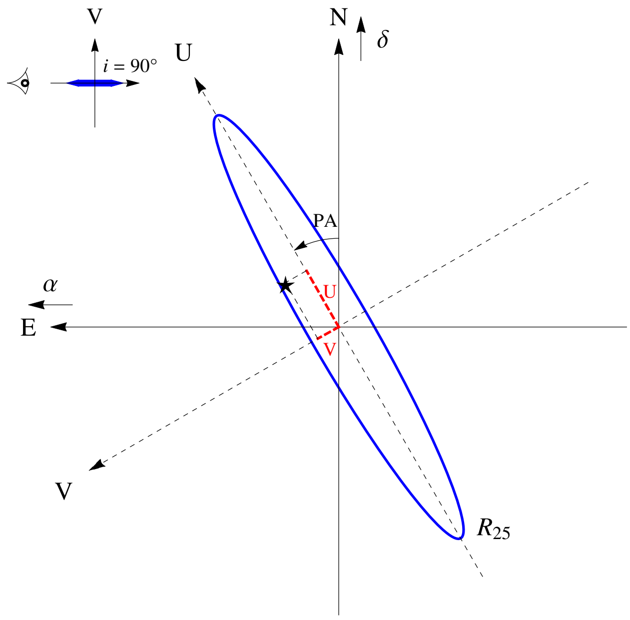

Figure 1.2: Location of the SN within its edge-on host galaxy. The center of the galaxy is at the origin of coordinate systems and the asterisk is the projected location of the SN. The U (the projected galactocentric radius) and V (the height) are coordinates of the SN in host galaxy coordinate system along the major (U) and the minor (V) axes, respectively. The inset in the upper-left corner illustrates the 90° inclination of the polar axis of the galaxy with respect to the line of sight.

arcsec) of the SN. A similar technique was also used in [92] on the Digital Sky Survey images to determine the V and U coordinates of SNe.

It is important to note that as in the case of the radial distribution of SNe in face-on galaxies [3], the distribution of linear distances in the vertical direction is biased by the greatly different intrinsic sizes of host discs. Fig. 1.3 illustrates the comparison of the heights V of SNe and R_{25} of host galaxies in kpc. Also shown are the best fit lines

$$\log(\text{V}_{\text{Ia}}) = (-1.10 \pm 0.11) + (0.89 \pm 0.08)\ \log(R_{25})\ ,$$

$$\log(\text{V}_{\text{CC}}) = (-1.68 \pm 0.15) + (1.07 \pm 0.13)\ \log(R_{25})$$

with near unity slopes. To check the significance of the correlations, we use the Spearman's rank correlation test, which indicates strong positive trend between the heights and R_{25} for Type Ia SNe ($r_{\text{s}} = 0.382, P = 0.005$), while not significant for CC SNe ($r_{\text{s}} = 0.166, P =$

0.255). Therefore, in the remainder of this Chapter, we use only relative heights and projected galactocentric radii of SNe, i.e., normalized to $R_{25} = D_{25}/2$ of host galaxies in g-band.

The full data base of 102 individual SNe (SN designation, type, equatorial coordinates, V and U) and their 100 host galaxies (galaxy SDSS designation, distance, morphological type and corrected g-band D_{25}) is available online [110].

1.3 The model of stellar disc

In our model, the volumetric density $\rho^{\rm SN}(\tilde{r}, \tilde{z})$ of SNe in the host axisymmetric stellar discs is assumed to vary as follows in the radial $\tilde{r}$ and vertical $\tilde{z}$ directions:

$$\rho^{\rm SN}(\tilde{r}, \tilde{z}) = \rho_0^{\rm SN} \exp(-\tilde{r}/\tilde{h}_{\rm SN}) f(\tilde{z}) \ , \tag{1.3}$$

where $\tilde{r} = R_{\rm SN}/R_{25}$, $\tilde{z} = z_{\rm SN}/R_{25}$ and $(R_{\rm SN}, z_{\rm SN} \equiv \text{V})$ are cylindrical coordinates, $\rho_0^{\rm SN}$ is the central volumetric density, $\tilde{h}_{\rm SN} = h_{\rm SN}/R_{25}$ is the radial scale length, and $f(\tilde{z})$ is a function describing the vertical distribution of SNe.

In equation (1.3), we adopt a generalized vertical distribution

$$f(\tilde{z}) = {\rm sech}^{2/n}(n\tilde{z}/\tilde{z}_0^{\rm SN}) \ , \tag{1.4}$$

where $\tilde{z}_0^{\rm SN} = z_0^{\rm SN}/R_{25}$ is the vertical scale height of SNe and n is a parameter controlling the shape of the profile near the plane of host galaxy. Following the vertical surface brightness distribution of edge-on galaxies [111, 112], we also assume that the scale height of SNe is independent of projected galactocentric radius (see also [113], for late-type galaxies), i.e., there is no disc flaring.

Recent photometric fits to the surface brightness distribution of a large number of edge-on galaxies in near-infrared [114] and SDSS g-, r-, and i-bands [95] (see also [96] for other photometric bands) suggest that a value of $n = 1$ is an appropriate model of stellar discs. When $n \to \infty$, equation (1.4) reduces to $f(\tilde{z}) \sim \exp(-|\tilde{z}|/\tilde{H}_{\rm SN})$, where $\tilde{H}_{\rm SN} = \tilde{z}_0^{\rm SN}/2$ at large

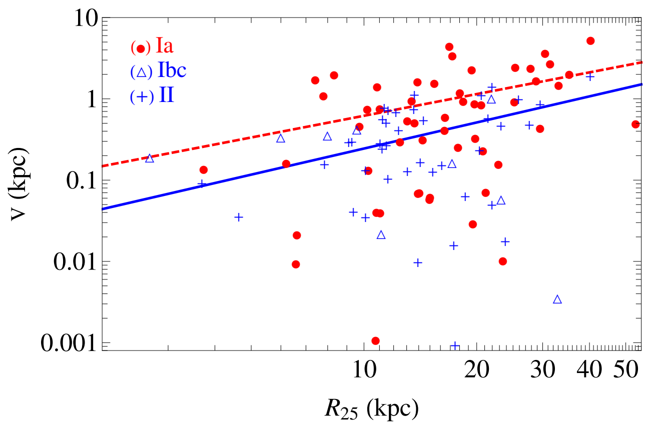

Figure 1.3: Comparison of the heights v of SNe and R_{25} of host galaxies in kpc. Red circles, blue triangles and crosses respectively show Types Ia, Ibc and II SNe. Red dashed (Ia) and blue solid (Ibc+II) lines are best fits to the samples.

heights, and is widely used to successfully fit the dust distribution in edge-on galaxies [95, 115].

In linear units, the exponential (exp) form of $f(\tilde{z})$ is used to model the distribution of Galactic stars [98, 99], novae [116], SNe [117, 118], SN remnants [119], pulsars [120], and extragalactic SNe [91–93], while the sech^2 form is used to fit the vertical distribution of resolved stars [97] and CC SNe [94] in highly inclined nearby galaxies.

Note that sech^2 profile ($n = 1$) is expected for an isothermal stellar population [121], while exp profile ($n \to \infty$) can be obtained by a combination of isothermal stellar populations with different "temperatures" (velocity dispersions). While at large heights, $\text{sech}^2(x) \to 4\exp(-2x)$, at low heights, the sech^2 profile is uniform, while the exp profile is cuspy.

1.4 Results and discussion

1.4.1 The vertical distribution and scale height of SNe

We fit sech^2 and exp forms of $f(\tilde{z})$ profile to the distribution of normalized absolute heights ($|\tilde{z}| \equiv |\text{v}|/R_{25}$) of SNe, using maximum likelihood estimation (MLE). Here, because of the small number statistics of Type Ibc SNe (see Table 1.1), we group them with Type II SNe in a larger CC SNe sample. Fig. 1.4 shows the histograms of the normalized heights with the fitted sech^2

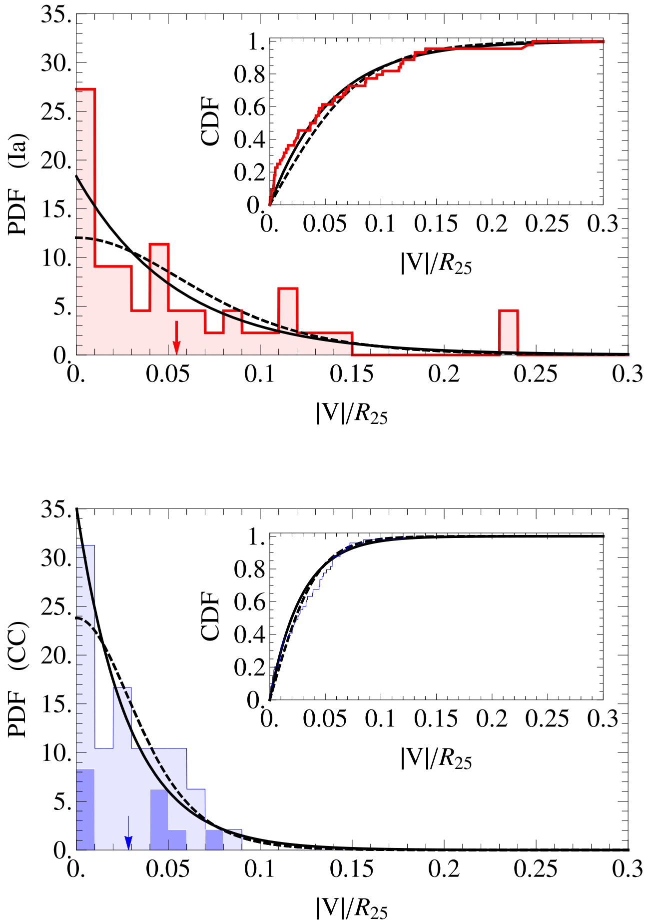

Figure 1.4: Vertical distribution of SNe (scaled to isophotal radius of disc) in Sa–Sd galaxies. Upper panel: fitted sech^2 (dashed curve) and exp (solid curve) PDFs of the normalized absolute heights ($|\tilde{z}| \equiv |\mathrm{V}|/R_{25}$) of Type Ia SNe (red histogram). Bottom panel: the same for CC SNe (blue histogram). The dark blue histogram presents the distribution of Type Ibc SNe only. The insets present the different forms of fitted CDFs in comparison with the SN distribution. The mean values of the distributions are shown by arrows.

and exp probability density functions (PDFs) for Type Ia and CC SNe in Sa–Sd galaxies.[4] In columns 4, 7, and 10 of Table 1.2, we list the mean values of $|\tilde{z}|$ and the maximum likelihood scale heights for both types of SNe in various subsamples of host galaxies.

From column 4 of Table 1.2, it immediately becomes clear that in all the subsamples of host galaxies the vertical distribution of CC SNe is about twice closer to the plane of host disc than the distribution of Type Ia SNe. In fact, the two-sample Kolmogorov–Smirnov (KS) and

[4]For this comparative illustration, we do not include S0–S0/a galaxies because they host almost only Type Ia SNe (see Table 1.1). For the sake of visualization, the distribution of Type Ibc SNe is also presented in the bottom panel of Fig. 1.4.

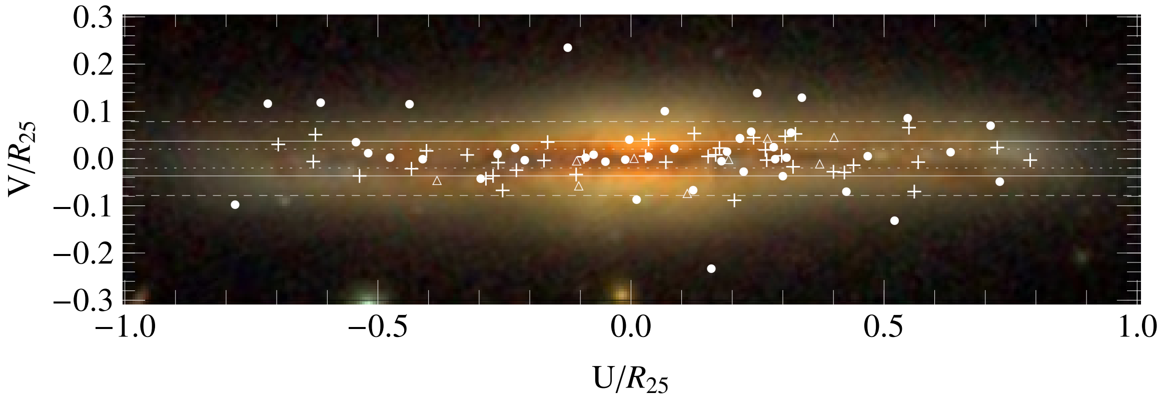

Figure 1.5: Distribution of coordinates of SNe along the major (U/R_{25}) and minor axes ($\tilde{z} \equiv$ V/R_{25}) of their Sa–Sd host galaxies. Circles, triangles and crosses respectively show Types Ia, Ibc and II SNe. One-sigma intervals of the distributions of the $\tilde{z}$ coordinates for Type Ia and CC (Ibc+II) SNe are presented by dashed ($\sigma = 0.078$) and solid ($\sigma = 0.037$) lines, respectively. Background SDSS image shows the PGC 037591 galaxy (scaled to the distribution), which is one of the representatives of the edge-on galaxies with a prominent dust line along the major axis. Dotted lines show the $|\tilde{z}| \leq 0.02$ opaque region.

Anderson–Darling (AD) tests,[5] shown in Table 1.3, indicate that this difference is statistically significant in Sa–Sd galaxies, although not significant if only late-type hosts are considered.

Note that four Type IIb SNe are included in Type II SNe sample (see Table 1.1). For Sa–Sd galasies, it might be reasonable also to group Types IIb and Ibc SNe as a wider 'stripped-envelop' (SE) SN class (13 objects) and compare them with pure Type II SNe (35 objects). However, we find no difference between the vertical distributions of SE and pure Type II SNe ($P_{\rm KS} = 0.401$, $P_{\rm AD} = 0.320$), resulting in statistically indistinguishable scale lengths between these SN types. Therefore, in the remainder of this study, we will group all these subtypes as the main CC SN sample and compare that with Type Ia SN sample.

It is important to note that dust extinction in edge-on SN host galaxies might have an impact on our estimated scale heights.[6] In [102], we demonstrated that in general there is a lack of SNe host galaxies with high inclinations, which can be explained by a bias in the

[5] The two-sample AD test is more powerful than the KS test [122], being more sensitive to differences in the tails of distributions. Traditionally, we chose the threshold of 5% for significance levels of the different tests.

[6] Another factor, such as a deviation from perfectly edge-on orientation of the host discs, may also affect our estimation of the scale heights, increasing them. However, we are quite confident that our galaxies can vary by a few degrees only from perfectly edge-on orientation (see Section 1.2.1). In addition, other authors have demonstrated that slight deviations from $i = 90°$ have minimal impact on the derived structural parameters of the vertical distributions of different stellar populations [111].

Table 1.2: Consistency and scale heights of the vertical distributions of Type Ia and CC SNe in edge-on galaxies with sech^2 ($n = 1$) and exp ($n \to \infty$) models.

				$n=1$			$n \to \infty$		
Host (1)	SN (2)	$N_{\rm SN}$ (3)	$\langle\lvert\tilde{z}\rvert\rangle$ (4)	$P_{\rm KS}$ (5)	$P_{\rm AD}$ (6)	$\tilde{z}_0^{\rm SN}$ (7)	$P_{\rm KS}$ (8)	$P_{\rm AD}$ (9)	$\tilde{H}_{\rm SN}$ (10)
S0–Sd	Ia	53	0.058 ± 0.009	0.068	**0.012**	0.089 ± 0.015	0.196	0.165	0.058 ± 0.009
Sa–Sd	Ia	44	0.055 ± 0.009	0.147	**0.031**	0.083 ± 0.012	0.319	0.239	0.055 ± 0.007
Sa–Sd	CC	48	0.028 ± 0.003	0.644	0.209	0.042 ± 0.004	0.648	0.287	0.028 ± 0.003
Sa–Sd†	Ia	28	0.082 ± 0.011	0.983	0.973	0.098 ± 0.014	0.970	0.973	0.062 ± 0.012
Sa–Sd†	CC	28	0.044 ± 0.003	0.459	0.723	0.041 ± 0.006	0.331	0.525	0.024 ± 0.004
Sa–Sbc	Ia	21	0.061 ± 0.014	0.168	0.055	0.094 ± 0.014	0.371	0.151	0.061 ± 0.011
Sa–Sbc	CC	21	0.028 ± 0.004	0.860	0.299	0.040 ± 0.005	0.492	0.239	0.028 ± 0.003
Sc–Sd	Ia	23	0.049 ± 0.011	0.627	0.354	0.073 ± 0.018	0.849	0.919	0.049 ± 0.009
Sc–Sd	CC	27	0.029 ± 0.005	0.493	0.353	0.044 ± 0.007	0.497	0.684	0.029 ± 0.004
Sb–Sc	Ia	30	0.064 ± 0.011	0.476	0.212	0.096 ± 0.016	0.679	0.482	0.065 ± 0.012
Sb–Sc	CC	32	0.028 ± 0.004	0.476	0.203	0.042 ± 0.007	0.586	0.264	0.028 ± 0.003
Sb–Sc†	Ia	21	0.089 ± 0.013	0.853	0.962	0.108 ± 0.021	0.594	0.821	0.070 ± 0.014
Sb–Sc†	CC	19	0.044 ± 0.004	0.908	0.948	0.041 ± 0.008	0.728	0.794	0.024 ± 0.006
Sb–Sc*	Ia	24	0.065 ± 0.014	0.686	0.281	0.097 ± 0.020	0.927	0.657	0.065 ± 0.014
Sb–Sc*	CC	31	0.028 ± 0.004	0.422	0.224	0.042 ± 0.007	0.576	0.335	0.028 ± 0.004

Notes. Columns 1 and 2 give the subsample; Col. 3 is the number of SNe in the subsample; Col. 4 is the mean of normalized absolute vertical distribution with the error of the mean; Cols. 5 and 6 are the $P_{\rm KS}$ and $P_{\rm AD}$ probabilities from one-sample KS and AD tests, respectively, that the vertical distribution of SNe is drawn from the best-fitting sech^2 profile; Col. 7 is the maximum likelihood value of the scale height with bootstrapped error (repeated 10^3 times); Cols. 8, 9, and 10 are, respectively, the same as Cols. 5, 6, and 7, but for the best-fitting exp profile. The subsamples labeled with '†' symbols correspond to SNe with $\lvert\tilde{z}\rvert > 0.02$. The subsamples labeled with '∗' symbols correspond to SNe with distances ≤ 200 Mpc. We calculate the $P_{\rm KS}$ and $P_{\rm AD}$ using the calibrations by [123] and [124], respectively. The statistically significant deviations from the best-fitting profile are highlighted in bold.

Table 1.3: Comparison of the normalized absolute vertical distributions ($|\tilde{z}| \equiv |\mathrm{V}|/R_{25}$) of SNe among different pairs of subsamples.

Subsample 1				Subsample 2				
Host	SN	$N_{\rm SN}$		Host	SN	$N_{\rm SN}$	$P_{\rm KS}$	$P_{\rm AD}$
Sa–Sd	Ia	44	versus	Sa–Sd	CC	48	**0.045**	**0.025**
Sa–Sd†	Ia	28	versus	Sa–Sd†	CC	28	**0.011**	**0.003**
Sa–Sbc	Ia	21	versus	Sa–Sbc	CC	21	**0.041**	**0.037**
Sc–Sd	Ia	23	versus	Sc–Sd	CC	27	0.690	0.310
Sa–Sbc	Ia	21	versus	Sc–Sd	Ia	23	0.387	0.440
Sa–Sbc	CC	21	versus	Sc–Sd	CC	27	0.765	0.802
Sb–Sc	Ia	30	versus	Sb–Sc	CC	32	**0.039**	**0.009**
Sb–Sc†	Ia	21	versus	Sb–Sc†	CC	19	**0.013**	**0.001**
Sb–Sc*	Ia	24	versus	Sb–Sc*	CC	31	0.112	**0.028**

Notes. The subsamples labeled with '†' symbols correspond to SNe with $|\tilde{z}| > 0.02$. The subsamples labeled with '$*$' symbols correspond to SNe with distances ≤ 200 Mpc. The $P_{\rm KS}$ and $P_{\rm AD}$ are the probabilities from two-sample KS and AD tests, respectively, that the two distributions being compared are drawn from the same parent distribution. The $P_{\rm KS}$ and $P_{\rm AD}$ are calculated using the calibrations by [123] and [125], respectively. The statistically significant differences between the distributions are highlighted in bold.

discovery of SNe due to strong dust extinction [126], particularly in edge-on hosts [127].

The vertical distribution of dust in disc galaxies has an exponential profile with about three times smaller scale height in comparison with distribution of all stars ($H_{\rm stars}/H_{\rm dust} \approx 3$, [115]).[7] Analysing the vertical distribution of the resolved stellar populations in nearby edge-on galaxies, [97] found that the dust has negligible impact on the distribution parameters of stars at $|z| \gtrsim H_{\rm dust}$ heights (for the edge-on surface brightness profiles of unresolved populations, see e.g. [115]). Therefore, in Table 1.2, to check the impact of the dust extinction on the obtained scale heights, we also estimate the distribution parameters considering the SNe in Sa–Sd galaxies only at $|\tilde{z}| > \tilde{H}_{\rm dust}$ heights. For the average dust scale height, we use $\tilde{H}_{\rm dust} = 0.02$, roughly considering that $H_{\rm dust} \approx H_{\rm Ia}/3$ (see also [128]). In Fig. 1.5, we show the distribution of coordinates of SNe along the major (U/R_{25}) and minor axes ($\tilde{z} \equiv \mathrm{V}/R_{25}$) of their Sa–Sd host galaxies with the $|\tilde{z}| \leq 0.02$ opaque region, and for the sake of visualization, we scale the distribution to the PGC 037591 galaxy (also shown in Fig. 1.1, better known as NGC 3987), which is one of the representatives of the edge-on galaxies with a prominent dust line along the

[7] This value can vary from two to four, depending, respectively, on early- and late-type morphology of edge-on spiral galaxies [129].

major axis.

From columns 7 and 10 of Table 1.2 (the subsamples of Sa–Sd hosts labeled with '†' symbols), despite the small number statistics (column 3), we see that the extinction by dust near to the plane of host galaxies does not strongly bias the estimated scale heights of SNe. The scale height of CC SNe with $|\tilde{z}| > 0.02$ is almost equal to that with the $|\tilde{z}| \geq 0$, while the scale height of Type Ia SNe with $|\tilde{z}| > 0.02$ is only $\sim 15\%$ greater (still statistically insignificant) than that with the $|\tilde{z}| \geq 0$. In the remainder of this study, we will generally use the scale heights of SNe without height-truncation due to the small number statistics and insignificance of the effect, however, if needed, we will emphasize the impact of the dust extinction on the scale heights.

To check whether the distribution of SN heights follows the best-fitting profiles, we perform one-sample KS and AD tests on the cumulative distribution of the normalized absolute heights ($|\tilde{z}|$), where the sech^2 and exp models have $E(|\tilde{z}|) = \tanh(|\tilde{z}|/\tilde{z}_0^{\rm SN})$ and $E(|\tilde{z}|) = 1 - \exp(-|\tilde{z}|/\tilde{h}_{\rm z}^{\rm SN})$ cumulative distribution functions (CDFs), respectively. Columns 5, 6, 8 and 9 of Table 1.2 show the KS and AD probabilities that the vertical distributions are drawn from the best fitting profile. Cumulative distributions of the heights and CDFs of the fitted forms for Type Ia and CC SNe in Sa–Sd galaxies are presented in the insets of Fig. 1.4.

From columns 5, 6, 8 and 9 of Table 1.2, we see that the vertical distribution is consistent with both profiles in most subsamples of Type Ia SNe and in all subsamples of CC SNe. For Type Ia SNe in Sa–Sd (also in S0–Sd) galaxies, the vertical distribution is consistent with the exp profile, but not with the sech^2 one (as seen in the AD statistic but only very marginally in the KS statistic). When we separate SNe Ia between early- and late-type host galaxies, the inconsistency vanishes with only barely AD test significance in early-type spirals (see the $P_{\rm AD}$ value in column 6 of Table 1.2 for SNe Ia in Sa–Sbc galaxies). The $\langle|\tilde{z}|\rangle$ value (scale heights too) for SNe Ia is $\sim 25\%$ greater in Sa–Sbc galaxies than that in Sc–Sd hosts (although the difference is not significant, see Table 1.3), while for CC SNe this parameter has a nearly constant value in the mentioned subsamples. This effect can be attributed to the earlier and wider morphological distribution of SNe Ia host galaxies (from S0/Sa to Sd, see Table 1.1 and also [102] and [105]) in comparison with CC SNe hosts, and the systematically thinner vertical distribution of the host stellar population from early- to late-type discs [95, 96, 130].

In the first attempts to estimate the mean value of the vertical coordinates of SNe, [131, 132] used the distribution of SN colour excesses without precise information on their spectroscopic types and host galaxy morphology in a sample of non-edge-on spirals. No difference was found in the vertical distributions of Type I and II SNe with indication that both types belong to the young population I. However, the inclinations of host galaxies and the uncertain separation[8] of SN types might be the reason for the similarity between the vertical distributions of the mentioned SN types. Using a similar colour excess data of the best photometrically studied Type Ia SNe in late-type galaxies, [128] showed that these SNe have a considerably broader vertical distribution than the dust discs of their hosts and concluded that SNe Ia are older than the old disc population.

Direct measurements of the heights of SNe and estimation of the scales of their vertical distributions were performed only in a small number of cases [92–94]. [93] examined the offsets between the major axes of a sample of highly inclined ($i \geq 60°$) galaxies and the SNe they hosted in an attempt to measure the scale heights of Type Ia and II SNe. Unfortunately, the sample of such objects was quite small (66 galaxies), especially when restricted to galaxies at $i \geq 75°$, which resulted in statistically indistinguishable vertical distributions (in kpc) between the mentioned types of SNe. [94] used data from the ASC to study the vertical distribution (in kpc) of 64 CC SNe in highly inclined ($i \geq 80°$) Sa–Sd host galaxies. He showed that the distribution can be well fitted by a sech^2 profile. However, these studies only used linear scales to estimate the vertical distribution of SNe. This is somewhat undesirable because the absolute distribution of SN heights (in kpc) is biased by the greatly different intrinsic sizes of host discs (as already shown in Fig. 1.3).

[92] studied the absolute (in kpc) and relative (normalized to radius of host galaxy) vertical distributions of SNe using a sample of 26 Type Ia, 8 Ibc, and 44 II SNe in spiral host galaxies with $i \geq 85°$. They found that the distributions can be fitted by exp profiles with scale heights $\tilde{H}_{\rm Ia} = 0.030 \pm 0.006$, $\tilde{H}_{\rm Ibc} = 0.024 \pm 0.006$, and $\tilde{H}_{\rm II} = 0.029 \pm 0.005$. The scale heights for

[8] Type Ibc SNe were labelled as 'I pec' types during observations before 1986 and included in the sample of Type I SNe.

Type Ibc and II SNe are in good agreement with our $\tilde{H}_{\rm CC} = 0.028 \pm 0.003$ in Sa–Sd galaxies, while their scale height for Type Ia SNe is much smaller than our $\tilde{H}_{\rm Ia} = 0.055 \pm 0.007$ in the same morphological bin. However, the direct comparison of the scale heights obtained by [92] with ours is difficult because they used the Digital Sky Survey images for reduction of SNe host galaxies without mentioning the photometric band (we assume that they used B-band), while we use the SDSS g-band to normalize the heights to the 25$^{\rm th}$ magnitude isophotal semimajor axes of host galaxies. On the other hand, we are not able to check the consistency between the morphological distributions of edge-on galaxies hosting Type Ia and CC SNe in their and our samples because morphological types were not provided by [92].

To exclude any dependence of scale height of host stellar population on the morphological type, we analyse the vertical distribution of SNe in the most populated morphological bins, i.e., in the narrower Sb–Sc subsample (see Table 1.1).[9] In addition, the Sb–Sc subsample is more suitable for comparison of the estimated vertical scale heights of SNe with those of different stellar populations of thick and thin discs of the MW galaxy (see Section 1.4.2), and to exclude a small number of very thin discs [133], which usually appear in late-type galaxies.

From Table 1.2, we conclude that the vertical distributions of Type Ia and CC SNe in Sb–Sc galaxies can be well fitted by both the sech^2 and exp profiles. The vertical distribution of CC SNe is significantly different from that of Type Ia SNe (Table 1.3), being 2.3 ± 0.5 times more concentrated to the plane of the host disc (Table 1.2). This difference also exists when the above-mentioned effect of the dust extinction is considered for the particular subsample (Sb–Sc hosts labeled with '†' symbols in Tables 1.2 and 1.3). In Fig. 1.6, we present the comparison of vertical distributions as well as the fitted sech^2 and exp CDFs between both the types of SNe in Sb–Sc host galaxies.

It is important to note that Type Ia SNe, because of their comparatively high luminosity (in about two absolute magnitudes in B-band [134]) and the presence of dedicated surveys, are discovered at much greater distances than CC SNe [102]. To check the possible distance

[9] On the other hand, by selecting these bins we reduce the possible contribution by SNe Ia from central bulges of host galaxies, although the bulge contribution is only up to 9% of the total SN Ia population in Sa–Sd host galaxies [135].

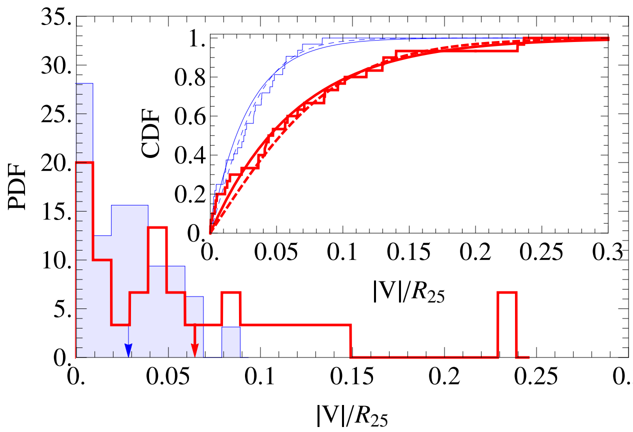

Figure 1.6: Vertical distributions of Type Ia (red thick line) and CC (blue thin line) SNe in Sb–Sc galaxies. The inset presents the cumulative distributions of SNe and fitted sech^2 (dashed curve) and exp (solid curve) CDFs. The mean values of the distributions are shown by arrows.

biasing on the vertical distribution of SNe, we truncate the sample of Sb–Sc galaxies to distances ≤ 200 Mpc.[10] In Table 1.2, the comparison of $\langle|\tilde{z}|\rangle$, $\tilde{z}_0^{\rm SN}$, and $\tilde{H}_{\rm SN}$ as well as $P_{\rm KS}$ and $P_{\rm AD}$ values of distance-truncated sample (labeled with '$*$' symbols) with those of Sb–Sc host galaxies allows to conclude that possible distance biasing in our sample is negligible. Due to the smaller number statistics, we get larger error bars in Table 1.2, and lose only the KS test significance in Table 1.3. Therefore, in the remainder of this Chapter, we will use SNe in Sb–Sc galaxies without distance-truncation.

1.4.2 The thick and thin discs

It is largely accepted that the disc of the MW, one of the well-studied representatives of Sb–Sc classes, is separated into at least three components/populations: (1) the youngest star-forming disc ($\tilde{H} \lesssim 0.01$), including molecular clouds and massive young stars; (2) the younger thin disc ($\tilde{H} \sim 0.02$), which contains stars with a wide range of ages; and (3) the old thick disc ($\tilde{H} \sim 0.06$), composed almost exclusively of older stars [98–100, 136–142]. For extragalactic discs of nearby edge-on spirals, the thick and thin components are also resolved [96, 97]. In this

[10] It would be more effective to check this with distance-truncation at 150 (100) Mpc (see [105] and [84]), however the remaining statistics in this case is very low, which destroys any comparison with significance. With the mentioned distance-truncation, we have only 19 (9) Type Ia SNe with $\langle|\tilde{z}|\rangle = 0.071 \pm 0.019$ (0.086 ± 0.025) and 30 (24) CC SNe with $\langle|\tilde{z}|\rangle = 0.027 \pm 0.005$ (0.031 ± 0.006).

Table 1.4: Comparison of the $\tilde{H}_{\rm SN}$ values of Type Ia and CC SNe in edge-on Sb–Sc galaxies with those of the MW thick and thin discs.

Host	$\tilde{H}$	Reference
MW thin disc	0.020 ± 0.005	[100]
MW thin disc	0.022 ± 0.003	[98]
MW thin disc	0.022 ± 0.005	[99]
SNe CC (Sb–Sc)	**0.028 ± 0.003**	**This study**
MW thick disc	0.050 ± 0.005	[98]
MW thick disc	0.051 ± 0.005	[137]
MW thick disc	0.057 ± 0.014	[140]
MW thick disc	0.058 ± 0.005	[99]
MW thick disc	0.060 ± 0.013	[100]
MW thick disc	0.061 ± 0.020	[139]
SNe Ia (Sb–Sc)	**0.065 ± 0.012**	**This study**
MW thick disc	0.067 ± 0.008	[138]

Notes. The MW $\tilde{H}$ values are calculated using the original values of H from the references and assuming $R_{25}^{\rm MW} = 15 \pm 1$ kpc. The $\tilde{H}$ values are listed in ascending order.

sense, we may be able to put constraints on the nature of the progenitors of Type Ia and CC SNe by comparing the parameters of their distributions ($\tilde{H}_{\rm SN}$ or $\tilde{z}_0^{\rm SN}$ and $h_{\rm SN}/z_0^{\rm SN}$ or $h_{\rm SN}/H_{\rm SN}$) in edge-on Sb–Sc galaxies with those of different stellar populations of thick and thin discs of MW and other similar galaxies. Note that the mean luminosity of our sample of Sb–Sc host galaxies ($\langle M_{\rm g} \rangle = -20.5 \pm 1.0$) is in good agreement with that of the MW ($\langle M_{\rm g}^{\rm MW} \rangle = -21.0 \pm 0.5$, [143]).

In Table 1.4, we list the exp scale heights of SNe estimated in this study and the exp scale heights of the MW thick and thin discs derived from star counts (from hundreds of thousands to millions of individual stars) by other authors. As can be seen, the scale height of the vertical distribution of CC SNe is consistent with those of younger stellar population in the thin disc (a wide range of ages up to a few Gyr, [144]), while the scale height of Type Ia SNe is consistent with those of old population in the thick disc (from a few Gyr up to ~ 10 Gyr, [144]) of the MW galaxy.

Note that, in Table 1.4, the MW $\tilde{H}$ values are calculated using the original values of H (in kpc) from the references and assuming $R_{25}^{\rm MW} = 15 \pm 1$ kpc, i.e., $\tilde{H} = H/R_{25}^{\rm MW}$, while the ratio of radial to vertical scales (h/H) would be better for a comparison of SNe distribution with the distribution of stars in the MW, avoiding the use of ambiguous value of $R_{25}^{\rm MW}$.

Table 1.5: Comparison of the length/height ratios of Type Ia and CC SNe in Sb–Sc galaxies with those of the MW stars in the thick and thin discs.

Host	h/H	Reference
SNe Ia (Sb–Sc)	$\mathbf{3.08 \pm 0.65}$	**This study**
MW thick disc	3.30 ± 1.97	[139]
MW thick disc	3.68 ± 1.08	[137]
MW thick disc	4.00 ± 1.13	[100]
MW thick disc	4.30 ± 1.29	[140]
MW thick disc	4.50 ± 0.46	[138]
MW thick disc	5.41 ± 0.41	[99]
MW thin disc	6.82 ± 3.03	[98]
SNe CC (Sb–Sc)	$\mathbf{7.14 \pm 1.05}$	**This study**
MW thin disc	8.67 ± 2.45	[100]
MW thin disc	10.86 ± 2.70	[99]

Notes. For both the types of SNe, we use $\tilde{h}_{\rm SN} = 0.20 \pm 0.02$ [84]. The h/H values are listed in ascending order.

[84] studied the radial distributions of SNe and estimated the scale lengths of Type Ia and CC SNe using a well-defined sample of 500 nearby SNe and their low-inclined ($i \leq 60°$) and morphologically non-disturbed S0–Sm host galaxies from the SDSS.[11] In particular, the radial distributions of Type Ia and CC SNe in spiral galaxies are consistent with one another and with an exponential surface density according to $\exp(-\tilde{r}/\tilde{h}_{\rm SN})$ in equation (1.3) where $\tilde{r} = R_{\rm SN}/R_{25}$ and $\tilde{h}_{\rm SN} = h_{\rm SN}/R_{25} = 0.21 \pm 0.02$. However, to be consistent with the present study, we use the estimation of the scale lengths of SNe restricted to Sb–Sc host galaxies from that sample. Note that the similar determination of the sample of the present paper is not possible because of its extreme inclination. For both types of SNe, we find $\tilde{h}_{\rm SN} = 0.20 \pm 0.02$ using 79 Type Ia and 198 CC SNe.

In Table 1.5, we list the ratios of radial to vertical scales of SNe ($h_{\rm SN}/H_{\rm SN}$) estimated in this study and the analogous ratios of MW thick and thin discs derived from star counts by other authors. The ratio of scales of CC SNe appears consistent with those of the younger stellar population in the thin disc, while the corresponding ratio of Type Ia SNe is consistent with the old population in the thick disc of the MW (although on the small side).

[11] At these inclinations, dust extinction has minimal impact on the efficiency of SNe discovery [126], making the estimation of the scale lengths as the most reliable.

Table 1.6: Comparison of the length to sech^2 height ratios of Type Ia and CC SNe in Sb–Sc galaxies with those detected from resolved stars in nearby edge-on galaxies and from unresolved populations of extragalactic thick and thin discs.

Host	h/z_0	Reference
Edge-on Sc galaxies^a (RGB-box)	1.83 ± 0.99	[97]
SNe Ia (Sb–Sc)	$\mathbf{2.08 \pm 0.40}$	**This study**
Edge-on Sc galaxies^a (AGB-box)	2.40 ± 1.30	[97]
Edge-on galaxies^b (thick+thin disc)	2.67 ± 0.86	[95]
Edge-on Sd galaxies^c (thick disc)	2.87 ± 0.72	[96]
Edge-on Sc galaxies^a (MS-box)	3.83 ± 1.79	[97]
SNe CC (Sb–Sc)	$\mathbf{4.76 \pm 0.93}$	**This study**
Edge-on Sd galaxies^c (thin disc)	5.48 ± 1.15	[96]

Notes. For both the types of SNe, we use $\tilde{h}_{\rm SN} = 0.20 \pm 0.02$ [84]. The h/z_0 values are listed in ascending order.
^{a}The mean ratio of all six galaxies with the additional components of NGC 55 and NGC 4631 (from table 4 in [97]). These galaxies have lower masses than the MW.
^{b}To be consistent with the present study and the mentioned references, the mean ratio in g-band is estimated for a subsample of 529 galaxies from table 4 in [95] with bulge-to-total luminosity ratio (B/T) in r-band between 0.2 to 0.4 and distances ≤ 200 Mpc (a few galaxies, with obviously incorrect B/T values, are removed). The mean luminosity of this subsample ($\langle M_{\rm g} \rangle = -20.9 \pm 0.7$, corrected for Galactic extinction) is in good agreement with that of our Sb–Sc host galaxies ($\langle M_{\rm g} \rangle = -20.5 \pm 1.0$).
^{c}The mean ratio of all 34 galaxies in R-band from table 4 in [96]. These galaxies have lower kinematic masses than the MW.

It should be noted that the parameters of the vertical distributions of different stellar populations in the MW are determined using samples dominated by stars relatively near the Sun, not including the sizable population of the disc (see the discussion in [145]). Therefore, the structural parameters of the MW may be different from those of other galaxies. In particular, [97] analysed the vertical distribution of the resolved stellar populations in nearby six edge-on Sc galaxies observed with the Hubble Space Telescope and found that the ratios of radial to vertical scales of young star-forming discs are much smaller ($\sim$ 3-4 times) than that of the MW. In other words, the young star-forming discs of their sample galaxies are much thicker in comparison with that of the MW. Their results are in agreement with those of [96], who analysed the vertical structure of 34 late-type, edge-on, undisturbed disc galaxies using the two-dimensional fitting to their photometric profiles.

Interestingly, [97] found that the scale height of a stellar population increases with age, which is also correct for the MW galaxy [141, 145]. They used colour-magnitude diagrams to estimate the ages of resolved stellar populations (see figs. 1 and 4 in [97]). The young population in their MS box of the colour-magnitude diagram is dominated by stars with ages from ~ 10 Myr up to ~ 100 Myr, the intermediate population in the asymptotic giant branch (AGB) box is dominated by stars with ages from a few 100 Myr up to a few Gyr, while the old population in the red giant branch (RGB) box is dominated by stars with ages from a few Gyr up to ~ 10 Gyr. In light of this, we compare in Table 1.6 the ratios of radial to vertical scales of SNe with those detected from resolved stars in nearby edge-on late-type galaxies [97] and from unresolved populations of extragalactic thick and thin discs estimated using the edge-on surface brightness profiles [95, 96].[12]

In Table 1.6, we see that the ratio of scales of the distribution of CC SNe is consistent with those of the resolved MS-box stars in [97] and unresolved stellar population of the thin disc in [96]. On the other hand, the $h_{\rm SN}/z_0^{\rm SN}$ ratio of Type Ia SNe is consistent and located between the values of the same ratios of resolved RGB- and AGB-box stars, respectively [97]. In addition, the $h_{\rm SN}/z_0^{\rm SN}$ ratio of Type Ia SNe is consistent with those of the unresolved population of the thick disc in [96] and with the thick+thin disc population in [95].

These results are in good agreement with the age-scale height relation of stars in galaxy discs [97, 145], and that Type Ia SNe result from stars of different ages (from ~ 0.5 Gyr up to ~ 10 Gyr, see [146]), with even the shortest lifetime progenitors having much longer lifetime than the progenitors of CC SNe (from a few Myr up to ~ 0.2 Gyr, see [147]).

1.5 Chapter Conclusions

Using a well-defined and homogeneous sample of SNe and their edge-on host galaxies from the coverage of SDSS DR12, we analyse the vertical distributions and estimate the sech^2 and exp scale heights of the different types of SNe, associating them to the thick or thin disc populations of galaxies. Our sample consists of 100 nearby (the mean distance is 100 ± 8 Mpc), high-inclination ($i \geq 85^\circ$), and morphologically non-disturbed S0–Sd galaxies, hosting 102 SNe in total.

[12]Here, to be consistent with the original values from the references, we use the $h_{\rm SN}/z_0^{\rm SN}$ ratios.

The extinction by dust near to the plane of edge-on host galaxies has an insignificant impact on our estimated SN scale heights, although as was shown previously [102], it is significantly decreasing the efficiency of SN discovery in these galaxies. We also check that there is no strong redshift bias within our SNe and host galaxies samples, which could drive the observed behaviours of the vertical distributions of the both SN types in host galaxies with edge-on discs.

The results obtained in this Chapter are summarized below, along with their interpretations.

For the first time, we show that in both early- and late-type edge-on spiral galaxies the vertical distribution of CC SNe is about twice more concentrated to the plane of host disc than the distribution of Type Ia SNe (Fig. 1.4 and Table 1.2). The difference between the distributions of the SN types is statistically significant with only the exception in late-type hosts (Table 1.3).

When considering early- and late-type spiral galaxies separately, the vertical distributions of Type Ia and CC SNe are consistent with both the sech^2 and exp profiles (Table 1.2). In wider morphological bins (S0–Sd or Sa–Sd), the vertical distribution of Type Ia SNe is not consistent with sech^2 profile, most probably due to the earlier and wider morphological distribution of SNe Ia host galaxies in comparison with CC SNe hosts (Table 1.1), and the systematically thinner vertical distribution of the host stellar population from early- to late-type discs.

By narrowing the host morphologies to the most populated Sb–Sc galaxies (close to the MW morphology) of our sample, we exclude the morphological biasing of host galaxies between the SN types and the dependence of scale height of host stellar population on the morphological type. In these galaxies, we find that the sech^2 scale heights ($\tilde{z}_0^{\mathrm{SN}}$) of Type Ia and CC SNe are 0.096 ± 0.016 and 0.042 ± 0.007, respectively. The exp scale heights ($\tilde{H}_{\mathrm{SN}}$) are 0.065 ± 0.012 and 0.028 ± 0.003, respectively. In Sb–Sc galaxies, the vertical distribution of CC SNe is significantly different from that of Type Ia SNe (Table 1.3), being 2.3 ± 0.5 times more concentrated to the plane of the host disc (Table 1.2).

In Sb–Sc hosts, the exp scale height (also the $h_{\mathrm{SN}}/H_{\mathrm{SN}}$ ratio) of CC SNe is consistent with that of the younger stellar population in the thin disc of the MW, derived from star counts, while the scale height (also the ratio) of SNe Ia is consistent with that of the old population in the thick disc of the MW (Tables 1.4 and 1.5).

For the first time, we show that the ratio of scale lengths to scale heights ($h_{\rm SN}/z_0^{\rm SN}$) of the distribution of CC SNe is consistent with those of the resolved young stars with ages from ~ 10 Myr up to ~ 100 Myr in nearby edge-on galaxies and the unresolved stellar population of extragalactic thin discs (Table 1.6). On the other hand, the corresponding ratio for Type Ia SNe is consistent and located between the values of the same ratios of the two populations of resolved stars with ages from a few 100 Myr up to a few Gyr and from a few Gyr up to ~ 10 Gyr, as well as with the unresolved population of the thick disc of nearby edge-on galaxies.

All these results can be explained considering the age-scale height relation of the distribution of stellar population and the mean age difference between Type Ia and CC SNe progenitors.

Chapter 2

Constraining Type Ia SNe through their heights in edge-on galaxies

2.1 Introduction

In Chapter 1, taking into account that the height from the disc plane is an indicator of stellar population age [96, 97, 148], we showed that the majority of SNe Ia are localized in the discs of edge-on galaxies and they have about two times larger scale height than CC SNe, whose progenitors' ages are up to $\sim$100 Myr. Also, we showed that the scale height of SNe Ia is compatible with that of the older MW thick disc. Nevertheless, we did not investigate different SN Ia subclasses separately. However, many studies demonstrated that the progenitor population age of SN Ia subclasses is increasing in the sequence of 91T-, normal, and 91bg-like events [48, 67]. Therefore, in this Chapter, for the first time, we attempt to accomplish this by studying the heights distributions of the SN Ia subclasses from the host discs.

In [149], we verified an earlier finding on the correlation between LC decline rates of SNe Ia and the global ages of their host galaxies: SNe Ia from older and younger stellar populations, respectively, have larger and smaller Δm_{15} values. This result can be interpreted within the frameworks of the sub-M_{Ch} WD explosion models. As mentioned in the Introduction, for this explosion model, it should follow that the LC decline rate Δm_{15} of SN Ia is correlated with the age of the SN progenitor system [58, 63]. Given this, in this Chapter we simply check the potential correlation between the SN Ia heights from host discs and their LC decline rates, which may provide an indication that both parameters are appropriate stellar population age indicators.

2.2 Sample selection and reduction

For this Chapter, to ensure a sufficient number of SNe and to appropriately measure the SN heights from their host galactic discs, we selected the spectroscopically classified SN Ia subclasses (normal, 91T- and 91bg-like) with distances ≤ 200 Mpc from the Open Supernova Catalog [150]. In order to have high confidence on the SN subclasses, the information is additionally verified utilizing data from the Weizmann Interactive Supernova data REPository [151], Astronomer's Telegram, website of the Central Bureau for Astronomical Telegrams, etc.[1]

Since we are interested in SNe Ia that exploded in highly inclined spiral galaxies, we need to roughly classify the morphology and estimate the inclination of hosts. To perform this we employed the SDSS DR16 [152], the SkyMapper DR2 [153], and the Panoramic Survey Telescope and Rapid Response System (Pan-STARRS) DR2 [154], which together cover the whole sky and provide the gri bands composed images for each host galaxy. Hosts with visible low inclinations ($i \lesssim 60^{\circ}$) and obviously elliptical, lenticular, or irregular morphology were excluded from the study. Following [149], we further morphologically classified the hosts and created the 25 mag arcsec^{-2} elliptical apertures for each galaxy on the surveys' g-band images enabling exact measurements of the SN hosts' inclinations, semi-major (R_{25}) and semi-minor (Z_{25}) axes.

The next step was to use the estimated elongations (R_{25}/Z_{25}) and morphological types of galaxies to calculate inclinations, following the approach of [106]. It is worth noting that the calculated inclinations for galaxies with prominent bulges are inaccurate, as the isophotes of bulges in highly inclined galaxies reduce the real galaxy disc inclinations. Such scenarios got

[1] The sources provide also the equatorial coordinates of the selected SNe Ia.

Table 2.1: Broadly binned morphological distribution of SN Ia subclasses in edge-on spiral host galaxies.

SN	S0/a–Sab	Sb–Sc	Scd–Sdm	All
Normal	46	81	17	144
91T	5	18	7	30
91bg	13	10	0	23
All	67	108	22	197

special attention for exact inclination calculation, with only the isophotes of discs being taken into account [85]. Finally, we limited the sample of host galaxies to those with an inclination of $80^\circ \leq i \leq 90^\circ$. As a result, we sampled 196 S0/a–Sdm galaxies with a nearly edge-on view, where a total of 197 SNe Ia were discovered (Table 2.1).

It is important to test the representativeness of our edge-on SN host sample compared to a sample of galaxies arbitrarily aligned along line-of-sight. Using the two-sample KS and AD tests, we compared the distributions of the sampled SN Ia subclasses and the morphological types of their hosts with the same distributions of nearly complete volume-limited (≤ 80 Mpc) sample of the Lick Observatory Supernova Search (LOSS; [28]). In our and LOSS samples, the representations of SN Ia subclasses are not statistically different (the probabilities that the distributions are drawn from the same parent sample are > 0.6). The frequencies of morphologies in our and LOSS samples are also consistent between each other (probabilities are > 0.1). Therefore, any artificial loss or excess of SN subclasses and/or host's morphologies should be not significant in our sample.

We used the methods described in our earlier study on edge-on SN hosts [85] to determine the height (V) of a SN from the plane of its host disc (i.e. the vertical distance of a SN from the major axis of host), as well as the projected radius (U) along the plane. The g-band images were used for these measurements. The values of U and V are given in arcsec units. In this study, we used the R_{25} normalization (in arcsec) to bring the galaxies to relatively the same size (normalized height is V/R_{25}, normalized projected radius is U/R_{25}). For more details on the measurement techniques, the reader is referred to [84, 85]. We also applied Z_{25} normalization to the V parameter (V/Z_{25}).

Recall that the galaxies in our sample have an inclination of $80° - 90°$, which can introduce discrepancies in (projected) height measurements when compared to physical heights in the same galaxies with inclination of $90°$. To check the impact of this effect, using a Monte Carlo (MC) simulation, we generated 1000 SN heights in $i = 90°$ disc adopting a generalized vertical distribution ($f(\tilde{z}) = \text{sech}^2(\tilde{z}/\tilde{z}_0)$, where $\tilde{z} = V/R_{25}$) and its scale heights for SNe Ia in spiral galaxies ($\tilde{z}_0 = 0.083$; [85]). Then, we randomly assigned an inclination within $80° - 90°$ to the disc for each SN and estimated the projected SN height from the major axis of the host. Eventually, the comparison of the generated and projected heights showed that the differences between them is not significant ($P_{\text{KS}} = 0.130$, $P_{\text{AD}} = 0.200$). Thus, the mentioned effect has a minor impact on the real height measurements, which accounts, on average, for about 10% of the measured value (± 0.01 in absolute units, typically within the range of measurement errors).

Because we aim to investigate the possible relationships between photometric features like Δm_{15} and the heights of SNe Ia from the disc, following [149], we conducted a thorough literature search to assemble the B-band LC decline rates for our 197 SNe. Only 69 of the SNe Ia in our sample have available Δm_{15} values.

The database of 197 individual SNe Ia (SN designation, U and V, spectroscopic subclass and Δm_{15} with their sources) and their 196 hosts (galaxy designation, distance, morphological type, R_{25}, and Z_{25}) is available online [155].

2.3 Results and discussion

2.3.1 Directional distributions of SNe Ia in edge-on spiral hosts

Following [156], for the SNe Ia in edge-on spirals of the current study, we perform the two-sample KS and AD tests comparing the $|V|/R_{25}$ and $|U|/R_{25}$ distributions between each other. Table 2.2 shows that the bulk of SNe Ia in all of the SN subclasses are localized in the host galaxies' discs. For 91bg-like SNe only, the AD test shows barely significance, unlike the KS test, which is probably due to the statistics with the smallest sample size.

We then compare the projected and normalized radii $|U|/R_{25}$ and the heights $|V|/R_{25}$ be-

Table 2.2: Comparison of the positional distributions of the SN Ia subclasses along major U and minor V axes.

SN	$N_{\rm SN}$	$\langle\lvert U\rvert/R_{25}\rangle$	versus	$\langle\lvert V\rvert/R_{25}\rangle$	$P_{\rm KS}^{\rm MC}$	$P_{\rm AD}^{\rm MC}$
Normal	144	$0.28^{+0.05}_{-0.04}$	versus	$0.07^{+0.01}_{-0.01}$	**<0.001**	**<0.001**
91T	30	$0.25^{+0.12}_{-0.07}$	versus	$0.05^{+0.03}_{-0.02}$	**<0.001**	**<0.001**
91bg	23	$0.25^{+0.15}_{-0.08}$	versus	$0.14^{+0.08}_{-0.04}$	**0.022**	0.145
All	197	$0.27^{+0.04}_{-0.03}$	versus	$0.07^{+0.01}_{-0.01}$	**<0.001**	**<0.001**

Notes. The $P_{\rm KS}$ and $P_{\rm AD}$ probabilities that the distributions are drawn from the same parent sample are calculated using a MC simulation with 10^5 iterations. Each subsample's mean values with their 95% confidence intervals (CIs) are presented. The P-values are bolded when differences between the distributions are statistically significant ($P \leq 0.05$).

Table 2.3: Comparison of the $\lvert U\rvert/R_{25}$ and $\lvert V\rvert/R_{25}$ distributions between different subclasses of SNe Ia.

Subsample 1	$N_{\rm SN}$	versus	Subsample 2	$N_{\rm SN}$	$P_{\rm KS}^{\rm MC}$	$P_{\rm AD}^{\rm MC}$
$\lvert U\rvert/R_{25}$ of Normal	144	versus	$\lvert U\rvert/R_{25}$ of 91bg	23	0.279	0.166
$\lvert U\rvert/R_{25}$ of Normal	144	versus	$\lvert U\rvert/R_{25}$ of 91T	30	0.828	0.835
$\lvert U\rvert/R_{25}$ of 91bg	23	versus	$\lvert U\rvert/R_{25}$ of 91T	30	0.756	0.611
$\lvert V\rvert/R_{25}$ of Normal	144	versus	$\lvert V\rvert/R_{25}$ of 91bg	23	0.079	**0.010**
$\lvert V\rvert/R_{25}$ of Normal	144	versus	$\lvert V\rvert/R_{25}$ of 91T	30	0.685	0.588
$\lvert V\rvert/R_{25}$ of 91bg	23	versus	$\lvert V\rvert/R_{25}$ of 91T	30	**0.033**	**0.022**

Notes. The explanations for the P-values are identical to those in Table 2.2.

tween different SN Ia subclasses. In Table 2.3, the KS and AD tests show that the radial distributions of normal, 91T- and 91bg-like SNe are consistent with one another. In addition, the height distributions of normal and 91T-like SNe are consistent between each other. At the same time, the height distributions of 91T- and 91bg-like SNe are significantly different. The same is happens for the distributions of normal and 91bg-like SNe (with barely KS test significance). Fig. 2.1 shows a scatterplot of $\lvert V\rvert/R_{25}$ versus $\lvert U\rvert/R_{25}$, and the cumulative distributions of $\lvert V\rvert/R_{25}$ values for different SN Ia subclasses. The 91T-like SNe have the smallest height distributions, closest to the disc plane, whereas the 91bg-like SNe have the highest distribution (see also the $\langle\lvert V\rvert/R_{25}\rangle$ values in Table 2.2). Normal SNe Ia have a height distribution that is somewhat between those of the two others, but closer to 91T-like events.

The results, in Table 2.2, are in agreement with those of [84,85,156]. As already stated, the disc, rather than the spherical component, is where the majority of normal, 91T- and 91bg-like SNe Ia in spiral galaxies arise. In particular, [71] showed that SN Ia progenitor age distribution

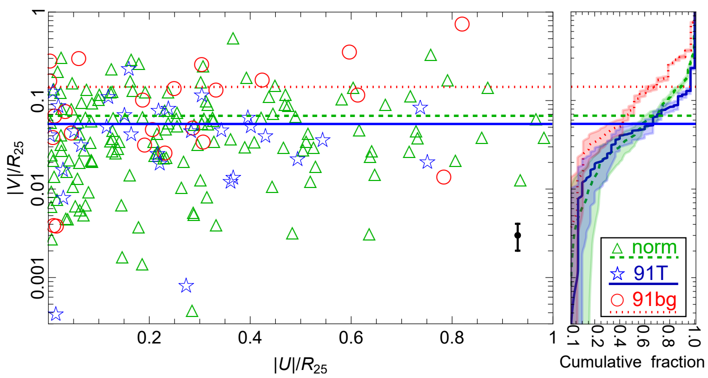

Figure 2.1: Left panel: distributions of $|V|/R_{25}$ versus $|U|/R_{25}$ for normal, 91T-, and 91bg-like SNe. The error bar on the right side of the panel shows the characteristic error in the height estimation due to possible inclination floating in $80° - 90°$. The lines show the mean $|V|/R_{25}$ values for each SN Ia subclass. Right panel: the heights' cumulative distributions for different SNe Ia. The light coloured regions around each curve represent the appropriate spreads considering the uncertainties in height measurements.

Table 2.4: Comparison of the $|V|/Z_{25}$ distributions between different subclasses of SNe Ia.

Subsample 1	$N_{\rm SN}$	versus	Subsample 2	$N_{\rm SN}$	$P_{\rm KS}^{\rm MC}$	$P_{\rm AD}^{\rm MC}$
Normal	144	versus	91bg	23	0.112	**0.005**
Normal	144	versus	91T	30	0.311	0.307
91bg	23	versus	91T	30	**0.042**	**0.048**

Notes. The explanations for the P-values are identical to those in Table 2.2.

in spirals peaks up to several hundred Myr (< 1 Gyr) and has a long tail up to ~ 10 Gyr, implying that the bulk of progenitors come from young/intermediate stellar component [146], which is mostly found in discs [157]. Although the old stars (> 1 Gyr) are distributed in both disc and spherical components of spiral galaxies, most of the old progenitors of SNe Ia also distributed in discs, as evidenced by the behaviour of the bulge to disc (B/D) flux ratio [158] or mass ratio [157]. For example, the B/D flux ratio in the K-band, which is a tracer of the old population, decreases passing from early- to late-type spirals [158]: the average B/D flux ratios are ~ 0.33 and ~ 0.07 for S0/a–Sbc and Sc–Sdm galaxies, respectively.

Now let us look at the results in Table 2.3. Recall that we only use edge-on host galaxies, therefore it is practically impossible to correct the discs for the inclination effect and properly study the de-projected radial distributions of SNe. This could explain why the projected radial distributions of normal, 91bg, and 91T-like SNe are all consistent (see Table 2.3), although it is known that the ages and other parameters of various stellar populations in spiral galaxies demonstrate radial dependency [159].

Table 2.3 also shows, statistically, that 91T- and 91bg-like SNe Ia are distributed differently toward the plane of their host disc. The mean heights are growing, starting with 91T-like events and progressing through normal and 91bg-like SNe (Table 2.2). On the other hand, it is well-known that spiral galaxies have a vertical stellar age gradient, with the age increasing as the vertical distance from the disc plane increases [96, 97, 148]. Therefore, from the perspective of the vertical distribution (an age tracer) it may be deduced that the progenitors of 91T-like and normal SNe Ia are relatively younger than those of 91bg-like events. At least the age differences should be significant for 91T- versus 91bg-like SNe (Table 2.3, Fig. 2.1). The results are unaffected when the Z_{25} normalization is applied (Table 2.4). We emphasize that the current study is the first to demonstrate the observational differences in the heights of the SN Ia subclasses.

In fact, more luminous 91T-like SNe could be found more easily at the brighter host galaxy background than less luminous 91bg-like events. This would mean that 91T-like SNe could be observed closer to the disc than 91bg-likes. If so, the observed effect would be a selection bias. However, it is crucial to note that 91T-like SNe are not as frequently detected at higher heights as 91bg-likes (see Fig. 2.1). More luminous 91T-like SNe would undoubtedly be found if they had exploded at the higher heights from the disc. Hence, it is likely that the detection of 91T-like SNe at lower heights as opposed to 91bg-likes is a real effect rather than the product of the mentioned selection bias. This is further supported by the observation that 91T-like SNe are mostly associated with star-forming environments [149, 160, 161] than 91bg-like SNe, which are more frequently seen in older environments [162]. On the other hand, the star-forming environment has the lowest height in the galactic disc [100].

2.3.2 Constraining the age of SN Ia progenitors

It is noteworthy that along with the qualitative age constraints of SN Ia progenitors we can add also quantitative ones. Table 2.5 compares the scale heights of SN Ia subclasses in our

Table 2.5: Comparison of exponential scale heights of SN Ia subclasses with those of CC SNe, and thick and thin discs of edge-on galaxies.

Disc	N	$\widetilde{H}$	Reference
Early-type galaxies			
S0/a–Sc thin disc	122	$0.02^{+0.01}_{-0.01}$	[163]
S0/a–Sab thin disc	38	$0.04^{+0.02}_{-0.01}$	[163]
Normal (S0/a–Sab)	46	$\mathbf{0.07^{+0.03}_{-0.02}}$	**This study**
S0/a–Sc thick disc	122	$0.11^{+0.02}_{-0.02}$	[163]
91bg (S0/a–Sc)	23	$\mathbf{0.14^{+0.08}_{-0.04}}$	**This study**
91bg (S0/a–Sab)	13	$\mathbf{0.16^{+0.15}_{-0.06}}$	**This study**
S0/a–Sab thick disc	38	$0.17^{+0.07}_{-0.04}$	[163]
Late-type galaxies			
MW thin disc	–	0.02 ± 0.01	[100]
Sb–Sc thin disc	84	$0.02^{+0.01}_{-0.01}$	[163]
CC SNe	27	$0.03^{+0.02}_{-0.01}$	[85]
91T (Sb–Sdm)	25	$\mathbf{0.04^{+0.02}_{-0.01}}$	**This study**
Normal (Scd–Sdm)	17	$\mathbf{0.05^{+0.04}_{-0.02}}$	**This study**
MW thick disc	–	0.06 ± 0.01	[100]
Normal (Sb–Sc)	81	$\mathbf{0.07^{+0.02}_{-0.01}}$	**This study**
Scd–Sd thick disc	19	$0.08^{+0.06}_{-0.03}$	[163]
Sb–Sc thick disc	84	$0.08^{+0.02}_{-0.02}$	[163]
91bg (Sb–Sc)	10	$\mathbf{0.12^{+0.13}_{-0.05}}$	**This study**

Notes. $\widetilde{H}_{\rm SN} = \langle |V|/R_{25} \rangle$. Morphological classification of galaxies from [163] is available via the HyperLeda and/or NED. The $\widetilde{H}$ values are displayed in ascending order.

sample with the exponential scale heights of the MW thin and thick discs, as well as with those of 141 edge-on S0/a–Sd galaxies from [163], sampled according to the different morphological groups. The scale height of CC SNe in late-type host galaxies is also shown from our previous paper [85]. Here an exponential vertical distribution $\exp(-|\tilde{z}|/\widetilde{H})$ is used, where the scale height $\widetilde{H}$ is normalized to the galaxy R_{25} radius. The scale height of SNe $\widetilde{H}_{\rm SN} = \langle |V|/R_{25} \rangle$ for an exponential vertical distribution (see [85], for more details). Because the scale height of a stellar population depends on the morphological type of galaxies, being larger in early-types [95, 96], we split the sample into early- and late-type hosts in Table 2.5 to accurately compare different scales. Note that in spiral galaxies the majority of 91T-like events are found in Sb–Sdm (late-type) morphological bin, while most of normal SNe Ia and 91bg-like events are distributed in S0/a–Sc (early-type) bin (Table 2.1, see also [149]).

As shown in Table 2.5, in early-type spirals, the scale height of normal SNe Ia is found

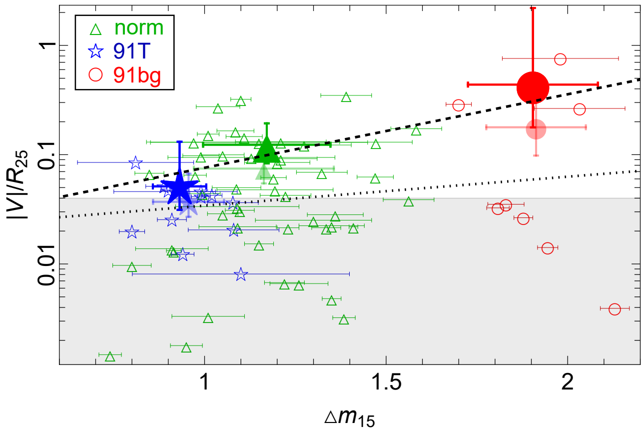

Figure 2.2: Distributions of $|V|/R_{25}$ versus Δm_{15} for different SN Ia subclasses. The dotted and dashed lines, which encompass all SN Ia subclasses, present the best-fitting lines for entire and dust-truncated (outside the shaded area) discs, respectively. Averaged values of $|V|/R_{25}$ (and Δm_{15}) with their 95% CIs (and 1σ errors) for entire and dust-truncated samples are presented by medium-transparent and big-filled symbols, respectively.

between those of the thick and thin discs, while the scale height of 91bg-like events is clearly consistent with the thick disc. In late-type spirals, the scale height of 91T-like SNe Ia is close to that of CC SNe, while being larger. The average height of normal SNe Ia again is between thin and thick discs. The scale height of 91bg-like events again is in agreement with those of thick discs. This is a rough comparison when taking into account the error bars of the mean heights, it nevertheless gives us a numerical understanding of the relative vertical distributions of SN subclasses in comparison with thin and thick components of galactic disc.

On the other hand, [96] found that the scale height of thin disc of 34 late-type spiral galaxies corresponds to those of young/intermediate stellar populations with ages from ~ 10 Myr up to a few Gyr, while the scale height of thick disc is comparable to those of old stellar population with ages from a few Gyr up to ~ 10 Gyr [97, 164]. A similar result was obtained by [165] for the thick disc, where the age of stellar population increases from ~ 5 to ~ 10 Gyr [163,166,167]. Similarly, the ages of stellar populations of the MW thin and thick discs are estimated to be up to a few Gyr and from a few Gyr up to ~ 10 Gyr, respectively [100,168]. Notably, CC SNe arise from young progenitors with ages up to ~ 100 Myr and their vertical extend is accordingly less than the thin disc [85].

Thus, the various SN Ia subclasses correspond to different stellar population ages being distributed at the various average heights from the disc [85, 97, 164]. From Table 2.5, we can impose rough numerical constraints on the SN progenitors: 91T-like events arise from progenitors with ages about several 100 Myr, the ages of progenitors of 91bg-like SNe are comparable to ~ 10 Gyr, while normal SNe Ia arise from progenitors with ages from about one up to ~ 10 Gyr.

It is important to note that the delay time[2] of the SN progenitor system could be dominated by the timescale of the gravitational inspiral of WDs in comparison with the stellar age (a lifetime till it becomes WD, see [50, 52]). In this study, however, we consider the stellar age of SN progenitors rather than the system's entire delay time when comparing their average heights with those of various disc components. Note that a significant change in the mean vertical scales of the young and old stellar populations is not expected during the SN progenitor stellar age or the delay time of the systems. As mentioned above, 91T-like events (and the most of normal SNe Ia) are associated with star-forming environments ($\lesssim 500$ Myr; [160, 161]), therefore the effect of the gravitational inspiral's timescale should play a role mostly for 91bg-like SNe.

2.3.3 Relating LC decline rates with SN heights from host disc

SNe Ia span a variety of properties from subluminous SNe with fast-declining LCs to over-luminous and slowly evolving events [25]. The majority of earlier theoretical studies have failed to fit the full range of observed SNe Ia properties with a single explosion/progenitor scenario (see reviews by [50, 52]). Fortunately, recent theoretical studies in the sub-$M_{\rm Ch}$ WD explosion models showed an excellent quantitative agreement with observed photometrical behaviours of SNe Ia in the entire range of the [47] relation [57, 58, 63]. As mentioned in the Introduction, the explosion is realized in the double detonation of a sub-$M_{\rm Ch}$ WD, where the LC decline rate Δm_{15} of SN Ia is positively correlated with the age of the SN progenitor system [58, 63].

Numerous researches extensively studied the links between the SNe Ia LC decline rates and the global age (or age tracers) of host galaxies, as well as local age at SN explosion

[2] Time interval between the progenitor formation and the SN explosion.

Table 2.6: The correlation test for the $|V|/R_{25}$ versus Δm_{15} parameters.

SN	$N_{\rm SN}$	$\langle\lvert V\rvert/R_{25}\rangle$	versus	$\langle\Delta m_{15}\rangle$	$r_{\rm s}$	$P_{\rm s}^{\rm MC}$
All	69	$0.08^{+0.02}_{-0.02}$	versus	1.21±0.32	0.118	0.334
All†	36	$0.14^{+0.06}_{-0.04}$	versus	1.18±0.29	0.471	**0.004**

Notes. A coefficient of Spearman's rank correlation ($r_{\rm s} \in [-1;1]$) is a metric for determining how closely two variables are related by a monotonic function. The variables are not independent when $P \leq 0.05$ (highlighted in bold). The $P_{\rm s}^{\rm MC}$ values are generated using permutations with 10^5 MC iterations. The subsample marked with † symbol corresponds to SNe with $|V|/R_{25} \geq 0.04$.

sites [48, 73, 74, 76, 149, 169]. These studies demonstrated that, at different levels of significance, the LC decline rate is correlated with the global/local age: the B-band Δm_{15} values increase with stellar population age. However, the correlation between SNe Ia decline rate and the height from the host disc, which is a reliable age indicator of stellar population, has not yet been investigated. Here, we intend to fill this gap.

Fig. 2.2 and the Spearman's rank correlation test in Table 2.6 show that the trend between $|V|/R_{25}$ and Δm_{15} is positive, but not statistically significant. At low heights, in Fig. 2.2, we observe all the SN Ia subclasses (full range with slower and faster declining LCs), but with increasing height, the decline rate of objects increases on average. However, it should be taken into account that due to the dust extinction in galactic disc the discovery of SNe Ia in edge-on galaxies is complicated and biased against objects at lower heights from the disc [127]. The impact of this effect would be greatest on subluminous SNe (91bg-like events).

In late-type galaxies, the vertical distribution of dust has a scale height that is ~ 3 times less than that of thick disc stars [115]. While the dust layer is ~ 1.5 times thicker in early-type galaxies [129, 170], which is closer to our sample of SNe Ia host galaxies (see Table 2.1). Therefore, to avoid the possible impact of dust we truncate the heights of SNe with $|V|/R_{25} \geq 0.04$, leaving 36 SNe Ia in our sample. For this dust-truncated sample, the Spearman's rank test reveals a significant positive correlation between the $|V|/R_{25}$ and Δm_{15} parameters (Table 2.6, Fig. 2.2). The results are unaffected when the Z_{25} normalization is applied (Table 2.7). Thus, despite the limited sample size, we demonstrate for the first time a significant correlation between LC decline rates and SNe Ia heights, which is consistent with a sub-$M_{\rm Ch}$ WD explosion models [57–59] and vertical age gradient of stellar population in discs [96, 148].

Table 2.7: The correlation test for the $|V|/Z_{25}$ versus Δm_{15} parameters.

SN	$N_{\rm SN}$	$\langle\|V\|/Z_{25}\rangle$	versus	$\langle\Delta m_{15}\rangle$	$r_{\rm s}$	$P_{\rm s}^{\rm MC}$
All	69	$0.24^{+0.07}_{-0.05}$	versus	1.21±0.32	0.058	0.633
All†	36	$0.41^{+0.18}_{-0.11}$	versus	1.18±0.29	0.396	**0.016**

Notes. For the explanations of the parameters see Table 2.6. The subsample marked with † symbol corresponds to the dust-truncated SNe with $|V|/Z_{25} \geq 0.123$. For our host galaxy sample, the truncation is obtained by considering that $\langle Z_{25}/R_{25}\rangle \approx 0.325$.

It would be important to verify the results in Tables 2.3 and 2.4 while accounting for the selection effects brought by dust extinction. However, in these tables we compare the SN positions (heights) between the subclasses, and after the dust-truncation the samples for 91T- and 91bg-like SNe become, unfortunately, insufficient to perform the statistical tests.

2.4 Chapter Conclusions

We analyse the height distributions of the SN Ia subclasses from their host disc plane using spectroscopically classified 197 SNe in edge-on spiral galaxies with distances ≤ 200 Mpc. In addition, this study is performed to examine potential links between photometric characteristics of SNe Ia, like LC decline rates (Δm_{15}), and SN heights from the disc.

For the first time, we demonstrate that 91T- and 91bg-like subclasses of SNe Ia are distributed differently toward the plane of their host edge-on disc. On average, the SN heights are rising, beginning with 91T-like events and progressing through normal and 91bg-like SNe Ia. Considering that the height from the disc is a stellar population age indicator and comparing the mean heights of the SN Ia subclasses with those of thin and thick discs with known ages, we roughly estimate that 91T-like events originate from relatively younger progenitors with ages of about several 100 Myr, the ages of progenitors of normal SNe Ia are from about one up to ~ 10 Gyr, and 91bg-like SNe Ia arise from progenitors with significantly older ages ~ 10 Gyr. In addition, we show that the SN Ia LC decline rates correlate with their heights from the host disc, after excluding the selection effects brought by dust extinction. The observed correlation is consistent with the explosion models of a sub-$M_{\rm Ch}$ mass WD [57, 58, 63] and the vertical age gradient of stellar population in discs [96, 97, 148].

Chapter 3

The diversity of Type Ia SN progenitors

3.1 Introduction

In [135], we comparatively studied nearby elliptical host galaxies of 66 normal SNe Ia and 41 subluminous/91bg-like events from the footprint of the SDSS, without considering SN Ia LC properties. Our results supported the earlier suggestion [68, 81] that the characteristics of normal SNe Ia and 91bg-like events depend more on age than on mass or metallicity of the elliptical host galaxies. We showed, that the majority of the elliptical hosts of 91bg-like events are very old (> 8 Gyr) in comparison with those of normal SNe Ia, which are on average bluer and might have more residual star formation that gives rise to younger/prompt SNe Ia progenitors. In other words, we showed that the age distribution of 91bg-like SNe hosts does not extend down to the stellar ages that produce significant u-band fluxes in early-type hosts of normal SNe Ia, thus younger stars in these hosts do not produce 91bg-like SNe. Therefore, we concluded that the delay time distribution (DTD) of 91bg-like SNe is likely weighted toward long delay times, larger than several Gyr [162, 171]. These results led us to favour SN Ia progenitor models such as He-ignited violent mergers [172] that have the potential to explain the different DTDs of normal SNe Ia and 91bg-like events.

In this Chapter, we significantly improved the inclusion of various spectroscopic subclasses of Type Ia SNe (normal SN Ia and peculiar 91T-, 91bg- and 02cx-like events) from host galaxies with almost all Hubble morphological types, including objects not only from the SDSS, but also from the Pan-STARRS and the SkyMapper Southern Sky Survey, thus covering the entire sky. In addition, instead of relying only on the discrete spectroscopic classifications, SNe Ia in our sample now have the available continuous and extinction-independent LC decline rate (Δm_{15}) values in the B-band. The goals of this Chapter are to properly identify the diversity of SNe Ia and better constrain the nature (i.e. the progenitor channel, through the DTD) of their different subclasses through a comprehensive study of SN Ia LC decline rates and global properties of their hosts (e.g. morphology, stellar mass, colour, and age of stellar population).

3.2 Sample selection and reduction

3.2.1 SN Ia sample

For this Chapter, we used the Open Supernova Catalog [150] to collect spectroscopically classified SNe Ia with distances ≤ 150 Mpc ($z \lesssim 0.036$),[1] discovered up to 2019 May 1. All SNe Ia are required to have a B-band LC decline rate (Δm_{15}). We compiled the LC decline rates with their errors from various publications where different LC fitters were applied on the B-band photometry (or measured directly from the LCs) with wide temporal coverage for individual SNe [41, 48, 173–175]. Note that the B-band is historically the most often used in SN studies, and therefore the data is best sampled in this band. It should be noted also that the Δm_{15} of an SN Ia is a weak function of the line-of-sight dust extinction towards the SN in host galaxy, which affects the LCs [49]: $\Delta m_{15}^{\rm true} = \Delta m_{15}^{\rm obs} + 0.1\,E(B-V)$, where the last term in the equation contains colour excess towards the SN. The $E(B-V)$ values are mostly distributed within 0 to 0.3 mag, with the mean value of ~ 0.1 mag [48, 49]. Therefore, the term in the equation is between 0 to 0.03 mag, while the mean error in Δm_{15} estimation is ~ 0.1 mag.[2] For this reason, we consider the B-band Δm_{15} as a practically extinction-independent parameter.

[1] The luminosity distances of SNe and/or host galaxies are calculated using the recession velocities both corrected to the centroid of the Local Group and for the Virgocentric infall (see [102], for more details).

[2] In some cases, the values of $E(B-V)$ towards SN can reach up to ~ 0.5 mag, and only in unique cases up to around 1 mag [48, 176]. However, in all these cases the errors in Δm_{15} estimations are higher, reaching up to about 0.2 mag.

Table 3.1: Numbers and fractions of SNe Ia subclasses in our (distances $\leq$ 150 Mpc) and LOSS (distances $\leq$ 80 Mpc) volume-limited samples.

	Our		LOSS	
SN subclass	$N_{\rm SN}$	fr	$N_{\rm SN}$	fr
normal	303	$73.5^{+2.8}_{-3.0}$	52	$70.3^{+7.0}_{-7.8}$
91T	42	$10.2^{+2.2}_{-1.9}$	7	$9.4^{+5.9}_{-4.1}$
91bg	50	$12.1^{+2.3}_{-2.0}$	11	$14.9^{+6.7}_{-5.2}$
02cx	12	$4.1^{+1.5}_{-1.2}$	2	$5.4^{+5.1}_{-3.0}$
02es	5		2	
06gz	2	–	0	–
All	414	–	74	–

Notes. To be comparable with the LOSS sample, the fractions (in %) of SN subclasses in our sample are calculated, using the approach of [177], without two 06gz-like SNe. Despite the different nature of 02cx- and 02es-like events [178], the LOSS merged these SNe in a single bin, and we therefore presented the corresponding merged fraction in our sample as well (however the SN numbers are presented separately).

In the compilation of SNe Ia LC decline rates, we avoided using any transformation from LC stretch[3] to Δm_{15}, because it is unclear how reliable such a transformation is [48, 179].

The collected SNe Ia are also required to have available subclasses of their spectroscopy (e.g. normal, 91T-, 91bg-, and 02cx-like). Following [135], we carried out an extensive literature search to compile the information on the subclasses. As an interactive archive of SN spectra and corresponding references, we mostly used the Weizmann Interactive Supernova data Repository [151]. We considered also the websites of Central Bureau for Astronomical Telegrams[4], the Astronomer's Telegram[5], and other references with information on the SN subclasses [174, 180, 181]. Note that we included in the 91T-like SNe subclass the transitional 99aa-like events. Very early spectra of these SNe resemble those of 91T-like events. The difference with 91T-like SNe is that in the spectra of 99aa-like SNe the Ca II lines are always prominent. However, at maximum light the 99aa-like SNe spectra are similar to those of normal SNe Ia. In addition, the photometry shows that 99aa-like SNe are similarly luminous and slow-declining as 91T-like SNe. At the same time, we included two transitional 86G-like events in the 91bg-like SNe subclass. Spectroscopically, these events show properties intermediate between normal

[3]The stretch parameter, usually used in cosmological studies for the standardization of SN Ia, is related to the width of the SN Ia LC (see [182], for more details).

[4]http://www.cbat.eps.harvard.edu/iau/cbat.html

[5]http://www.astronomerstelegram.org/

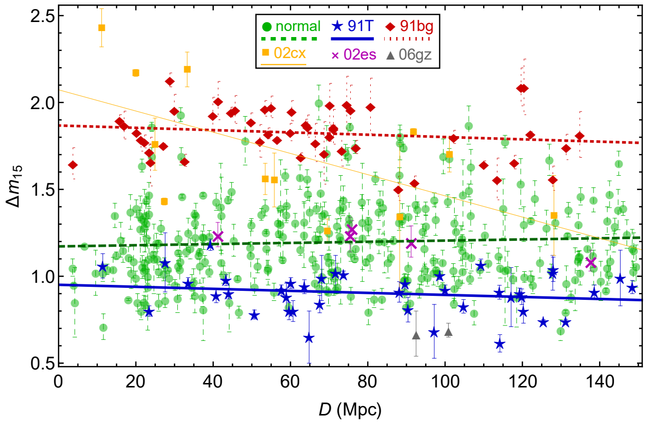

Figure 3.1: Variation of the B-band LC drop, Δm_{15}, of different subclasses of SNe Ia as a function of the host galaxy distance. Because of very few data points for 02es- and 06gz-like SNe, their best-fitting lines are useless and not presented.

and 91bg-like SNe. The Si II lines are as strong as in 91bg-like spectra, while Ti II lines are somewhat weaker. The LCs of 86G-like events peak at magnitudes intermediate between those of normal and 91bg-like SNe, and decline rapidly similar to the latter. For more details on the properties of these transitional events, the reader is referred to [25]. In total, we succeeded to collect the subclasses for 414 SNe Ia with available LC decline rates. The second column of Table 3.1 shows the numbers of different subclasses of the collected Type Ia SNe.

We compared the fractions of SN subclasses in our sample with those in the volume-limited sample of the LOSS [28]. Based on the detection efficiency of LOSS, the authors noted that their survey did not miss any SNe Ia that exploded within the sample of targeted galaxies out to 80 Mpc, achieving a completeness more than 98% (74 events). Table 3.1 shows that the representation of the SN subclasses in our sample is in good agreement within errors with that in the LOSS. We checked this by applying the two-sample KS and AD tests on the reconstructed two discrete data sets (distributions) with sizes of 414 and 74, using the ordered frequencies $\{303, 42, 50, 12, 5, 2\}_{\rm Our}$ and $\{52, 7, 11, 2, 2, 0\}_{\rm LOSS}$ from Table 3.1, respectively. The P-value of two-sample KS (AD) test represents the probability that the two distributions being compared are randomly drawn from the same parent distribution. The KS and AD tests showed that the frequencies of SN subclasses in our and LOSS samples are not significantly different ($P_{\rm KS} = 0.728$ and $P_{\rm AD} = 0.929$).

Table 3.2: Numbers of SNe Ia subclasses and coefficients of the linear best-fits ($\Delta m_{15} = a + b\, D$[Mpc]) from Fig. 3.1 with results of the Spearman's rank correlation test.

SN subclass	$N_{\rm SN}$	a	$b \times 10^{-3}$	$r_{\rm s}$	$P_{\rm s}$
normal	303	1.17 ± 0.03	0.3 ± 0.3	0.057	0.320
91T	42	0.95 ± 0.05	-0.6 ± 0.5	-0.131	0.407
91bg	50	1.87 ± 0.04	-0.7 ± 0.6	-0.135	0.350
02cx	12	2.07 ± 0.18	-6.1 ± 2.6	-0.559	0.058

Notes. See Table 2.6, for the explanations of $r_{\rm s}$ and $P_{\rm s}$.

For small-size samples like in Table 3.1, in addition to the original two-sample KS (or AD) test, a MC simulation is usually used for a better approximation of the P-value [183]. If the original two data samples have m and n members, the MC simulation randomly generates partitions of joint $m + n$ size sample into an m-set and an n-set, computing the two-sample KS (or AD) test statistic $D(m, n)$ for the generated sets. The $P_{\rm KS}^{\rm MC}$-value (or $P_{\rm AD}^{\rm MC}$-value) is the proportion of $D_i(m, n)$ values that are greater than d, where i is the number of iterations (we used $i = 10^5$) and d is the test statistic based on the original two data samples. The described analysis also showed that the frequencies of SN subclasses in our and LOSS samples are consistent between each other ($P_{\rm KS}^{\rm MC} = 0.710$ and $P_{\rm AD}^{\rm MC} = 0.650$). Thus, we believe that the artificial loss/excess of any of the SN subclasses in our sample is not significant.

It is important to recall that the 91T-like SNe have peak luminosities that are ~ 0.6 mag overluminous than do normal SNe Ia, while 91bg-like SNe have luminosities that are ~ 2 mag lower in comparison with normal ones. In general, the peak luminosities of 91bg- and 02es-like SNe are comparable. On the other hand, the peak luminosities of some 06gz-like events are even higher than those of 91T-like SNe, while the 02cx-like SNe can be less luminous than 91bg-like SNe (see [25] for a review on the extremes of SNe Ia). Therefore, the discoveries of the events with lower luminosities might be complicated at greater distances.

To check the possible influence of the distance effect, in Fig. 3.1 we illustrated the dependence of extinction-independent Δm_{15}, which is a good proxy for the intrinsic luminosity of a SN Ia [47], on distance for the different SN subclasses. The parameters of best-fitting lines from Fig. 3.1 and results of the Spearman's rank correlation test for Δm_{15} versus distance (in Mpc) are presented in Table 3.2. The Spearman's rank test shows not significant trends between the

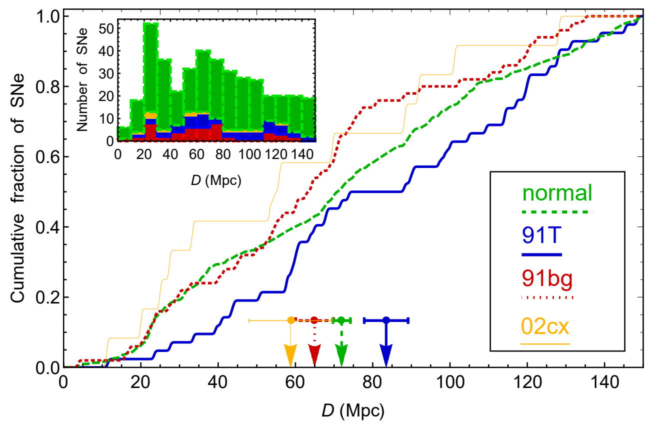

Figure 3.2: Cumulative distributions and stacked histogram (upper left inset) of distances of the subclasses of Type Ia SNe. The mean values (with standard errors) of the distributions are shown by arrows (with error bars).

Δm_{15} and distances for all the SN subclasses. Only for 02cx-like SNe, the $P_{\rm s}$-value of negative trend ($r_{\rm s} < 0$) is close to the 0.05 threshold, but still statistically not significant (see Table 3.2).

Note that, in this study we avoided merging 02cx- and 02es-like SNe subsamples, because they are two distinct subclasses based on their spectroscopic, photometric, and host galaxy properties [178]. For this reason and due to a small number of 02es-like events, we simply removed these five SNe from our analysis. For the same reasons, we also removed two 06gz-like SNe from our statistical/comparative study.

To further check the redshift-dependent biases in our SN sample, in Fig. 3.2 we compared the cumulative distance distributions of the SN subclasses. In Table 3.3, the two-sample KS and AD tests showed that the distance distributions of normal, 91T-, and 91bg-like events are not significantly different from one another and could thus be drawn from the same parent distribution. However, only in the AD statistic, the distance distributions of 91T- and 02cx-like SNe are not consistent between each other. At the same time, the corresponding P-value for a MC simulation is slightly higher than the significance threshold (see Table 3.3). Therefore, in comparison with more luminous SNe, the detection of 02cx-like events might be biased/complicated at greater distances (see Fig. 3.1 and the mean values in Fig. 3.2), most probably due to their low intrinsic luminosity at maximum light [25]. With this in mind, we will be cautious in our comparison of the properties of 02cx-like SNe and their host galaxies

Table 3.3: Comparison of the distributions of distances D (in Mpc) among different SN subclasses.

SN subsample 1		vs	SN subsample 2		P_{KS}	P_{AD}	$P_{\mathrm{KS}}^{\mathrm{MC}}$	$P_{\mathrm{AD}}^{\mathrm{MC}}$
Subclass	$\langle D \rangle$		Subclass	$\langle D \rangle$				
normal	72 ± 2	vs	91T	83 ± 6	0.094	0.071	0.089	0.074
normal	72 ± 2	vs	91bg	65 ± 5	0.137	0.206	0.131	0.216
normal	72 ± 2	vs	02cx	59 ± 11	0.613	0.426	0.594	0.471
91T	83 ± 6	vs	91bg	65 ± 5	0.060	0.055	0.056	0.061
91T	83 ± 6	vs	02cx	59 ± 11	0.126	**0.038**	0.104	0.051
91bg	65 ± 5	vs	02cx	59 ± 11	0.863	0.843	0.822	0.867

Notes. The explanations for the P-values are identical to those in Table 2.2. The statistically significant difference between the distributions is highlighted in bold.

with those of other SN subclasses. None of our SN Ia subsamples (except perhaps 02cx-like) should be affected by redshift-dependent biases.

3.2.2 SN Ia host galaxy sample

Our sample of SN Ia host galaxies was obtained by cross-matching the coordinates of our 407 SNe Ia with the footprints of the SDSS DR16 [152], the Pan-STARRS DR2 [154], and the SkyMapper DR2 [153], using the techniques described in [102]. Note that these surveys cover together the entire sky, complementing one another, and with some intersection. As a result, we identified 394 individual host galaxies of all collected SNe Ia: 1, 2, and 4 SNe are found in 383, 10, and 1 galaxies, respectively. It should be noted that some of the identified host galaxies from the footprint of SDSS DR16 are already listed in databases of [84, 85, 102, 135, 184], which are based on older DRs of SDSS. We nevertheless re-implemented the entire reduction process for all SDSS host galaxies using the DR16 properties.

Following the approach described in detail in [102], we morphologically classified all 394 host galaxies by visual inspection of images of hosts from the SDSS[6], Pan-STARRS[7], and SkyMapper[8] imaging servers, all of which build RGB colour images from the g, r, and i data channels. Note that SDSS, Pan-STARRS, and SkyMapper use different *ugriz*, *grizy*, and

[6]http://skyserver.sdss.org/dr16/en/tools/chart/listinfo.aspx
[7]https://ps1images.stsci.edu/cgi-bin/ps1cutouts
[8]http://skymapper.anu.edu.au/sky-viewer/

Table 3.4: Numbers of the subclasses of Type Ia SNe at distances ≤ 150 Mpc as a function of morphological types of host galaxies.

	E	E/S0	S0	S0/a	Sa	Sab	Sb	Sbc	Sc	Scd	Sd	Sdm	Sm	All
normal	20	7	20	22	20	15	57	63	47	13	8	7	4	303
91T	0	0	1	1	1	5	7	13	4	4	2	2	2	42
91bg	17	3	3	8	5	5	1	4	4	0	0	0	0	50
02cx	0	0	0	1	0	0	2	3	2	1	0	2	1	12
All	37	10	24	32	26	25	67	83	57	18	10	11	7	407

uvgriz filters, respectively. However, the *gri* sets of Pan-STARRS and SkyMapper are very similar to the SDSS filters of the same names [154, 185]. The SDSS RGB colour images of typical examples of SNe host galaxies with morphological classification according to the modified Hubble sequence (E-E/S0-S0-S0/a-Sa-Sab-Sb-Sbc-Sc-Scd-Sd-Sdm-Sm) can be found in [102]. Table 3.4 displays the distributions of the subclasses of SNe Ia among the various morphological types of host galaxies.

We first applied corrections to transform the Pan-STARRS and SkyMapper photometry to the SDSS system [153, 185, 186]. For all host galaxies, we fitted 25 mag arcsec^{-2} elliptical apertures in the SDSS g-band according to the approach presented in [102]. Following [135], for each host galaxy the corresponding SDSS *ugriz* fluxes (apparent magnitudes[9]) are measured using the mentioned elliptical apertures in g-band. The u-band flux measurements are performed only for host galaxies located on the footprints of SDSS and SkyMapper survey, which have the corresponding filter support. During the flux measurements, we masked out bright projected/saturated stars. The absolute/apparent magnitudes are corrected for Galactic extinction based on the [187] recalibration of the [188] dust map. In addition, these values are corrected for elongation/inclination effects and for the host galaxy internal extinction according to [189]. Finally, the colour-based K-corrections [190] are mostly negligible (< 0.15 mag), since the host redshifts are $\lesssim 0.036$.

The database of 407 individual SNe Ia (SN designation, spectroscopic subclass, Δm_{15}, and corresponding sources of the data) and their 394 hosts (galaxy designation, distance, corrected

[9] The magnitudes are in the AB system (https://www.sdss.org/dr16/algorithms/fluxcal/).

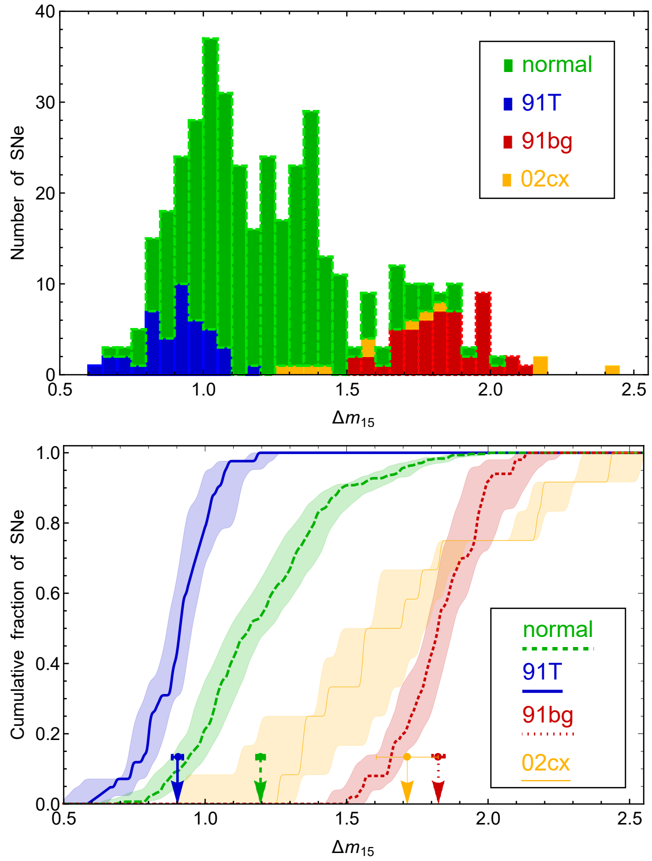

Figure 3.3: Upper panel: stacked histogram of the B-band Δm_{15} values of different SN Ia subclasses. Bottom panel: cumulative Δm_{15} distributions for the SN subclasses. The light shaded regions around each cumulative curve show the corresponding spreads considering the uncertainties in Δm_{15} values. The mean values (with standard errors) of the distributions are shown by arrows (with error bars).

$ugriz$ apparent magnitudes, and morphological type) is available online [191].

3.3 Results and discussion

With the aim of clarifying the progenitor natures of normal and peculiar (91T-, 91bg-, and 02cx-like) SN Ia subclasses, in this section we comparatively study the important relations between the LC decline rates of these SNe Ia and the global properties of the stellar population of their host galaxies with different morphological types.

Table 3.5: Comparison of the B-band Δm_{15} distributions among different SN Ia subclasses.

SN subsample 1		vs	SN subsample 2		$P_{\rm KS}$	$P_{\rm AD}$	$P_{\rm KS}^{\rm MC}$	$P_{\rm AD}^{\rm MC}$
Subclass	$\langle\Delta m_{15}\rangle$		Subclass	$\langle\Delta m_{15}\rangle$				
normal	1.19 ± 0.01	vs	91T	0.90 ± 0.02	<**0.001**	<**0.001**	<**0.001**	<**0.001**
normal	1.19 ± 0.01	vs	91bg	1.82 ± 0.02	<**0.001**	<**0.001**	<**0.001**	<**0.001**
normal	1.19 ± 0.01	vs	02cx	1.71 ± 0.11	<**0.001**	<**0.001**	<**0.001**	<**0.001**
91T	0.90 ± 0.02	vs	91bg	1.82 ± 0.02	<**0.001**	<**0.001**	<**0.001**	<**0.001**
91T	0.90 ± 0.02	vs	02cx	1.71 ± 0.11	<**0.001**	<**0.001**	<**0.001**	<**0.001**
91bg	1.82 ± 0.02	vs	02cx	1.71 ± 0.11	**0.031**	**0.002**	**0.025**	**0.003**

Notes. The explanations for the P-values are identical to those in Table 2.2. The statistically significant difference between the distributions is highlighted in bold.

3.3.1 Light curve decline rates of SN Ia subclasses

Fig. 3.3 shows the histogram and cumulative distributions of B-band Δm_{15} values for the different SN Ia subclasses in our sample. The Δm_{15} distribution appears to be bimodal, with the second (weaker) mode mostly distributed within $\sim 1.5-2.1$ mag range. This faster declining SN range is dominated by 91bg-like (subluminous) events, while the Δm_{15} of 91T-like (overluminous) SNe are distributed only within the first mode at slower declining range with $\Delta m_{15} \lesssim 1.1$ mag. This picture of the Δm_{15} distributions of faster and slower declining Type Ia SNe is very similar to the Δm_{15} distribution found by [48], who studied a data set of 165 low redshift ($z<0.06$) SNe Ia [172, 179]. It should be noted that the separate ranges of Δm_{15} distributions of 91T- and 91bg-like SNe are almost equal to each other (~ 0.6 mag), but about 2.2 times narrower than that of normal SNe Ia (~ 1.3 mag). At the same time, despite the small number statistics of 02cx-like SNe, their B-band decline rates with some extremes are spread in the faster side of the Δm_{15} distribution of normal SNe Ia [192]. The range of Δm_{15} distribution of these peculiar events is ~ 1.2 mag.

In Table 3.5, two-sample KS and AD tests show that the Δm_{15} distributions are inconsistent significantly between any pairs of SN Ia subclasses of our sample. Therefore, the Δm_{15} distributions of 91T- and 91bg-like SNe, which cross the tails of Δm_{15} distribution of normal SNe Ia, without crossing one another (see Fig. 3.3), suggest that these SN Ia subclasses may come from different stellar populations [48, 172]. A similar idea can be viable also for the progenitor population of 02cx-like SNe (see [26] and references therein), when comparing the Δm_{15}

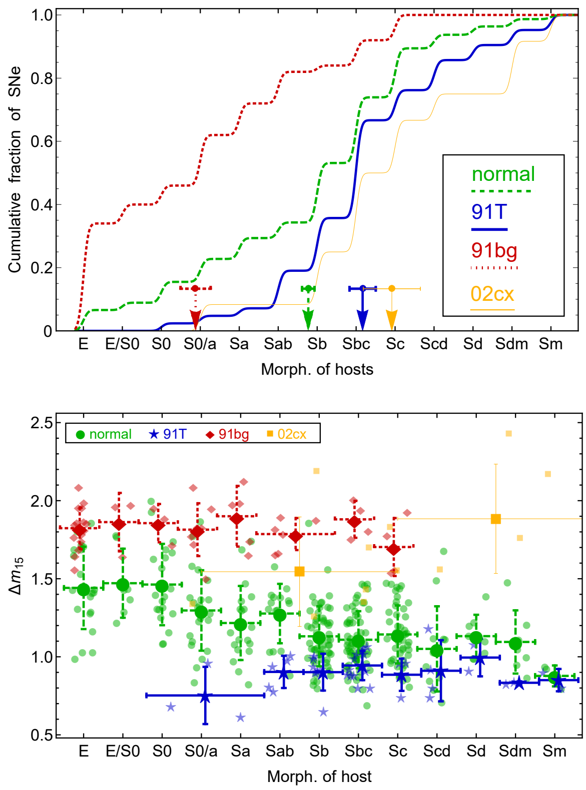

Figure 3.4: Upper panel: cumulative distributions of host galaxy morphological types of the subclasses of Type Ia SNe. The mean morphological types (with standard errors) of the host subsamples are shown by arrows (with error bars). Bottom panel: B-band Δm_{15} versus host galaxy morphology for different SNe Ia subclasses, displayed as a scatter plot (smaller symbols) and averaged in bins of morphological type (bigger symbols). The abscissae of the smaller symbols are randomly shifted by ± 0.3 in t for clarity, while they are slightly shifted according to SN Ia subclass for the bigger symbols. The S0, S0/a, and Sa morphological bins of 91T-like SNe are merged because each of them contains only one 91T-like event. For 91bg-like SNe, the Sb bin contains only one SN, therefore it is merged with the Sab bin. Similarly, given their small number, the hosts of 02cx-like SNe are merged into two broad morphological bins.

properties of normal SNe Ia with those of 02cx-like events (Fig. 3.3 and Table 3.5).

In next subsections, we obtain more robust constraints on the SN Ia progenitor populations, by studying the host galaxy global properties combined to the distributions of LC decline rates of the SN subclasses.

3.3.2 Morphologies of host galaxies of SN Ia subclasses

The upper panel of Fig. 3.4 presents the cumulative distributions of host galaxy morphological types of the subclasses of SNe Ia. It is clear that the host galaxies of normal, 91T-

Table 3.6: Comparison of the distributions of host galaxy morphological types among different SN Ia subclasses.

Host subsample 1 SN subclass	$\langle t \rangle$-type	vs	Host subsample 2 SN subclass	$\langle t \rangle$-type	$P_{\rm KS}$	$P_{\rm AD}$	$P_{\rm KS}^{\rm MC}$	$P_{\rm AD}^{\rm MC}$
normal	2.8 ± 0.1	vs	91T	4.2 ± 0.3	**0.015**	**0.004**	**0.015**	**0.007**
normal	2.8 ± 0.1	vs	91bg	-0.1 ± 0.4	**<0.001**	**<0.001**	**<0.001**	**<0.001**
normal	2.8 ± 0.1	vs	02cx	4.9 ± 0.7	0.134	**0.006**	0.122	**0.015**
91T	4.2 ± 0.3	vs	91bg	-0.1 ± 0.4	**<0.001**	**<0.001**	**<0.001**	**<0.001**
91T	4.2 ± 0.3	vs	02cx	4.9 ± 0.7	0.673	0.470	0.668	0.475
91bg	-0.1 ± 0.4	vs	02cx	4.9 ± 0.7	**<0.001**	**<0.001**	**<0.001**	**<0.001**

Notes. The explanations for P-values are the same as in Table 2.2. The statistically significant differences between the distributions are highlighted in bold.

Table 3.7: Comparison of the B-band Δm_{15} distributions of SNe Ia among different subsamples of host morphologies.

Subsample 1 Host	SN	$N_{\rm SN}$	$\langle \Delta m_{15} \rangle$	vs	Subsample 2 Host	SN	$N_{\rm SN}$	$\langle \Delta m_{15} \rangle$	$P_{\rm KS}$	$P_{\rm AD}$	$P_{\rm KS}^{\rm MC}$	$P_{\rm AD}^{\rm MC}$
E–S0	normal	47	1.45 ± 0.04	vs	S0/a–Sm	normal	256	1.15 ± 0.01	**<0.001**	**<0.001**	**<0.001**	**<0.001**
E–S0	91bg	23	1.83 ± 0.03	vs	S0/a–Sm	91bg	27	1.82 ± 0.03	0.876	0.840	0.806	0.842
E–S0	normal	47	1.45 ± 0.04	vs	S0/a–Sbc	normal	177	1.16 ± 0.02	**<0.001**	**<0.001**	**<0.001**	**<0.001**
E–S0	normal	47	1.45 ± 0.04	vs	Sc–Sm	normal	79	1.11 ± 0.02	**<0.001**	**<0.001**	**<0.001**	**<0.001**
S0/a–Sbc	normal	177	1.16 ± 0.02	vs	Sc–Sm	normal	79	1.11 ± 0.02	**0.050**	0.067	**0.048**	0.068
S0/a–Sbc	91T	27	0.91 ± 0.02	vs	Sc–Sm	91T	14	0.89 ± 0.03	0.608	0.322	0.557	0.366
E–S0	91bg	23	1.83 ± 0.03	vs	S0/a–Sbc	91bg	23	1.84 ± 0.03	0.991	0.936	0.931	0.937

Notes. The explanations for P-values are the same as in Table 2.2. The statistically significant differences between the distributions are highlighted in bold. Due to small number statistics of 02cx-like SNe, their study in the subsamples of host morphology is statistically useless, and therefore not presented.

(overluminous), and 91bg-like (subluminous) SNe Ia have morphological type distributions that are significantly mutually inconsistent (see Table 3.6). Host galaxies of 91bg-like SNe have, on average, earlier morphological types ($\langle t \rangle \approx 0$), with 46% of the events discovered in E–S0 galaxies. In contrast, host galaxies of 91T-like SNe have, on average, later morphological types ($\langle t \rangle \approx 4$), with a single 91T-like event in E–S0 hosts (only $\sim 2\%$ of the subsample, see Table 3.4). The morphological distribution of host galaxies of spectroscopically normal SNe Ia occupies an intermediate position between the host morphologies of 91T- and 91bg-like events. The morphological distribution of 02cx-like SNe hosts is similar to that of 91T-like SNe hosts, though the LC decline rates of the former SN subclass are significantly larger than those of the latter subclass (see Fig. 3.3 and Table 3.5).

These results are in good agreement with those of [65], who presented a photometric identification technique for 91bg-like SNe, separating them from the normal Type Ia population, and comparatively studied SNe host galaxy morphologies (see also [109, 193, 194] for other SN Ia subclasses). [65] showed that the morphological distribution of host galaxies of 91bg-like candidates is significantly earlier ($P_{\rm KS} \simeq 0.002$) from that of normal SNe Ia.[10] In addition, using a Fisher exact test, [65] noted that the number ratio of normal SNe Ia in passive (E–S0) to star-forming (S0/a–Sm) galaxies is statistically different (smaller) from the same ratio of 91bg-like SNe with a probability $P_{\rm F} \simeq 0.002$. For our SN sample in Table 3.4, the behaviour of the ratios is the same as in [65], with $P_{\rm F} < 0.001$. For the hosts of other SN Ia subclasses, [193] and [109] mentioned that 91T- and 02cx-like objects have consistent host morphologies, while hosts of 91T-like SNe have later morphological types in comparison with normal SNe Ia.

Taking into account that the mean stellar population age of galaxies is steadily decreasing along the Hubble sequence from early- to late-type galaxies [159], the results in the upper panel of Fig. 3.4 and Table 3.6 indicate that the progenitor population age of SN Ia subclasses in the sequence of 91bg-, normal, and 91T(or 02cx)-like events is decreasing as well.

In the bottom panel of Fig. 3.4, we show the distribution of the B-band Δm_{15} values as a function of morphological type of host galaxies, for different SN Ia subclasses. When dividing SNe Ia hosts between E–S0 (galaxies with only old stellar component) and S0/a–Sm morphological types (galaxies with both old and young stellar components), Table 3.7 shows that the distributions of Δm_{15} values of 91bg-like SNe are not different between the host subsamples, being distributed mainly within old ellipticals/lenticulars and early-type spirals (Fig. 3.4). In contrast, the Δm_{15} distribution of normal SNe Ia in E–S0 hosts is not consistent with that in S0/a–Sm galaxies.

Using narrow morphological bins, i.e. E–S0, S0/a–Sbc, and Sc–Sm, shows that the Δm_{15} values of normal SNe Ia are decreasing on average from early- to late-type galaxies. Indeed, the Spearman's rank test shows that the significant correlation between Δm_{15} and host t-

[10] It should be noted that [65] also identified other peculiar SNe Ia subgroup, which includes 02cx- and 06gz-like events. However, the results concerning to the hosts morphologies of this peculiar subgroup are not comparable with those of our case, because their subgroup include nearly equal numbers of 02cx- and 06gz-like SNe whose hosts morphologies have different distributions [135, 194, 195], thus mixing the morphological types.

types exists only for normal SNe Ia ($r_s = -0.416$, $P_s < 0.001$), although the discrete t-type values are not convenient for the test. The Δm_{15} distributions of 91T-like events are not different in S0/a–Sbc and Sc–Sm galaxies (Table 3.7), which lie mostly within spiral hosts (Fig. 3.4). Without a clear separation between the SN Ia spectroscopic subclasses, similar results have been obtained in the past with samples of SNe Ia and their host galaxies at different redshifts [48, 66–68, 77, 196, 197]. Note that, because of few data points for 02cx-like SNe, their study in the subsamples of host morphology is statistically useless, and therefore not presented in Table 3.7.

Recall that the intrinsic ranges of Δm_{15} distributions of 91T- and 91bg-like SNe are narrower than that of normal SNe Ia (see Subsection 3.3.1). Could these narrow ranges of Δm_{15} prevent us from seeing any trends with host galaxy properties such as morphology? We probe this issue by searching for trends of Δm_{15} and morphology for normal SNe Ia, in the corresponding narrow ranges of Δm_{15} as for 91T-like events first and then as for 91bg-like SNe. For 189 normal SNe Ia with $\Delta m_{15} \lesssim 1.26$ mag, the $r_s = -0.177$ and $P_s = 0.015$, and for 64 normal events with $\Delta m_{15} \gtrsim 1.38$ mag, the $r_s = -0.305$ and $P_s = 0.014$. Thus, normal SNe Ia keep the Δm_{15} – morphology trend direction and significance even in each of the narrower Δm_{15} ranges, showing that the Δm_{15} ranges of 91T- and 91bg-like SNe should not play a significant role in the absence of the trends for peculiar events.

Along with the mean stellar population ages of galaxies, the ratio of bulge luminosity (old halo/bulge component) over disc luminosity (old and young star-forming disc components) is steadily decreasing along the Hubble sequence [198, 199]. There is no disc component in elliptical galaxies, while the stellar bulge component is negligible in late-type spiral galaxies where the star-forming disc is prominent. Therefore, most probably the results above indicate that 91bg-like SNe (subluminous SNe Ia) come only from the old stellar component (halo/bulge, old disc) of hosts, while 91T-like events (overluminous SNe Ia) originate only from the young component (star-forming disc) of galaxies. Faster and slower declining normal SNe Ia likely come from older and younger stellar populations of host galaxies, respectively. Despite their small numbers, 02cx-like SNe typically lie in star-forming galaxies with late-type morphology

(Fig. 3.4), hinting that these events likely originate from young stellar component.

It is instructive to consider counter-examples. The discovery of SN 2004br [200], a 91T-like event [180], in NGC 4493 of S0 morphology (see Table 3.4 and Fig. 3.4), which consists of only old stellar population from a naive point of view. In NGC 4493, another SN Ia was also discovered (SN 1994M; [201]) with a normal spectroscopic classification [202]. Interestingly, this host galaxy has a distorted stellar disc and shows obvious evidence of an interaction with neighbor/companion galaxy [102]. The age of the younger stellar component in this galaxy is estimated to be down to about a few hundred Myr [203]. There are many indications that residual star formation episodes (birth of relatively young stellar component) could also take place in elliptical or lenticular galaxies, due to galaxy-galaxy interaction with close neighbors [86, 87, 204, 205]. In such early-type galaxies, in very rare cases, even core-collapse SNe were discovered [2, 102, 206, 207] whose progenitor ages are thought to be up to about hundred Myr [147]. Therefore, in our sample, the presence of unique 91T-like SN in the mentioned interacting lenticular galaxy can be interpreted as a result of such a residual star formation that could deliver SN Ia from relatively young progenitors.

3.3.3 Colour–mass diagram of SNe Ia host galaxies

Galaxy colours represent a more quantitative measure of galaxy classes, albeit spectral classes. Therefore, in this subsection we only use the photometric data of SNe Ia hosts, accompanied with the values of SN LC decline rates. To analyse the distribution of SN host galaxies on the colour–mass diagram, we estimate the stellar masses (M_*) of our sample galaxies, using a simple empirical relation of [208] between $\log(M_*/\mathrm{M}_\odot)$, $g-i$ colour and i-band absolute magnitude, M_i (see [135] for details). While this mass estimate is rudimentary and may be biased relative to more refined mass measurements, it suffices for our aim to. In the colour–mass diagram (Fig. 3.5), we prefer to use $u-r$ colours, which present the largest contrast among optical colours between the inputs of young and old stellar populations [87, 135]. Recall that u-band measurements are available only for 326 SNe Ia host galaxies (80% of the sample) located in the footprints of the SDSS and SkyMapper survey, which provide the corresponding fits images

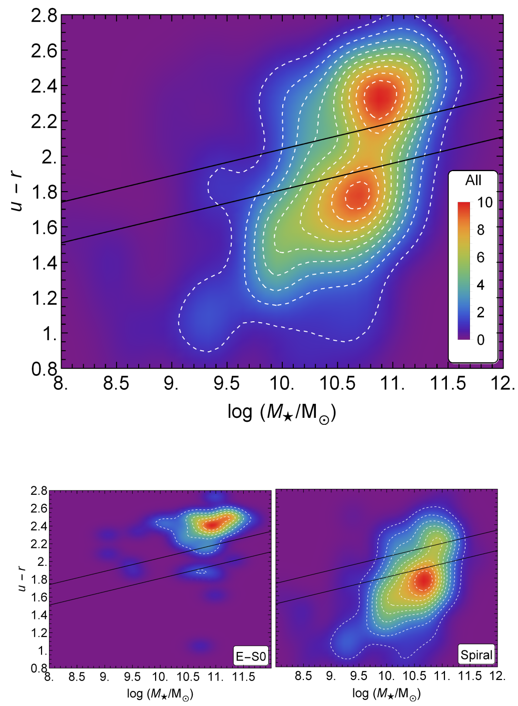

Figure 3.5: Colour–mass diagrams of SNe Ia host galaxies viewed as density and contours. The region between two solid lines marks the Green Valley (see text for details). Upper panel: all 326 SNe Ia host galaxies with measured u and r magnitudes. The colour bar shows the linear (arbitrary) units of density. Bottom panels: same for the E–S0 (*left*) and spiral (*right*) host morphologies.

(see Subsection 3.2.2).

In the upper panel of Fig. 3.5, the $u - r$ colour–mass diagram clearly displays a bimodal distribution of colours of SNe Ia host galaxies (see also [209] for the $g - i$ colours), as seen in general galaxy samples [210]. More precisely, galaxies with dominant old stellar populations and low specific SFRs (mostly massive galaxies) lie in the so-called Red Sequence of the diagram, which is located at $u - r \gtrsim 2$ mag, with a tail of about 10% of the population reaching down to $u - r \approx 1.5$ mag [87, 210]. Star-forming galaxies with prominent young stellar population are located in the so-called Blue Cloud of the diagram, mostly at $u - r \lesssim 2$ mag, with a tail to redder colours.

The bottom left panel of Fig. 3.5 shows the colour–mass relation for our E–S0 hosts with 83 SNe Ia. Similarly, spiral galaxies of the sample that host 243 SNe Ia are presented in the bottom right panel of Fig. 3.5. The bimodality in the diagram is due to the superposition of

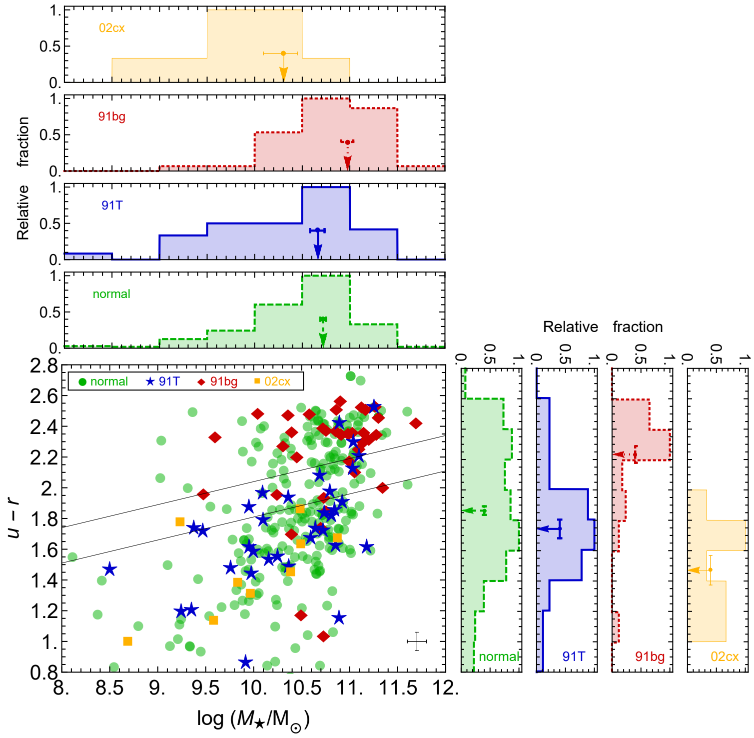

Figure 3.6: Colour–mass diagram for 326 SNe Ia host galaxies with measured u and r magnitudes, displayed as scatter plots and distributions. In the bottom right corner of the lower left panel, the error bar represents the characteristic errors in our estimations of colours and masses of galaxies. The region between two solid lines marks the Green Valley (see text for details). For host galaxies of different SN subclasses, the right and upper panels show separately the histograms (distributions of relative fractions) of the colours and masses, respectively. The mean values (with standard errors) of the distributions are shown by arrows (with error bars).

colours of these two distinct populations of galaxies [87]. A dip between bimodal (red and blue) colours in the colour–mass diagram is called Green Valley (the region between two solid lines in Fig. 3.5, see also [135]). This region is thought to include galaxies that are in transitional stage of the evolution between star-forming galaxies in the Blue Cloud and passively evolving quenched galaxies in the Red Sequence [87, 88, 210, 211].

Fig. 3.6 shows how the host galaxies of different SN Ia subclasses are distributed in the colour–mass diagram. The figure also displays the distributions of $u-r$ colours and masses for host galaxies for the different SN subclasses. Host galaxies of 91bg-like SNe are clearly located in the Red Sequence, and most of them have $u-r$ colours $\gtrsim 2$ mag (i.e. above the Green Valley). In comparison with hosts of normal, 91T-, and 02cx-like SNe, the colour distribution of host galaxies of 91bg-like SNe are significantly redder (see Table 3.8). Also, the bulk of

Table 3.8: Comparison of the distributions of host galaxy $u-r$ colours and stellar masses among different SN Ia subclasses.

Host subsample 1			vs	Host subsample 2			P_{KS}	P_{AD}	$P_{\mathrm{KS}}^{\mathrm{MC}}$	$P_{\mathrm{AD}}^{\mathrm{MC}}$
SN	N_{SN}	$\langle u-r \rangle$		SN	N_{SN}	$\langle u-r \rangle$				
normal	244	1.86 ± 0.03	vs	91T	34	1.74 ± 0.06	0.064	0.092	0.060	0.101
normal	244	1.86 ± 0.03	vs	91bg	39	2.23 ± 0.05	**<0.001**	**<0.001**	**<0.001**	**<0.001**
normal	244	1.86 ± 0.03	vs	02cx	9	1.47 ± 0.10	**0.020**	**0.007**	**0.016**	**0.013**
91T	34	1.74 ± 0.06	vs	91bg	39	2.23 ± 0.05	**<0.001**	**<0.001**	**<0.001**	**<0.001**
91T	34	1.74 ± 0.06	vs	02cx	9	1.47 ± 0.10	0.140	**0.041**	0.117	0.059
91bg	39	2.23 ± 0.05	vs	02cx	9	1.47 ± 0.10	**<0.001**	**<0.001**	**<0.001**	**<0.001**
		$\langle \log(M_*/\mathrm{M}_\odot) \rangle$				$\langle \log(M_*/\mathrm{M}_\odot) \rangle$				
normal	244	$10.72^{+0.03}_{-0.03}$	vs	91T	34	$10.66^{+0.07}_{-0.08}$	0.342	0.432	0.325	0.444
normal	244	$10.72^{+0.03}_{-0.03}$	vs	91bg	39	$10.98^{+0.06}_{-0.07}$	**<0.001**	**<0.001**	**<0.001**	**<0.001**
normal	244	$10.72^{+0.03}_{-0.03}$	vs	02cx	9	$10.30^{+0.14}_{-0.21}$	**0.030**	**0.014**	**0.027**	**0.024**
91T	34	$10.66^{+0.07}_{-0.08}$	vs	91bg	39	$10.98^{+0.06}_{-0.07}$	**0.019**	**0.001**	**0.016**	**0.001**
91T	34	$10.66^{+0.07}_{-0.08}$	vs	02cx	9	$10.30^{+0.14}_{-0.21}$	0.175	0.130	0.143	0.169
91bg	39	$10.98^{+0.06}_{-0.07}$	vs	02cx	9	$10.30^{+0.14}_{-0.21}$	**0.001**	**<0.001**	**<0.001**	**0.001**

Notes. The explanations for P-values are the same as in Table 2.2. The statistically significant differences between the distributions are highlighted in bold.

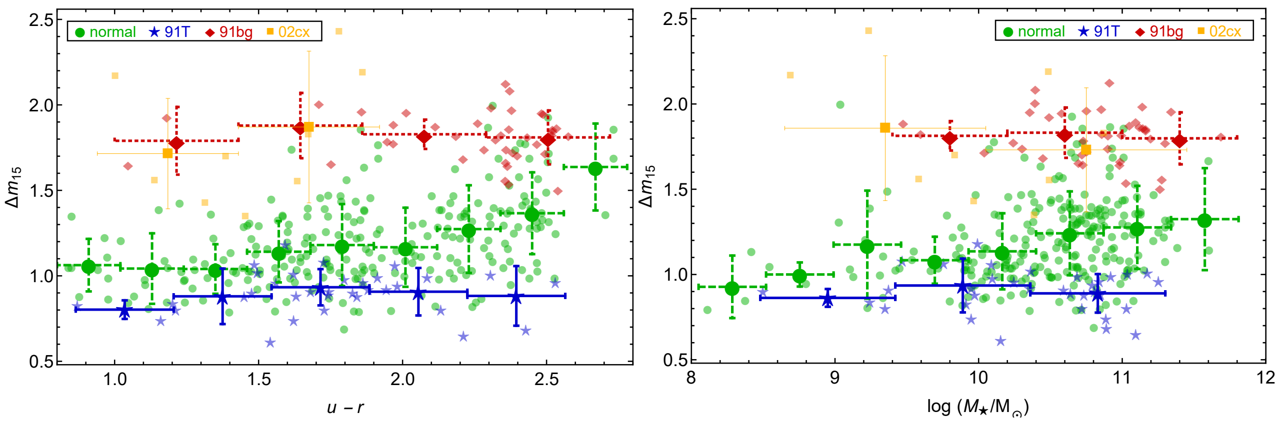

Figure 3.7: B-band Δm_{15} values of the SN Ia subclasses versus host galaxy colour (*left*) and host galaxy stellar mass (*right*). Binned and averaged values of Δm_{15} (bigger symbols) are superposed on the original distributions (smaller symbols). Horizontal bars show the bin sizes. Depending on the numbers of SNe Ia for certain subclasses, different binning sizes are selected to include sufficient numbers of the objects.

Table 3.9: Results of Spearman's rank correlation test for the B-band Δm_{15} values of the SN Ia subclasses versus $u-r$ colours and stellar masses of host galaxies.

SN subclass	$N_{\rm SN}$	Variable 1	vs	Variable 2	$r_{\rm s}$	$P_{\rm s}$
normal	244	Δm_{15}	vs	$u-r$	0.429	<**0.001**
normal[a]	149	Δm_{15}	vs	$u-r$	0.210	**0.010**
normal[b]	53	Δm_{15}	vs	$u-r$	0.285	**0.038**
91T	34	Δm_{15}	vs	$u-r$	0.143	0.421
91bg	39	Δm_{15}	vs	$u-r$	-0.092	0.576
02cx	9	Δm_{15}	vs	$u-r$	0.417	0.264
normal	244	Δm_{15}	vs	$\log(M_*/{\rm M}_\odot)$	0.286	<**0.001**
normal[a]	149	Δm_{15}	vs	$\log(M_*/{\rm M}_\odot)$	0.159	0.052
normal[b]	53	Δm_{15}	vs	$\log(M_*/{\rm M}_\odot)$	0.062	0.657
91T	34	Δm_{15}	vs	$\log(M_*/{\rm M}_\odot)$	-0.052	0.770
91bg	39	Δm_{15}	vs	$\log(M_*/{\rm M}_\odot)$	-0.091	0.582
02cx	9	Δm_{15}	vs	$\log(M_*/{\rm M}_\odot)$	-0.300	0.433

Notes. The explanations for $r_{\rm s}$ and $P_{\rm s}$-values are the same as in Table 2.6. [a]$\Delta m_{15} \lesssim 1.26$ mag, similar to 91T-like SNe. [b]$\Delta m_{15} \gtrsim 1.38$ mag, similar to 91bg-like events. Statistically significant correlations between the variables are highlighted in bold.

hosts of 91bg-like SNe are significantly massive ($\log(M_*/{\rm M}_\odot) > 10.5$). The distribution of host masses is significantly inconsistent with those of the other SN Ia subclasses (Table 3.8). At the same time, the colour (resp. mass) distributions are not statistically different between hosts of normal and 91T-like SNe, spanning almost the entire ranges of host colour (resp. mass). Finally, although the small number statistics, all the host galaxies of 02cx-like SNe are positioned in the Blue Cloud, mostly below the Green Valley in Fig. 3.6. Their colour (mass) distribution is significantly bluer (lower) in comparison with that of normal SNe Ia host galaxies, but closer to that of 91T-like SNe hosts (Table 3.8).

In Fig. 3.7, we show the distribution of the B-band Δm_{15} values of the SN Ia subclasses as a function of $u-r$ colours and stellar masses of host galaxies. Interestingly, only normal SNe Ia show average systematic increase in Δm_{15} values with an increase in colour (mass) values of hosts. The results of Spearman's rank test, shown in Table 3.9, confirm that only for normal SNe Ia we do see a significant correlation between LC decline rates and host galaxy colours (masses). We note that similar dependence of SNe Ia LC properties, such as decline rates, on the stellar masses of host galaxies have been shown in the literature using various SN Ia/host

Table 3.10: Comparison of the B-band Δm_{15} distributions of only normal SNe Ia among different subsamples of host parameters.

Subsample 1			vs	Subsample 2			$P_{\rm KS}$	$P_{\rm AD}$	$P_{\rm KS}^{\rm MC}$	$P_{\rm AD}^{\rm MC}$
Host parameter	$N_{\rm SN}$	$\langle\Delta m_{15}\rangle$		Host parameter	$N_{\rm SN}$	$\langle\Delta m_{15}\rangle$				
$u-r$ >2 mag	100	1.30 ± 0.02	vs	$u-r$ ≤2 mag	144	1.13 ± 0.02	**<0.001**	**<0.001**	**<0.001**	**<0.001**
$\log(M_*/{\rm M}_\odot)>10.5$	139	1.26 ± 0.02	vs	$\log(M_*/{\rm M}_\odot)\leq10.5$	105	1.13 ± 0.02	**<0.001**	**<0.001**	**<0.001**	**<0.001**
above Green Valley	81	1.33 ± 0.03	vs	below/in Green Valley	163	1.14 ± 0.02	**<0.001**	**<0.001**	**<0.001**	**<0.001**
above Green Valley	81	1.33 ± 0.03	vs	below Green Valley	133	1.13 ± 0.02	**<0.001**	**<0.001**	**<0.001**	**<0.001**

Notes. The explanations for P-values are the same as in Table 2.2. A 0.15 mag and 0.25 dex variations in colour and mass demarcations, respectively, do not change the statistical behaviour of the tests. The statistically significant differences between the distributions are highlighted in bold.

samples [69,70,73,76,78,169,212–214]. However, instead of Δm_{15}, these studies used the SN Ia LC shape parameter Δ (adding and subtracting template LC shapes) or stretch x_1 (stretching or compressing the time axis of the LC by a single "stretch factor") obtained from two commonly used LC fitters in cosmology: MLCS2k2 [215] and SALT2 [216], respectively. These parameters (Δ and x_1) show different correlations with the observed Δm_{15} [179]. In addition, these studies did not perform a clear separation between normal and peculiar (91T-, 91bg-, and 02cx-like) SN Ia spectroscopic subclasses. The dependence of SNe Ia LC properties on the $u-r$ colours of host galaxies was not directly studied in the literature,[11] although it is expected, because similar dependencies on host morphology and other colours were known [48, 66–68, 77, 169, 197, 215], again without clear separation between the spectroscopic subclasses of SNe Ia.

As in Subsection 3.3.2, for normal SNe Ia we check for the correlations between their Δm_{15} and host galaxy properties in two separate Δm_{15} ranges corresponding to the sizes of the Δm_{15} ranges of 91T- and 91bg-like SNe. Table 3.9 shows that normal SNe Ia keep the Δm_{15} – colour trend direction and significance in each of the narrower Δm_{15} ranges, while the Δm_{15} – $\log(M_*/{\rm M}_\odot)$ trend becomes insignificant, hinting that the Δm_{15} ranges might play a role in the absence of the Δm_{15} – $\log(M_*/{\rm M}_\odot)$ trend for peculiar SNe Ia.

Without mixing the SN Ia subclasses, we compare in Table 3.10 the distributions of LC decline rates of normal SNe Ia between two distinct populations of host galaxies in the colour–mass diagram. The separations between two populations of galaxies are done according to $u-r$ colour [87], stellar mass [213], or according to locations of galaxies above and below

[11] But see [214], for indirectly obtained $U-R$ colours of SNe Ia host galaxies.

the Green Valley. Indeed, the Green Valley separates best the two populations of passively evolving quenched (older) galaxies and of star-forming (younger) hosts. Table 3.10 shows that the distributions of Δm_{15} values of normal SNe Ia are significantly different between all the mentioned host subsamples. On average, those normal SNe Ia that are in galaxies above the Green Valley have faster declining LCs compared to those in galaxies below the Green Valley. This result suggests that the correlation seen in Fig. 3.7 and Table 3.9 is due to a superposition of faster and slower declining normal SNe Ia from old and young stellar populations of host galaxies, respectively dominating in the Red Sequence and Blue Cloud of the colour–mass diagram (see Fig. 3.6). In addition to the findings in Subsection 3.3.2, the colour–mass study of SN Ia hosts also suggest that there could be at least two distinct populations of normal SNe Ia: the halo/bulge and old disc components of galaxies most likely host faster declining normal SNe Ia, while star-forming component of galaxies hosts their slower declining counterparts.

Taken separately, the LC decline rates of 91bg-like SNe (subluminous SNe Ia) and 91T-like events (overluminous SNe Ia) do not show dependencies on host galaxy colour (Fig. 3.7 and Table 3.9). At the same time, the distribution of hosts on the colour–mass diagram confirms the known tendency for 91bg-like SNe to occur in globally red/old galaxies while 91T-like events prefer blue/younger hosts. Therefore, the results in Figs. 3.5, 3.6, and Table 3.8 reinforce those obtained in Subsection 3.3.2 that among the considered SN Ia subclasses, 91bg-like SNe come only from old stellar population of hosts (halo/bulge and old disc components), while 91T-like events originate only from young population of galaxies (star-forming component). Probably, the decline rates of 02cx-like SNe also do not show dependencies on host galaxy properties (Table 3.9), although we note that statistics of these events is based on small numbers. Complementing the results of Subsection 3.3.2, the positions of 02cx-like SNe hosts in the colour–mass diagram suggest that these events may all originate from the young stellar component, although they diverge from 91T-like events in their significantly higher LC decline rate.

Since the g- and i-bands photometry is available for all 407 SNe Ia host galaxies, we also check the stellar mass-based results in Tables 3.8-3.10 using the entire SN Ia subsamples. As a

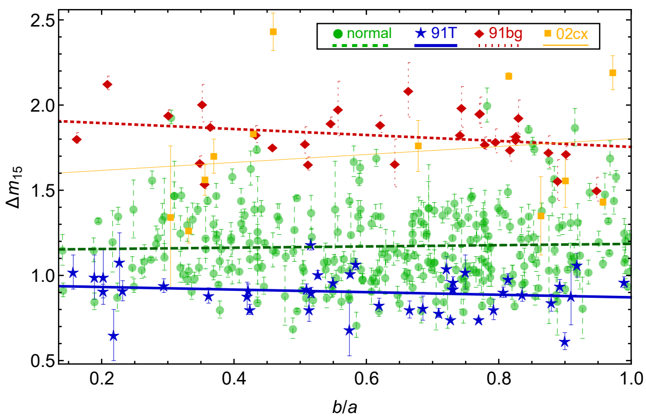

Figure 3.8: Distributions of the B-band Δm_{15} values of different subclasses of 360 SNe Ia as a function of b/a of S0–Sm host galaxies (a measure of galaxy inclination), and their best-fitting lines.

result, all behaviours of the dependencies (Δm_{15} vs $\log(M_*/\mathrm{M}_\odot)$) and statistical significances of the tests remain almost unchanged.

Interestingly, some studies suggested that the correlations between the optically-based LC properties and host galaxy mass might be due to differences in dust extinction in galaxies with different masses [217, 218]. However, most recently [176] observed near-constant correlations between SN Ia LC properties and host galaxy mass across near-infrared, which are less sensitive to dust, and optical bands. They suggested that dust extinction might not play a significant role in the observed correlation [219]. In this respect, the combination of the lack/non-significance of Δm_{15} – host stellar mass (morphology, colour) correlations for peculiar SNe Ia and the observed significant correlation for normal SNe Ia (Figs. 3.4, 3.7 and Table 3.9) also suggest that dust may not be the dominant process in the correlations of LCs and host properties for normal SNe Ia. If the impact of dust were strong, then one would expect that, contrary to what we found in Fig. 3.4, the B-band Δm_{15} of 91T-like SNe would be correlated with host galaxy properties, because the bulk of these events are discovered in star-forming galaxies with different masses and dust properties.

Indeed, one could also expect that SNe Ia in strongly inclined hosts are more extinguished and will show smaller Δm_{15} (see Subsection 3.2.1). Fig. 3.8 shows the distribution of Δm_{15}

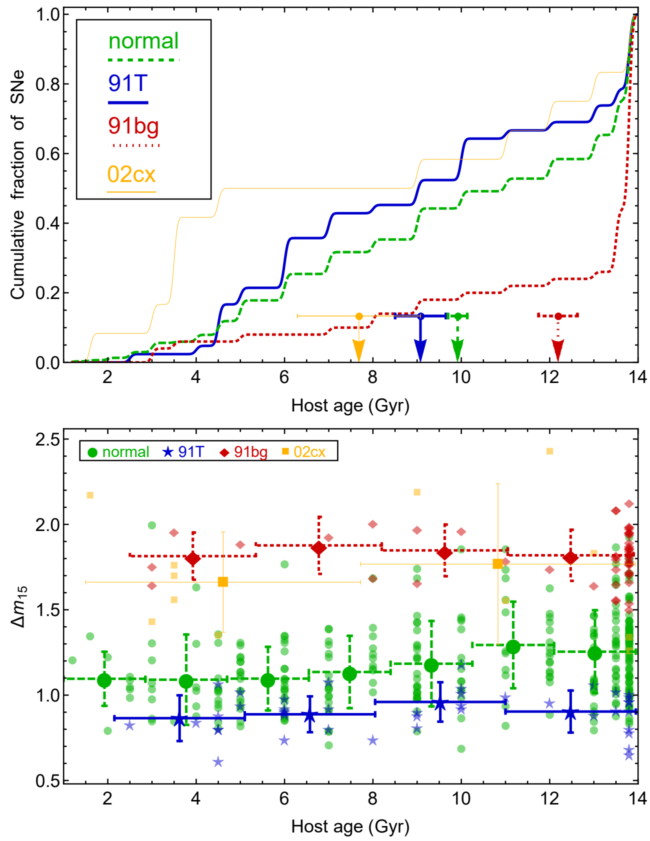

Figure 3.9: Upper panel: cumulative distributions of SNe Ia host galaxy luminosity-weighted ages. The mean ages (with standard errors) of the host subsamples are shown by arrows (with error bars). Bottom panel: B-band Δm_{15} values of the SN Ia subclasses versus luminosity-weighted ages of host galaxies. Binned and averaged values of Δm_{15} (bigger symbols) are superposed on the original distributions (smaller symbols). Horizontal bars show the bin sizes. Depending on the numbers of SNe Ia for certain subclasses, different binning sizes are selected to include sufficient numbers of the objects.

versus b/a of S0–Sm host galaxies,[12] which is a measure of galaxy inclination. However, the Spearman's rank test shows that these variables are not correlated: the $P_{\rm s}$-values are 0.745, 0.419, 0.123, and 0.275 for normal, 91T-, 91bg-, and 02cx-like SNe, respectively [213]. Therefore, we believe that the observed normal SN Ia-host relations are dominated by the diversity of SNe Ia progenitors.

Table 3.11: Comparison of the distributions of host galaxy luminosity-weighted ages among different SN Ia subclasses.

Host subsample 1			vs	Host subsample 2			$P_{\rm KS}$	$P_{\rm AD}$	$P_{\rm KS}^{\rm MC}$	$P_{\rm AD}^{\rm MC}$
SN subclass	$N_{\rm SN}$	$\langle$host age$\rangle$		SN subclass	$N_{\rm SN}$	$\langle$host age$\rangle$				
normal	303	9.9 ± 0.2	vs	91T	42	9.1 ± 0.6	0.211	0.310	0.211	0.325
normal	303	9.9 ± 0.2	vs	91bg	50	12.2 ± 0.4	**<0.001**	**<0.001**	**<0.001**	**<0.001**
normal	303	9.9 ± 0.2	vs	02cx	12	7.7 ± 1.4	**0.029**	**0.016**	**0.030**	**0.030**
91T	42	9.1 ± 0.6	vs	91bg	50	12.2 ± 0.4	**<0.001**	**<0.001**	**<0.001**	**<0.001**
91T	42	9.1 ± 0.6	vs	02cx	12	7.7 ± 1.4	0.052	**0.038**	0.051	**0.049**
91bg	50	12.2 ± 0.4	vs	02cx	12	7.7 ± 1.4	**0.001**	**<0.001**	**0.001**	**0.002**

Notes. The explanations for the P-values are identical to those in Table 2.2. The statistically significant difference between the distributions is highlighted in bold.

3.3.4 Luminosity-weighted ages of SNe Ia host galaxies

In order to move from the qualitative description of the progenitor population ages of the SN Ia subclasses to the quantitative ones, we determine the luminosity-weighted ages of their host galaxies.[13] To conform to values used in the Chapter 4, we use the fixed redshifts of the galaxies to fit the PÉGASE.2 templates library [220, 221], comprised of various morphological/spectral types, to the measured *ugriz* photometry of SN hosts. Five photometric values of a host galaxy (in some cases only four *griz* band values are available, see Subsection 3.2.2) and its fixed redshift are used to select the best locations of the values on the spectral energy distribution (SED) templates. Accordingly, the best matched SED model and corresponding luminosity-weighted age can be used from the collection of all possible synthetic templates for different galaxy ages (up to 19 Gyr). The luminosity-weighted stellar population ages are very sensitive to recent star formation, i.e. bright young stellar populations get more weight in the estimated ages. An example of SN Ia host galaxy photometry with its best template, and more information on the SED fitting method can be found in [135].

In the upper panel of Fig. 3.9, we present the cumulative distributions of luminosity-weighted ages of normal and peculiar (91T-, 91bg-, and 02cx-like) SNe Ia host galaxies. Note that only about 10% of the host galaxies in our sample have very late-type morphologies (Scd–Sm, see

[12]The elongations (b/a) of host galaxies are obtained from the fitted 25 mag arcsec^{-2} elliptical apertures in the g-band (see Subsection 3.2.2).

[13]The luminosity-weighted ages of host galaxies are available online in [191].

Table 3.12: Results of Spearman's rank correlation test for the B-band Δm_{15} values of the SN Ia subclasses versus luminosity-weighted ages of host galaxies.

SN subclass	$N_{\rm SN}$	Variable 1	vs	Variable 2	$r_{\rm s}$	$P_{\rm s}$
normal	303	Δm_{15}	vs	host age	0.314	**<0.001**
normal[a]	189	Δm_{15}	vs	host age	0.161	**0.027**
normal[b]	64	Δm_{15}	vs	host age	−0.059	0.644
91T	42	Δm_{15}	vs	host age	0.154	0.330
91bg	50	Δm_{15}	vs	host age	0.082	0.569
02cx	12	Δm_{15}	vs	host age	−0.264	0.406

Notes. The explanations for $r_{\rm s}$ and $P_{\rm s}$-values are the same as in Table 2.6. [a] $\Delta m_{15} \lesssim 1.26$ mag, similar to 91T-like SNe. [b] $\Delta m_{15} \gtrsim 1.38$ mag, similar to 91bg-like events. Statistically significant correlations between the variables are highlighted in bold.

Table 3.4) that generally exhibit stellar populations younger than a few Gyr [159]. Therefore, we have a deficit of hosts with ages less than a few Gyr in our age calculations. The two-sample KS and AD tests in Table 3.11 show that the age distribution of normal SNe Ia hosts is consistent with that of 91T-like SNe hosts, but significantly inconsistent with those of 91bg- and 02cx-like SNe hosts. In comparison with hosts of normal and 91T-like SNe, the ages of 91bg-like SNe hosts are older on average, while the ages of hosts of 02cx-like events are younger. These results are expected in light of those in Fig. 3.6 and Table 3.8, when considering the $u-r$ colour as a proxy for recent star formation or stellar population ages of galaxies.

In the bottom panel of Fig. 3.9, we show the distribution of the B-band Δm_{15} values of the SN Ia subclasses as a function of luminosity-weighted ages of host galaxies. In analogy with the results in Table 3.9, the Spearman's rank test, presented in Table 3.12, shows that the significant correlation exists only between normal SNe Ia LC decline rates and stellar population ages of their host galaxies. These SNe Ia show an average increase in Δm_{15} values with an increase in host's age. Using the SN Ia LC stretch instead of Δm_{15}, similar correlations between the SN LC and host parameters have been shown many times in the literature [69, 74, 76, 82, 212, 222]. The samples of these studies mostly include normal SNe Ia events, thus not studying separately the correlations for peculiar (91T-, 91bg-, and 02cx-like) SN Ia subclasses. While, importantly we show that these peculiar SNe Ia subclasses originate from host galaxies diverging in age (Table 3.11), however taken separately their LC decline rates do not show dependencies on host galaxy age, contrary to normal SNe Ia events (Table 3.12). These results are in good support of those obtained in Subsections 3.3.2-3.3.3 that 91bg-like SNe come only from old stellar population of hosts, while 91T-like events originate only from young population of galaxies, thus likely belonging to two unique classes of progenitors.

In Table 3.12, for normal SNe Ia we check for the Δm_{15} – age correlation in the two separate and narrower Δm_{15} ranges. In the slower declining range, normal SNe Ia keep the Δm_{15} – age trend direction and significance, while in the faster declining range, the trend becomes insignificant, hinting that the Δm_{15} ranges and/or small number statistics might play some role in the absence of the Δm_{15} – age trend for 91T- and 91bg-like SNe.

Interestingly, to study the connection between SNe Ia and their host characteristics, [79] estimated the hosts' global stellar population ages as well as the local environment ages around the sites of photometrically and spectroscopically classified SDSS II SNe Ia (103 events, $z < 0.2$). The authors noted that the significant correlation between SN Ia LC properties/luminosity and host stellar population age might be an effect of age step at ~ 8 Gyr (corresponding to the jump in the average LC properties). [79] also noted that both the local environment age and global one show the equivalent correlations with the SNe properties, however, as expected, the age of the local stellar population is younger than that of the global one for SN Ia in star-forming environments. With that in mind, we split the sample of normal SNe Ia into two subsamples according to the host age step at 8 Gyr, and compare the Δm_{15} distributions between the subsamples ($N_{\rm SN} = 107$, $\langle \Delta m_{15} \rangle = 1.10 \pm 0.02$ for host age ≤ 8 Gyr versus $N_{\rm SN} = 196$, $\langle \Delta m_{15} \rangle = 1.24 \pm 0.02$ for host age > 8 Gyr). The two-sample KS and AD tests show that the Δm_{15} distributions are significantly inconsistent between each other ($P_{\rm KS}^{\rm MC} < 0.001$, $P_{\rm AD}^{\rm MC} < 0.001$). As expected from Fig. 3.9 and Table 3.12, galaxies with ages ≤ 8 Gyr host on average slower declining/brighter SNe Ia (spectroscopically normal) in comparison with older hosts (see also [58]). Note that a 3 Gyr variation in the host age step does not change the statistical behaviour of the tests. Thus, the significant correlation seen in Table 3.12 is due to a superposition of faster and slower declining normal SNe Ia from older and younger stellar components of hosts, respectively (see also [83] as measured by the environmental Hα emission at the positions of SNe Ia).

This result can be explained considering the correlation between ^{56}Ni mass synthesized in SN Ia and host galaxy age [73]. In this respect, [69] suggested that the details of the ^{56}Ni mass – age correlations in their study and in [73] imply an age step/threshold of about several Gyr for SN Ia hosts, above which galaxies are less likely to produce SNe Ia with ^{56}Ni masses $\gtrsim 0.5 M_{\odot}$, i.e. slower declining/brighter events.

It is important also to mention that the Δm_{15} – morphology, Δm_{15} – colour, and Δm_{15} – $\log(M_{*}/\mathrm{M}_{\odot})$ correlations, we showed in previous subsections for spectroscopically normal SN Ia, and the Δm_{15} – age correlation agree with one another in the sense that host galaxy morphology, colour, mass, and age are correlated, with older galaxies mainly being earlier type, redder, and more massive [159]. Therefore, the previously reported correlations between LC properties of SNe Ia and physical parameters of their host galaxies are most likely originated from the differences in host stellar population ages (see also earlier discussions in [71, 74, 79, 82, 83]).

3.3.5 Constraints on delay time distributions of SNe Ia

Current theoretical models of spectroscopically normal SNe Ia progenitors predict that most likely their DTD peaks below/close to 1 Gyr, corresponding to the young/prompt component, then declines fast by over two orders of magnitude at several Gyr [71, 223, 224]. At redshifts near zero (as in our sample), the SN Ia rate in evolved galaxies, from a large volume, results in a bimodal shape of the distribution of SN Ia progenitor ages, with assumption that galaxies have nearly constant SFR [71]. In such a bimodal age distribution, the second peak includes old/delayed events at current epoch, which are naturally absent at high redshifts. Young/prompt SNe Ia originate in actively star-forming galaxies, predominantly from progenitors whose ages correspond to the first peak of the SN Ia progenitor age distribution. While old/delayed SNe Ia originate in galaxies that already have an old stellar component or they are entirely old whose star formation ceased in the past. In such old stellar systems, the DTD is lacking young/prompt events, meaning that delayed SNe Ia occur from different age group of progenitors [19, 71]. In this respect, the significant correlation between the LC decline rates and the global host galaxy ages of normal SNe Ia (see Subsection 3.3.4) is likely caused by the bimodal behaviour of the age distribution of normal SN Ia progenitors, which includes both the prompt events from young progenitors (slower declining SNe Ia) and delayed SNe Ia from old systems (faster declining events). On the other hand, the absence (non-significance) of the mentioned correlation for peculiar (91T-, 91bg-, and 02cx-like) SNe Ia and the observed differences in the properties of their host galaxies (see Subsections 3.3.2 and 3.3.3) can be considered as evidences for distinct (single-mode) behaviours of their progenitor age distribution, thus distinct progenitor channels.

Our results on peculiar 91bg-like events agree with those of [70], who found that subluminous/91bg-like SNe (18 events with $z \leq 0.6$) in their photometrically identified SNe sample are mainly found in early-type hosts with almost no star formation, and argued that these SNe come from a delayed progenitor component with a Gaussian DTD centered around 6 Gyr, but with large uncertainty up to ~ 11 Gyr. Recently, [162] studied integral field observations of the hosts' explosion sites of 11 spectroscopically identified 91bg-like events ($z \leq 0.04$) and found that the majority of the stellar populations in the vicinity of these SNe locations are dominated by old stars with a lack of recent star formation. The authors concluded that the DTD of 91bg-like SNe is likely weighted toward long delay times, larger than ~ 6 Gyr [171]. Most recently, in [135] we found that in elliptical host galaxies of SNe Ia, the age distribution of 91bg-like SNe hosts ($\gtrsim 8$ Gyr) does not extend down to the stellar ages that produce significant u-band fluxes of their early-type hosts, contrary to the hosts of normal SNe Ia. Therefore, younger stars in elliptical galaxies do not produce 91bg-like SNe.

Our study includes the largest sample of 50 subluminous 91bg-like SNe in a much wider morphological range of host galaxies than previous studies, and shows even more clearly that the progenitor population age of these events is strongly weighted toward very old ages (oldest among the other SN Ia subclasses, see Table 3.11 and Fig. 3.9). More than 85% of 91bg-like SNe hosts are older than 8 Gyr. As already mentioned, such delay times are much longer than the delays of normal Type Ia SNe from star-forming environments, whose DTD peaks between several hundred Myr and ~ 1 Gyr (a sharp initial peak) with a low tail at higher delay times [71]. Therefore, most likely 91bg-like events originate exclusively from old stellar population of host galaxies, and thus these peculiar SNe Ia have no prompt component.

As in [135], we favour the DD channel for the progenitors of these peculiar events that belong to the old stellar components of galaxies [21, 225, 226]: in particular the progenitor models such as He-ignited violent mergers (CO WD primary with He WD companion) might be appropriate for 91bg-like events [171, 172]. These models predict very long delay times for subluminous 91bg-like SNe ($\gtrsim$ several Gyr). On the other hand, the DD channel with CO WD primary and CO WD companion [172] can provide an appropriate DTD for normal SNe Ia with an initial peak below/close to 1 Gyr and a tail up to about 10 Gyr, while most SD models predict few or no SNe Ia at long delays [19, 71]. In addition, [227] showed that mergers of CO WD with hybrid He-CO WD could also give rise to normal Type Ia SNe whose synthetic LCs and spectra are consistent with those of observed SNe Ia (see also [228] for the properties of hybrid He-CO WDs). These authors noted that together with the contribution from mergers of massive double CO WDs that give rise to more luminous SNe Ia, their models can potentially reproduce the full range of normal SNe Ia, their DTD and rate.

Relatively younger global host ages of overluminous 91T-like SNe (Fig. 3.9) can be explained in the context of shorter DTD in comparison with that of 91bg-like events. In addition, 91T-like SNe strongly prefer blue (Fig. 3.6) and late-type hosts (Fig. 3.4), and no such an event is observed in old elliptical galaxies (Table 3.4), thus supporting shorter, i.e. relatively prompt DTD for these SNe. In this sense, the DTD of the SD channel is different from that of DD one and can be appropriate for 91T-like SNe [229]. The DTD of SD channel has a sharp cutoff at 2-3 Gyr, because in its original formulation a donor/companion star in an SD system is a main sequence or red giant star with only a narrow range of masses that could provide mass accretion at the sufficient rate resulting in a stable burning and an explosion of WD [230]. Also, note that massive CO WD primaries in DD models are naturally explode in more luminous SNe Ia (e.g. overluminous/91T-like events). Such massive WDs, which originated from more massive intermediate-mass stars, in DD systems have delay times $\lesssim$ several hundred Myr (e.g. the violent WDs merger scenario; [161]), and is therefore expected in late-type star-forming galaxies.

These DTDs may seem too young in comparison with the global age distribution of hosts (see Fig. 3.9 and Table 3.11), however, as mentioned in Subsection 3.3.4 for normal SN Ia in star-forming environments, the age of the local stellar population at the SN position is younger (on average) than the global age of its host galaxies [79]. Therefore, in an ideal case, the stellar population age obtained from the location of the SN in the host galaxy would be preferable to the global host age that we estimate in the current study (see also discussions in [74, 229]). Consequently, additional local age-estimations are needed for 91T-like SNe to better test the DTDs of the SD and DD progenitors models.

Despite the small number statistics of 02cx-like SNe, on average their host galaxies have the youngest global ages (Fig. 3.9), latest morphology (Fig. 3.4), bluest colour and lowest masses (Fig. 3.6) among the other SN Ia subclasses, again strongly pointing to a shorter DTD for the events. In our sample the host galaxy properties of 02cx-like SNe are close to those of star-forming hosts of 91T-like SNe [109, 193], however, their LC decline rates are significantly different from those of 91T-like events (Fig. 3.3 and Table 3.5) and fall off the SN Ia LC width-luminosity relation [25]. The properties of 02cx-like SNe and evidence of their short DTD suggest a binary system where 02cx-like SN arises from massive CO WD that quickly accretes helium from an He-star donor [231]. Then accretion-triggered explosion of a Chandrasekhar mass WD does not necessarily fully disrupt the star. Among a variety of proposed scenarios, this is now the leading model (see review by [26] and references therein). This channel might be the dominant one for delays of up to a few hundred Myr, above which hydrogen-accreting SD and DD systems dominate [232]. Again, the stellar population ages obtained at the locations of 02cx-like SNe in the host galaxies would be preferable to the global host ages to better test the DTD of the leading model.

3.4 Chapter Conclusions

In this Chapter, using a well-defined sample of Type Ia SNe and their host galaxies, we comparatively analyse the relations between the LC decline rates and the global properties of hosts of various SN Ia subclasses to better understand the diverse nature of SNe Ia progenitors. The spectroscopic subclasses of SNe Ia (normal, 91T-, 91bg-, and 02cx-like) and their B-band LC decline rates (Δm_{15}) are carefully compiled from the available literature, while the data of the SNe Ia host galaxies is a homogeneous set of consistent measurements performed by the authors of this study. Our sample consists of 394 relatively nearby ($\leq$ 150 Mpc, the mean distance is 72 Mpc) E–Sm galaxies, which host 407 SNe Ia in total.

There is no strong redshift bias within our sample, which could drive the observed relations between global properties of hosts and extinction-independent LC decline rates of the SN Ia subclasses. In addition, the representation of SN subclasses in our compilation and in nearly complete volume-limited sample of the LOSS are not different statistically. However, due to the small number statistics of 02cx-like SNe, the results on these peculiar events and their hosts should be considered with caution.

All the obtained results and their interpretations are summarized below.

1. In general, the B-band Δm_{15} distribution of SNe Ia seems to be bimodal (Fig. 3.3), with the second (weaker) mode mostly distributed within ~ 1.5 to 2.1 mag. This faster declining range is generally occupied by 91bg-like (subluminous) events, while the Δm_{15} of 91T-like (overluminous) SNe are distributed only within the first mode at slower declining range ($\Delta m_{15} \lesssim 1.1$ mag). The decline rates of 02cx-like SNe are spread on the faster side of the Δm_{15} distribution of normal SNe Ia. Statistically, all these distributions are significantly different from one another (Table 3.5).

2. The host galaxies of normal, 91T-, and 91bg-like SNe Ia have morphological type distributions that are significantly inconsistent between one another (Fig. 3.4 and Table 3.6). Hosts of 91bg-like SNe have, on average, earlier morphological types ($\langle t \rangle \approx 0$) with a large number of the events discovered in E–S0 galaxies. While hosts of 91T-like SNe have on

average later morphological types ($\langle t \rangle \approx 4$) with a single 91T-like event in the E–S0 bin (Table 3.4). The same distribution of hosts of normal SNe Ia occupies an intermediate position between the host morphologies of 91T- and 91bg-like events. The morphological distribution of 02cx-like SNe hosts is similar to that of 91T-like SNe hosts.

3. As for galaxies in general, the distribution of SNe Ia hosts in the $u-r$ colour–mass diagram is bimodal (Fig. 3.5). The hosts of 91bg-like SNe are located in the Red Sequence of the diagram, most of them have $u-r$ colours $\gtrsim 2$ mag (i.e. above the Green Valley). In comparison with hosts of normal, 91T-, and 02cx-like SNe, the colour distribution of hosts of 91bg-like SNe are significantly redder (Table 3.8). Importantly, the bulk of hosts of 91bg-like SNe are significantly massive ($\log(M_*/\mathrm{M}_\odot) > 10.5$) and old (more than 10 Gyr). The hosts' mass (age) distribution is significantly inconsistent with those of the other SN Ia subclasses (Tables 3.8 and 3.11). At the same time, the colour (mass, age) distributions are not statistically different between hosts of normal and 91T-like SNe. Finally, all the host galaxies of 02cx-like SNe are positioned in the Blue Cloud of the colour–mass diagram, mostly below the Green Valley (Fig. 3.6). Their colour (mass, age) distribution is significantly bluer (lower, younger) in comparison with that of normal SNe Ia hosts, but closer to that of 91T-like SNe hosts.

4. As previously shown with smaller nearby SN Ia samples, there is a significant correlation between normal SNe Ia LC decline rates and global ages (morphologies, colours, and masses) of their host galaxies (Tables 3.9 and 3.12). On average, those normal SNe Ia that are in galaxies above the Green Valley, i.e. in early-type, red, massive, and old hosts, have faster declining LCs in comparison with those in galaxies below the Green Valley, i.e. in late-type, blue, less massive, and younger hosts (Tables 3.7 and 3.10). The results suggest that the observed correlations between normal SNe Ia LC decline rates and global properties of host galaxies are due to a superposition of at least two distinct populations of faster and slower declining normal SNe Ia from old (halo/bulge and old disc) and young (star-forming disc) components of hosts, respectively dominating in the

Red Sequence and Blue Cloud of the colour–mass diagram.

5. For the first time we show that the LC decline rates of subluminous/91bg-like SNe and overluminous/91T-like events do not show dependencies on the host galaxy morphology and colour (Figs. 3.4, 3.7, and Table 3.9). The distribution of hosts on the colour–mass diagram (Fig. 3.6) confirms the known tendency for 91bg-like SNe to occur in globally red/old galaxies (from halo/bulge and old disc components) while 91T-like events prefer blue/younger hosts (related to star-forming component). Probably, the decline rates of 02cx-like SNe also do not show dependencies on hosts' properties. On average, the youngest global ages of 02cx-like SNe hosts and their positions in the colour–mass diagram hint that these events likely originate from the young stellar component, but they differ from 91T-like events in the LC decline rate.

6. As in [135], for the progenitors of 91bg-like events we favour the DD channel, in particular the progenitor models such as He-ignited violent mergers (CO WD primary with He WD companion, e.g. [171,172]). In agreement with our findings, these models predict very long delay times for subluminous 91bg-like SNe ($\gtrsim$ several Gyr). In addition, the DD channel with CO WD primary and CO (or hybrid He-CO) WD companion [172, 227] can provide an appropriate DTD for normal SNe Ia with an initial peak below/close to 1 Gyr and a tail up to about 10 Gyr [19, 71]. On the other hand, the DTD of the SD channel has a sharp cutoff at 2-3 Gyr [230] and can be appropriate for 91T-like SNe. Note that massive CO WD primaries in DD models are naturally explode in more luminous SNe Ia and also can be appropriate for these overluminous events [161]. Also, we show evidence of short DTD for 02cx-like SNe, which can be interpreted within the leading model for the events (a binary system where SN arises from massive CO WD that quickly accretes helium from an He-star donor, and then explosion of WD does not necessarily fully disrupt the star, e.g. [231]).

Chapter 4

Normal Type Ia and 91bg-like SNe in ellipticals

4.1 Introduction

In this Chapter, we morphologically select from the SDSS only elliptical host galaxies of SNe Ia, which are known to have the simplest structural properties of the composition in comparison with lenticular and spiral galaxies [233]. In these galaxies no 91T-like events have been discovered, they mostly host normal and 91bg-like SNe [67]. Therefore, these two subclasses of Type Ia SNe are the subject of study in this Chapter.

Recall that the 91bg-like SNe are unusually red and have peak luminosities that are 2 ± 0.5 magnitudes lower than do normal SNe Ia (the typical peak magnitude of normal SNe Ia is $M_B \simeq -19.1$ mag, see [234] and references therein. They have faster declining LCs $1.8 \lesssim \Delta m_{15} \lesssim 2.1$, compared with $\Delta m_{15} \lesssim 1.7$ for normal events, and their ejecta velocities are small at any epoch in comparison with normal SNe Ia [90, 235]. In the post-maximum spectra, particularly notable is the presence of unusually strong O I λ 7774 and Ti II absorption lines. Despite the recent detection of strong Hα in the nebular spectrum of ASASSN-18tb (a 91bg-like event; [236]), there is no evidence that fast declining SNe are more likely to have late time Hα emission [237]. For more details of the spectra and LC properties of 91bg-like events, the reader is referred to [25].

The explosion mechanism, which should explain the main characteristics of these events, including the low ^{56}Ni masses, is still under debate. The DD scenario, the helium layer detonation triggered sub-Chandrasekhar mass explosion, and the scenario of collision of two WDs are competing [171, 172, 238–240].

In the earlier literature, several attempts have been done to study the projected radial and surface density distributions of nearby SNe Ia in morphologically selected elliptical host galaxies [12, 241–243]. These studies showed that, in general, the distribution of Type Ia SNe is consistent with the light (de Vaucouleurs) profile of their elliptical host galaxies, which are dominated by old and metal-rich stellar populations [159]. However, mainly because of the lack of the spectral and LC data, these studies did not separate the normal and 91bg-like subclasses. For the first time, [92] attempted to compare the surface density distributions of the subclasses of nearby SNe Ia, in particular for those of the normal and 91bg-like events. However, the morphological types of SN hosts were not limited to elliptical galaxies only, thus mixing different progenitor populations from bulges and discs [81, 162].

On the other hand, [81] studied optical absorption-line spectra of 29 early-type host galaxies of local SNe Ia and found a higher specific SN rate in E–S0 galaxies with ages below 3 Gyr than in older hosts. Recall that the rate of Type Ia SNe can be represented as a linear combination of "prompt" and "delayed" (tardy) components [244]. The prompt component is more closely related with the recent SFR, and the delayed component with the total stellar mass of galaxy [245–248]. Therefore, according to [81], the higher rate seen in the youngest E–S0 hosts may be a result of recent star formation and represents a tail of the prompt SN Ia progenitors.

Recently, [162] analysed the explosion sites of eleven spectroscopically identified nearby 91bg-like SNe in hosts with different morphologies (including only six E–S0 galaxies) and found that the majority of the stellar populations that host these events are dominated by old stars with lack of recent star formation evidence. These authors concluded that the 91bg-like SN progenitors are likely to have delay times, i.e. the time intervals between the SN Ia progenitor formation and the subsequent thermonuclear explosion, much longer (> 6 Gyr, see also [171]) than the typical delay times of normal SNe Ia in star forming environments, whose delay times peak between several hundred Myr and ~ 1 Gyr [19, 71].

The goal of this Chapter is to properly address these questions through a comparative study of the galactocentric distributions of normal and 91bg-like SNe, as well as through an analysis of the global properties of SNe Ia hosts (e.g. stellar mass, metallicity, colour and age of stellar population) in a well-defined and morphologically non-disturbed sample of more than 100 relatively nearby elliptical galaxies.

4.2 Sample selection and reduction

For this Chapter, we used the updated versions of the ASC [104] and Open Supernova Catalog [150] to include all spectroscopically classified Type Ia SNe with distances ≤ 200 Mpc ($0.003 \leq z \leq 0.046$),[1] discovered before 9 October 2018. All SNe are required to have equatorial coordinates and/or offsets (positions in arcsec) with respect to host galactic nuclei. We cross-matched these coordinates with the coverage of the SDSS DR15 [249] to identify the host galaxies with elliptical morphology, using the techniques presented in [102]. Many of the identified SNe Ia host galaxies are already listed in database of [102], which is based on the SDSS DR8. However, because we added new SNe Ia, for homogeneity we redid the whole reduction for the sample of elliptical host galaxies of this study based only on DR15.

Following the approach of [105], we checked also the levels of morphological disturbances of the host galaxies using the SDSS images. Because we are interested in studying the distribution of SNe Ia in non-disturbed elliptical galaxies, the hosts with interacting, merging, and post-merging/remnant attributes are removed from the sample.

For three SNe (1980I, 2008gy and 2018ctv), the almost equality of projected distances from the few nearest elliptical galaxies did not allow to unambiguously assign them to certain hosts. Therefore, we simply excluded these objects from our sample.

[1] Following [102], to calculate the luminosity distances of SNe/host galaxies, we used the recession velocities both corrected to the centroid of the Local Group [250], and for infall of the Local Group toward Virgo cluster [251, 252].

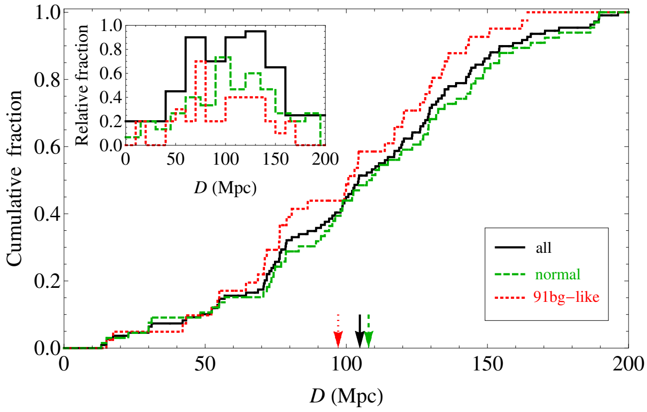

Figure 4.1: Cumulative and relative (inset) fractions of 109 Type Ia SNe (all – black solid, normal – green dashed, and 91bg-like – red dotted) in elliptical galaxies as a function of distance. The mean values of the distributions are shown by arrows.

For the remaining SNe Ia that satisfy the above-mentioned criteria, we carried out an extensive literature search to collect their spectroscopic subclasses (e.g. normal, 91T-like, 91bg-like and other peculiar events). To accomplish this, we mainly used the Weizmann Interactive Supernova data REPository [151], which is an interactive archive of SN spectra and photometry, including data of historical events and ongoing surveys/programs. The archive provides also the important references to the original publications, which we considered along with the Astronomer's Telegram, website of the Central Bureau for Astronomical Telegrams and other supporting publications [27, 180, 253]. In total, we managed to collect the subclasses for 109 SNe in 104 host galaxies: 66 SNe are normal, 41 SNe are 91bg-like, and two SNe are 06gz-like (super-Chandrasekhar) events. As expected [67, 68], 91T-like events have not been discovered in elliptical galaxies. On the other hand, less than a dozen of 06gz-like SNe have been discovered so far, and they have a tendency to explode in low-mass (low-metallicity) late-type galaxies [195]. Therefore, they are not the subject of our study, and because of only two such objects in our sample, further in the article we do not specifically discuss these events and their hosts, instead we just present them for illustrative purpose.

It is important to note that in this sample of SNe Ia only seven normal events ($\sim 6\%$ of objects: 1939A, 1957B, 1970J, 1981G, 1982W, 1993ae, and 1993C) were discovered photographically, while all the other 102 SNe were discovered by visual or mostly CCD searches.

Fig. 4.1 shows the distributions of relative and cumulative fractions of the subclasses of Type Ia SNe as a function of distances. As was mentioned, the 91bg-like SNe have peak luminosities that are ~ 2 magnitudes lower than do normal SNe Ia (see [234] and references therein), therefore the discoveries of 91bg-like events might be complicated at greater distances. The mean distances of all, normal and 91bg-like SNe are 105, 108 and 97 Mpc with standard deviations of 43, 44 and 38 Mpc, respectively. Meanwhile, the two-sample KS and AD tests showed that the distance distributions of normal and 91bg-like events are not significantly different ($P_{\rm KS} = 0.404$, $P_{\rm AD} = 0.238$) and could thus be drawn from the same parent distribution. Therefore, our subsamples of normal and 91bg-like SNe and their host galaxies should not be strongly affected by the redshift-dependent biases against or in favour of one of the SN subclasses.

We measured the photometry and geometry of the 104 host galaxies according to the approaches presented in [102]. For each host galaxy, we used the fitted 25 mag arcsec^{-2} elliptical aperture in the SDSS g-band to obtain the major axis (D_{25}), elongation (a/b), and PA of the major axis relative to North in the anticlockwise direction. The classification of hosts includes also the ratio $10(a-b)/a$: for a projection of a galaxy with a equal to b, the ratio is 0 and the morphological type is E0. There are only one E5 and ten E4 host galaxies ($\sim 10\%$ of the sample). The rest of the galaxies are almost evenly distributed in E0–E3 bins. The mean D_{25} of the hosts is 129 arcsec with the minimum value of 21 arcsec. The corresponding u-, g-, r-, i- and z-band fluxes (apparent magnitudes[2]) are measured using the g-band fitted elliptical aperture. During the measurements, we masked out bright projected and/or saturated stars. The apparent/absolute magnitudes and D_{25} values are corrected for Galactic extinction using the [187] recalibration of the [188] infrared-based dust map. These values are not corrected for host galaxy internal extinction because ellipticals have almost no global extinction, with mean $A_V = 0.01 \pm 0.01$ mag [159]. Since the redshifts of host galaxies are low ($z \leq 0.046$), the accounted K-corrections for the magnitudes are mostly negligible and do not exceed 0.2 mag in the g-band. The D_{25} values are also corrected for inclination/elongation effect [189].

[2]All magnitudes are in the AB system such that $u_{\rm AB} = u - 0.04$ mag and $z_{\rm AB} = z + 0.02$ mag (g, r and i are closer to AB system, see https://www.sdss.org/dr15/algorithms/fluxcal/).

In an elliptical galaxy the real galactocentric distance of SN can not be calculated using the SN offset from the host galaxy nucleus ($\Delta\alpha$ and $\Delta\delta$). Instead, we can only calculate the projected galactocentric distance of a SN ($R_{\rm SN} = \sqrt{\Delta\alpha^2 + \Delta\delta^2}$), which is the lower limit of the real galactocentric distance.[3] Following [1], we used the relative projected galactocentric distances ($\widetilde{R}_{\rm SN} = R_{\rm SN}/R_{25}$), i.e. normalized to $R_{25} = D_{25}/2$ in the g-band.

However, for the normalization, the effective radius ($R_{\rm e}$) could be more relevant being tighter correlated with the stellar surface density distribution or surface brightness profile of the host galaxy in comparison with the R_{25} photometric radius [233]. For elliptical galaxies, the surface brightness (I) profiles are described by the Sérsic law [254]:

$$I(R\,|R_{\rm e}) = I_0 \exp\left\{-b_{\rm n}\left(\frac{R}{R_{\rm e}}\right)^{\frac{1}{n}}\right\}, \tag{4.1}$$

where $R_{\rm e}$ is the radius of a circle that contains half of the light of the total galaxy (also known as half-light radius), I_0 is the central surface brightness of the galaxy, n is the Sérsic index, defining the shape of the profile. An analytical expression that approximates the $b_{\rm n}$ parameter is $b_{\rm n} \simeq 1.9992\,n - 0.3271$ [255]. When $n = 4$, the profile, which is called de Vaucouleurs profile, sufficiently describes the surface brightness distribution of elliptical galaxies [256]. Therefore, following [12], we also normalized $R_{\rm SN}$ to the $R_{\rm e}$ radii of host galaxies ($\widehat{R}_{\rm SN} = R_{\rm SN}/R_{\rm e}$).

The g-band $R_{\rm e}$ radii (in arcsec) of our host galaxies are extracted from the SDSS where a detailed photometric analysis of galaxies is performed [257]. Their pipeline fitted galaxies with a de Vaucouleurs profile and an exponential profile,[4] and asked for the linear combination of the two that best-fitted the image, providing the $R_{\rm e}$ and parameter `fracDeV`, which is the fraction of fluxes contributed from the de Vaucouleurs profile. An elliptical galaxy with a pure de Vaucouleurs profile should have `fracDeV` $= 1$, and a galaxy with pure exponential profile should have `fracDeV` $= 0$. In our morphologically selected sample of hosts, most (about 90%) of the galaxies have `fracDeV` > 0.8, where `fracDeV` $= 0.8$ roughly corresponds to S0

[3] In several cases when SNe offsets were not available in the above-mentioned catalogues, we calculated $\Delta\alpha$ and $\Delta\delta$ by $\Delta\alpha \approx (\alpha_{\rm SN} - \alpha_{\rm g})\cos\delta_g$ and $\Delta\delta \approx (\delta_{\rm SN} - \delta_{\rm g})$, where $\alpha_{\rm SN}$ and $\delta_{\rm SN}$ are SN coordinates and $\alpha_{\rm g}$ and $\delta_{\rm g}$ are host galaxy coordinates in equatorial system.

[4] The Sérsic index of $n = 1$ represents the exponential profile of S0–Sm galactic discs [258].

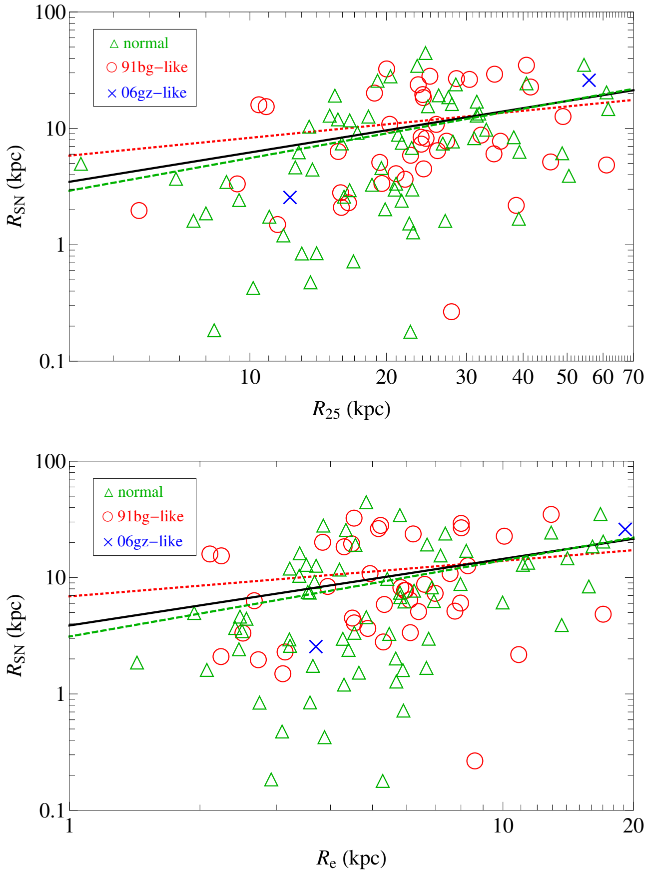

Figure 4.2: Upper panel: comparison of the projected galactocentric distances of SNe Ia and R_{25} of elliptical host galaxies in kpc. Green triangles, red circles and blue crosses show normal, 91bg-like and 06gz-like SNe, respectively. Black solid (all), green dashed (normal) and red dotted (91bg-like) lines are best-fits to the samples. Bottom panel: same as in upper panel but for R_{SN} versus R_e.

galaxies [259]. Only for 14 host galaxies (mostly with $D_{25} > 200$ arcsec), the SDSS lacks the mentioned model fits or provides unreliable parameters due to the blending/defragmenting of galaxies with large angular sizes. For these 14 galaxies, we used our estimations of half-light radii based on the SDSS g-band images.

The R_{25}- and R_e-normalizations are crucial for studying the projected radial distribution of SNe, because the distribution of linear values of R_{SN} is strongly biased by the greatly different intrinsic sizes of elliptical hosts. Fig. 4.2 illustrates the dependencies of the R_{SN} on R_{25} and R_{SN} on R_e of host galaxies in kpc. The best-fits from Fig. 4.2 and results of the Spearman's rank correlation test for R_{SN} versus R_{25} and for R_{SN} versus R_e (regardless of log or linear scales) are presented in Table 4.1. The Spearman's rank test indicates significant positive trends ($r_s > 0$)

Table 4.1: The best-fits from Fig. 4.2 with results of the Spearman's rank correlation test.

		$\log(R_{\rm SN}[\rm kpc]) = a + b\,\log(R_{25}[\rm kpc])$			
SN subclass	$N_{\rm SN}$	a	b	$r_{\rm s}$	P
all	109	0.16 ± 0.25	0.63 ± 0.17	0.457	$\mathbf{6 \times 10^{-7}}$
normal	66	0.04 ± 0.32	0.70 ± 0.22	0.481	$\mathbf{4 \times 10^{-5}}$
91bg-like	41	0.53 ± 0.44	0.39 ± 0.30	0.316	**0.044**
		$\log(R_{\rm SN}[\rm kpc]) = a + b\,\log(R_{\rm e}[\rm kpc])$			
all	109	0.59 ± 0.13	0.57 ± 0.14	0.364	$\mathbf{10^{-4}}$
normal	66	0.49 ± 0.17	0.65 ± 0.19	0.414	$\mathbf{5 \times 10^{-4}}$
91bg-like	41	0.84 ± 0.23	0.30 ± 0.28	0.162	0.313

Notes. The explanations for $r_{\rm s}$ and $P_{\rm s}$-values are the same as in Table 2.6. The statistically significant correlations (P-values ≤ 0.05) are highlighted in bold.

between the $R_{\rm SN}$ and R_{25} for all, normal and 91bg-like SNe, as well as between the $R_{\rm SN}$ and $R_{\rm e}$ for all and normal SNe Ia. Only for 91bg-like SNe in the latter case, the trend is positive again but not statistically significant. In the remainder of this study, we use only normalized projected galactocentric radii of Type Ia SNe, i.e. $\widetilde{R}_{\rm SN} = R_{\rm SN}/R_{25}$ and $\widehat{R}_{\rm SN} = R_{\rm SN}/R_{\rm e}$.

In addition, we measured the integrated g-band flux of the concentric elliptical aperture, which crosses the position of a SN, with the same elongation and PA as the host galaxy aperture. We then normalized this flux to the total flux contained within an elliptical aperture, retaining the same elongation and PA, out to distances where the host galaxy flux is consistent with the sky background values. This fractional radial g-band flux is commonly referred as Fr_g and can have values between 0 and 1, where a value of 0 means that an SN explodes at the center of its host, while a value of 1 means that the SN explodes at distances where no significant galaxy flux is detected, i.e. at the edge of the galaxy. As will be presented in Subsection 4.3.3, the distribution of Fr_g values allows to compare the radial distribution of SNe Ia with respect to that of the g-band light of host galaxies, irrespective of their different elongations and Sérsic indices (elliptical galaxies can have $n \approx 2$ to 6 in the g-band, see e.g. [260, 261]). Note that 15 SNe, which are located far outside the elliptical apertures where fluxes are consistent with the sky background values, are removed from the Fr_g analysis in Subsection 4.3.3.[5] For a complete

[5]Their inclusion would artificially increase the number of SNe Ia in the fractional radial flux distribution at $Fr_g = 1$ (see Subsection 4.3.3).

description of the adopted methodology of Fr_g measurement, the reader is referred to [262] and [263].

The full database of 109 individual SNe Ia (SN designation, subclass, source of the subclass, offset from host galaxy nucleus, and fractional radial g-band flux) and their 104 elliptical hosts (galaxy SDSS designation, distance, a/b, PA, $R_{\rm e}$, corrected D_{25} and u-, g-, r-, i-, z-band absolute magnitudes) is available online [264].

4.3 Results

With the aim of finding possible links between the properties of SN progenitors and host stellar populations of elliptical galaxies, we now study the distributions of projected and normalized galactocentric distances and fractional radial fluxes of the subclasses of Type Ia SNe (normal and 91bg-like events). In this section, we also study the possible differences of global properties (absolute magnitudes, colour, R_{25} and $R_{\rm e}$) and estimates of the physical parameters (stellar mass, metallicity and age) of the stellar population of elliptical galaxies in which the different subclasses of SNe Ia are discovered.

4.3.1 Directional (major vs. minor axes) distributions of SNe Ia in elliptical host galaxies

Because the elliptical host galaxies of Type Ia SNe have different elongations (noted in Section 4.2), it is possible that the distributions of projected galactocentric distances of SNe along major (U) and minor (V) axes, normalized to R_{25} or $R_{\rm e}$, would be different. Obviously, the projected U and V galactocentric distances (in arcsec) of an SN are

$$U = \Delta\alpha \, \sin {\rm PA} + \Delta\delta \, \cos {\rm PA} \, ,$$

$$V = \Delta\alpha \, \cos {\rm PA} - \Delta\delta \, \sin {\rm PA} \, .$$

Table 4.2: Comparison of the projected and normalized distributions of the subclasses of Type Ia SNe along major (U) and minor (V) axes of elliptical host galaxies.

SN subclass	$N_{\rm SN}$	Subsample 1	vs.	Subsample 2	$P_{\rm KS}$	$P_{\rm AD}$
		$\langle \lvert U\rvert/R_{25}\rangle$		$\langle \lvert V\rvert/R_{25}\rangle$		
all	109	0.31 ± 0.03	vs.	0.26 ± 0.03	0.141	0.052
normal	66	0.27 ± 0.03	vs.	0.27 ± 0.05	0.438	0.250
91bg-like	41	0.37 ± 0.06	vs.	0.26 ± 0.05	0.279	0.143
		$\langle \lvert U\rvert/R_{\rm e}\rangle$		$\langle \lvert V\rvert/R_{\rm e}\rangle$		
all	109	1.31 ± 0.13	vs.	1.13 ± 0.15	0.331	0.099
normal	66	1.09 ± 0.14	vs.	1.10 ± 0.21	0.721	0.352
91bg-like	41	1.68 ± 0.27	vs.	1.21 ± 0.23	0.420	0.210

Notes. The explanations for the P-values are similar to those in Table 2.2.

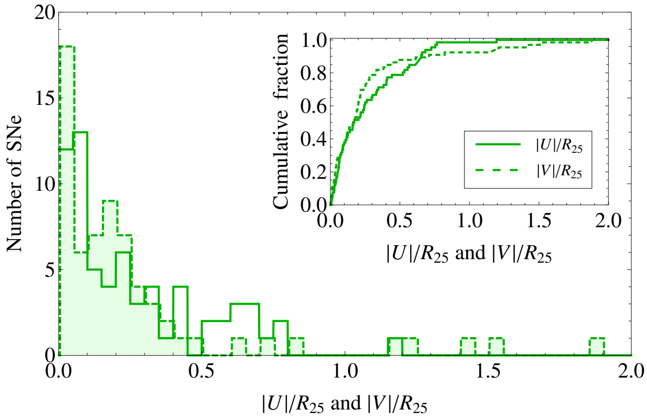

Figure 4.3: Distributions of $|U|/R_{25}$ (green solid) and $|V|/R_{25}$ (green dashed and filled) values for normal SNe Ia. The inset presents the corresponding cumulative distributions.

Here, as already noted, $\Delta\alpha$ and $\Delta\delta$ are offsets of the SN in equatorial system, and PA is position angle of the major axis of the elliptical host galaxy.

In the mentioned context, using the two-sample KS and AD tests, we compare the distributions of $|U|/R_{25}$ versus $|V|/R_{25}$, as well as the distributions of $|U|/R_{\rm e}$ versus $|V|/R_{\rm e}$ for all, normal and 91bg-like SNe. Here, the absolute values of U and V are used to increase the statistical power of the tests. The values of $P_{\rm KS}$ and $P_{\rm AD}$ in Table 4.2 show that the distributions of projected and normalized galactocentric distances of SNe along major and minor axes are consistent between each other. Only the $P_{\rm AD}$ values for the entire sample of SNe Ia are close to the rejection threshold of 0.05, however when we split the sample between normal and 91bg-like events, both the P-values of KS and AD tests become clearly above the threshold. Therefore,

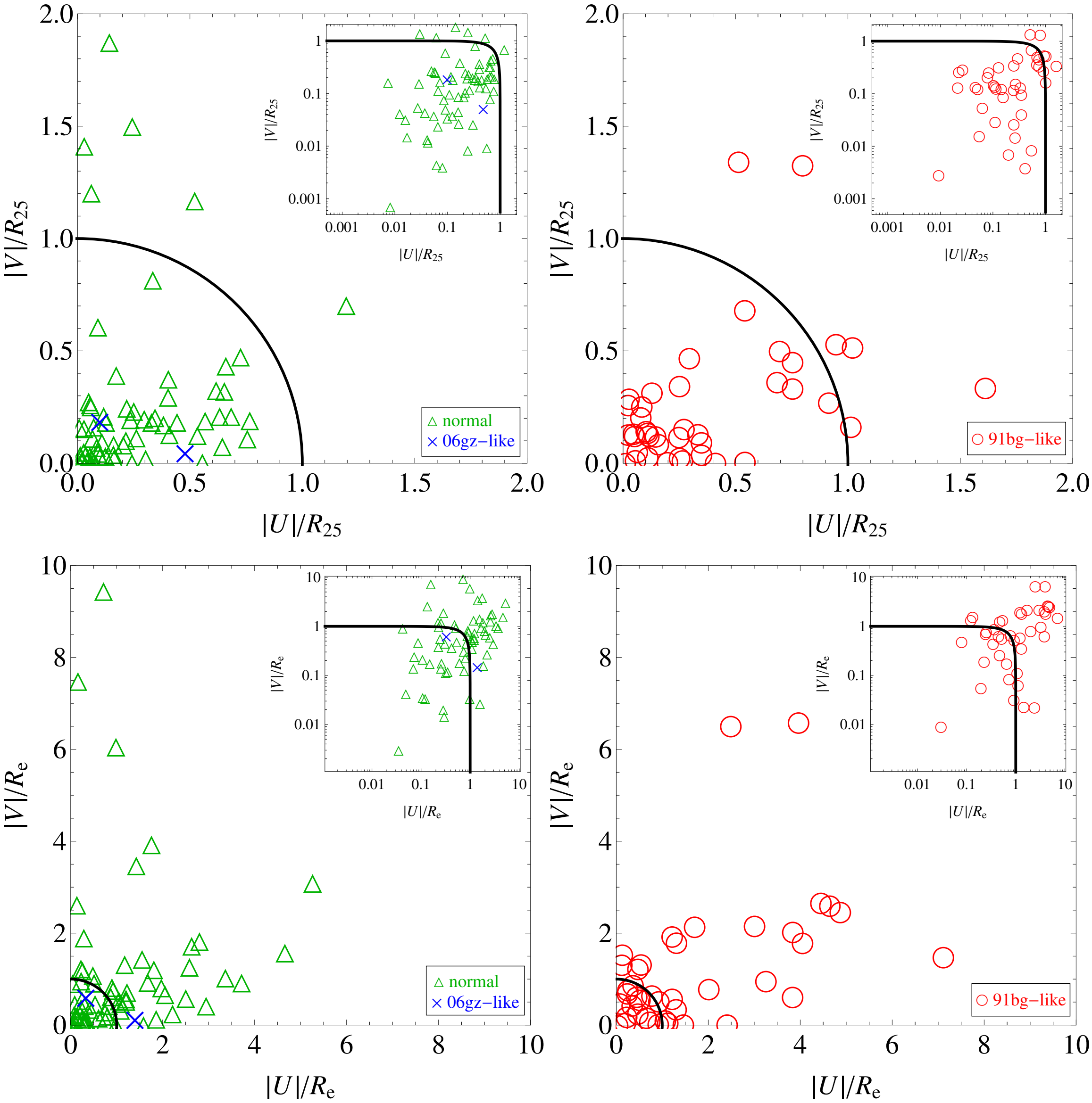

Figure 4.4: Upper panels: projected and R_{25}-normalized distributions of the different subclasses of Type Ia SNe along major (U) and minor (V) axes of elliptical host galaxies. The green triangles, blue crosses and red circles represent normal, 06gz-like and 91bg-like SNe, respectively. The quarters of big black circles are the host galaxy R_{25} sizes. Bottom panels: same as in upper panels but for $R_{\rm e}$ normalization. The quarter circles now represent $R_{\rm e}$. In the insets, we show the same distributions with log axes.

the different elongations of elliptical host galaxies in our sample have negligible impact, if any, on the sky plane projection of the spherical 3D distribution of SNe Ia. For illustration, in Fig. 4.3 we show the histograms and cumulative distributions of $|U|/R_{25}$ and $|V|/R_{25}$ for normal SNe Ia. Comparison of the same distributions for 91bg-like SNe looks similar (also for the cases with $R_{\rm e}$ normalization). Fig. 4.4 shows the projected distributions of the subclasses of Type Ia SNe with R_{25} and $R_{\rm e}$ normalizations.

4.3.2 The radial distributions of SNe Ia in ellipticals

As already mentioned above, the light profiles of elliptical galaxies are characterized with a continuous distribution according to the [254] law with mean index $n \approx 4$, when considering the families of ellipticals from dwarfs to giants (for the g-band see e.g. [260, 261]). In addition, [12] have already shown that the projected surface density distribution of Type Ia SNe in morphologically selected early-type host galaxies is consistent with the de Vaucouleurs profile ($n = 4$) in the $0.2 < R_{\rm SN}/R_{\rm e} < 4$ radial range [243, 265]. However, in the literature a comprehensive analysis of the surface density distributions of normal and 91bg-like SNe in well-defined elliptical host galaxies with different radius normalizations has not yet been performed and, as already mentioned, is one of the main goals of the present study.

Using MLE method, we fit the distribution of projected and R_{25}-normalized galactocentric radii of Type Ia SNe ($\widetilde{R}_{\rm SN} = R_{\rm SN}/R_{25}$) with the surface density model of Sérsic profile with $n = 4$. If the surface density (Σ) of SNe Ia is described by a Sérsic function of $\widetilde{R}_{\rm SN}$ (see Eq. [4.1]), then the probability that a SN is observed at $\widetilde{R}_{\rm SN}$ radius, i.e. PDF, is

$$p(\widetilde{R}_{\rm SN}|\widetilde{R}_{\rm e}^{\rm SN}) = \frac{\widetilde{R}_{\rm SN}\,\Sigma(\widetilde{R}_{\rm SN}|\widetilde{R}_{\rm e}^{\rm SN})}{\int_0^\infty \widetilde{R}_{\rm SN}\,\Sigma(\widetilde{R}_{\rm SN}|\widetilde{R}_{\rm e}^{\rm SN})\,{\rm d}\widetilde{R}_{\rm SN}}\,, \tag{4.2}$$

where $\widetilde{R}_{\rm e}^{\rm SN} = R_{\rm e}^{\rm SN}/R_{25}$ is normalized effective radius of SN distribution. The likelihood of the

Table 4.3: Consistency of the distribution of projected and normalized galactocentric distances of SNe Ia with the surface density model of Sérsic profile with $n = 4$ (de Vaucouleurs profile) in elliptical host galaxies.

SN subclass	$\widetilde{R}_{\rm SN} \geq$	$N_{\rm SN}$	$\widetilde{R}_{\rm e}^{\rm SN}$	$P_{\rm KS}$	$P_{\rm AD}$
all	0	109	0.28 ± 0.03	**0.008**	**0.014**
normal	0	66	0.26 ± 0.04	0.184	0.129
91bg-like	0	41	0.31 ± 0.04	**0.036**	**0.041**
all	0.1	94	0.18 ± 0.02	0.231	0.093
normal	0.1	54	0.18 ± 0.02	0.369	0.222
91bg-like	0.1	38	0.18 ± 0.04	0.263	0.185
	$\widehat{R}_{\rm SN} \geq$		$\widehat{R}_{\rm e}^{\rm SN}$		
all	0	109	1.15 ± 0.12	**0.016**	**0.034**
normal	0	66	1.03 ± 0.09	0.176	0.212
91bg-like	0	41	1.38 ± 0.15	0.059	0.068
all	0.4	92	0.80 ± 0.12	0.132	0.093
normal	0.4	52	0.78 ± 0.18	0.144	0.196
91bg-like	0.4	38	0.87 ± 0.21	0.514	0.206

Notes. The $P_{\rm KS}$ and $P_{\rm AD}$ are the probabilities from one-sample KS and AD tests, respectively, that the distributions of SNe Ia are drawn from the best-fitting de Vaucouleurs surface density profiles with the maximum likelihood values of $\widetilde{R}_{\rm e}^{\rm SN} = R_{\rm e}^{\rm SN}/R_{25}$ and $\widehat{R}_{\rm e}^{\rm SN} = R_{\rm e}^{\rm SN}/R_{\rm e}$ (with bootstrapped errors, repeated 10^3 times). The $P_{\rm KS}$ and $P_{\rm AD}$ are calculated using the calibrations by [123] and [124], respectively. The statistically significant deviations from de Vaucouleurs profile (P-values ≤ 0.05) are highlighted in bold.

set of $\{\widetilde{R}_{{\rm SN}\,i}\}$ is

$$\mathcal{L}(\widetilde{R}_{\rm e}^{\rm SN}) = \prod_{i=1}^{N_{\rm SN}} p(\widetilde{R}_{{\rm SN}\,i}|\widetilde{R}_{\rm e}^{\rm SN}) \,, \tag{4.3}$$

and thus maximizing $\ln(\mathcal{L})$ we get the effective radii of SN distributions for the subclasses of Type Ia SNe.

At the same time, to check whether the distributions of SNe Ia follow the best-fit de Vaucouleurs profiles, we perform one-sample KS and AD tests on the cumulative distributions of the projected and normalized galactocentric distances of SNe. In general, the CDF of Sérsic model can be expressed as the integral of its PDF (see Eq. [4.2]) as follows:

$$
\begin{aligned}
E(\widetilde{R}_{\rm SN}) &= \int_{-\infty}^{\widetilde{R}_{\rm SN}} p(t\,|\widetilde{R}_{\rm e}^{\rm SN})\,{\rm d}t \\
&= 1-\Gamma\Big(2n,\, b_{\rm n}\Big(\frac{\widetilde{R}_{\rm SN}}{\widetilde{R}_{\rm e}^{\rm SN}}\Big)^{\frac{1}{n}}\Big)\Big/\Gamma\Big(2n\Big)\,,
\end{aligned}
\tag{4.4}
$$

where

$$\Gamma(z)=\int_0^{\infty} t^{z-1}e^{-t}dt$$

and

$$\Gamma(a,\,z)=\int_z^{\infty} t^{a-1}e^{-t}dt$$

are the complete and upper incomplete gamma functions, respectively.

For the $R_{\rm e}$ normalization, in the above-mentioned formulae (Eqs. [4.2–4.4]) we simply replace $\widetilde{R}_{\rm SN}$ with $\widehat{R}_{\rm SN}=R_{\rm SN}/R_{\rm e}$ and therefore $\widetilde{R}_{\rm e}^{\rm SN}$ with $\widehat{R}_{\rm e}^{\rm SN}=R_{\rm e}^{\rm SN}/R_{\rm e}$. The estimated $\widetilde{R}_{\rm e}^{\rm SN}$ and $\widehat{R}_{\rm e}^{\rm SN}$ effective radii, and the $P_{\rm KS}$ and $P_{\rm AD}$ probabilities that the distributions of SNe Ia are drawn from the best-fitting de Vaucouleurs surface density profiles (Sérsic model with $n=4$) are listed in Table 4.3.

From the P-values in Table 4.3, we see that the global ($\widetilde{R}_{\rm SN}\geq 0$ and $\widehat{R}_{\rm SN}\geq 0$) surface density distributions of Type Ia SNe in elliptical host galaxies are not consistent with the de Vaucouleurs profiles. When splitting the sample between the subclasses of SNe Ia, we see that the significant inconsistency exists for the $\widetilde{R}_{\rm SN}$ distribution of 91bg-like events, and the marginal inconsistency takes place for the $\widehat{R}_{\rm SN}$ distribution of the same SNe (Table 4.3). The left panel of Fig. 4.5 illustrates that the main inconsistency is likely attributed to the slower growth or decline (in case of 91bg-like events) of the SN surface density at the central region of hosts with the radius of about one tenth of the optical radius of galaxies (gray shaded region in the figure). In our sample, the mean $R_{\rm e}/R_{25}$ is about four, and a similar behavior of the $R_{\rm e}$-normalized surface density is seen at the central $0.4R_{\rm e}$ region (gray shaded region in the

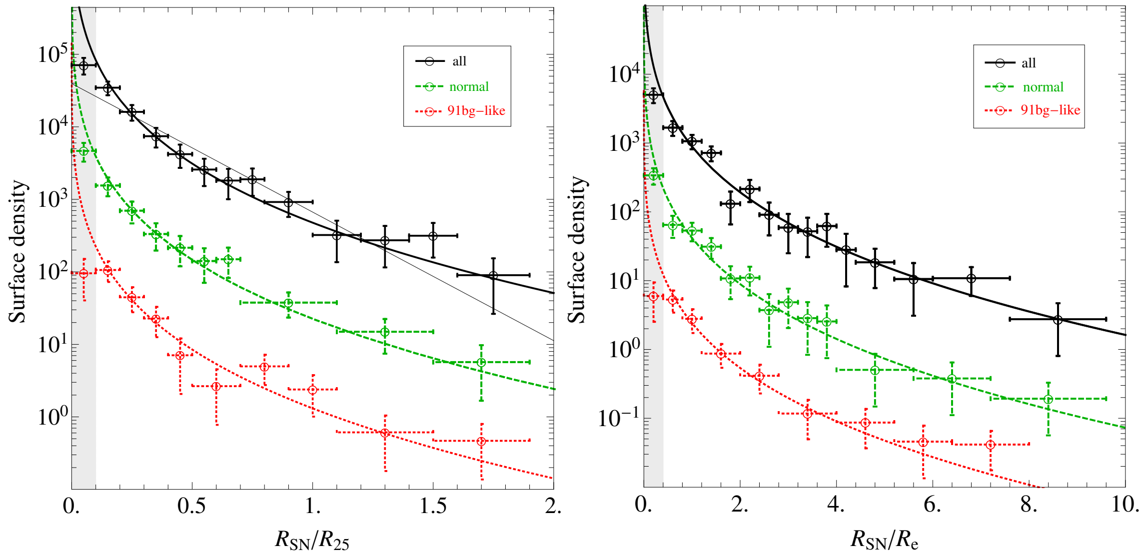

Figure 4.5: Left: R_{25}-normalized surface density distributions (arbitrary scaled) of all (black solid), normal (green dashed) and 91bg-like (red dotted) SNe Ia in elliptical host galaxies. The vertical error bars assume a Poisson distribution. The horizontal bars show the bin sizes that are increased at the edges of galaxies to include at least two SNe in each. The different curves show the maximum likelihood de Vaucouleurs surface density profiles, estimated using the inner-truncated distributions (outside the shaded area). For all SNe, the best-fitting inner-truncated exponential profile (black thin line) is also shown. For better visibility, the distributions with their best-fitting profiles are shifted vertically (to avoid falling one onto another). Right: same as in left panel but for R_e normalization.

right panel of Fig. 4.5).

It is important to note that different SN surveys are biased against the discovery of SNe near the centers of host galaxies [266]. This happens because central SNe have lower contrast with respect to the bright and often overexposed background of elliptical hosts, increasing the difficulty of their detection in a scan of the survey figures [267]. In addition, host galaxy internal extinction $A_V < 0.2$ mag exists only within the central region, while A_V is almost zero outside that region till to the end of optical radius of an elliptical galaxy [159]. Since 91bg-like events have peak luminosities that are ~ 2 magnitudes lower than do normal SNe Ia (e.g. [234] and references therein), 91bg-like SNe are more strongly affected by these effects than are normal Type Ia SNe (as seen in Fig. 4.5).

We now exclude SNe from the central regions of hosts ($\widetilde{R}_{SN} \geq 0.1$, $\widehat{R}_{SN} \geq 0.4$) and compare the SN distributions with the best-fitting inner-truncated de Vaucouleurs profiles. From the

P-values in Table 4.3, we see that all the inconsistencies vanish. In Fig. 4.5, we show the inner-truncated de Vaucouleurs profiles, extended to the central regions of host galaxies,[6] and the global surface density distributions of SNe, enabling to roughly estimate the loss in SNe Ia discoveries, most expressive for 91bg-like events, compared with their expected densities. The mean loss of SNe in the central regions of elliptical galaxies is $22 \pm 4\%$ of the expected total number of Type Ia SNe. This value is in good agreement with the similar estimation of $23 \pm 12\%$ in E–S0 galaxies by [126], though a different method and sample were used in their study. In our sample, the mean central losses of normal and 91bg-like SNe are 17 ± 5 and $27 \pm 7\%$, respectively.

In addition, we check the dependence of the described bias, i.e. the central loss of SNe, on the distances of their host galaxies (the *Shaw effect*; [268]), splitting the sample between near (≤ 100 Mpc) and far (> 100 Mpc) objects. This separation is done to have adequate numbers of objects in the subsamples. The surface density distributions of SNe in these distance bins show the equivalent central losses of SNe. In this sense, it is well known that the Shaw effect is important for photographic searches and negligible for visual/CCD searches [269]. Similarly, the Shaw effect is negligible in our sample, in which $\sim 94\%$ of SNe Ia are discovered via visual and CCD searches (see Section 4.2).

4.3.3 SNe Ia locations vs. fractional radial light distributions of elliptical hosts

In the analysis above, we fixed the Sérsic index to $n = 4$ in Eq. [4.1] when describing the surface density distribution of SNe Ia, while different elliptical host galaxies have $n \approx 2$ to 6 in the SDSS g-band [260, 261]. Fortunately, the distribution of fractional radial g-band fluxes of SNe (Fr_g, see Section 4.2 for definition) allows to compare the distribution of SNe with respect to that of the g-band light of elliptical host galaxies, irrespective of their different Sérsic indices

[6] For illustrative purpose, in the left panel of Fig. 4.5 we also present the best-fitting inner-truncated exponential profile (black thin line, i.e. $n = 1$ in Eq. [4.1]). The one-sample KS and AD tests show that the surface density distribution of SNe Ia is strongly inconsistent with the global ($P_{\rm KS} = 0.050$, $P_{\rm AD} = 0.005$) and inner-truncated ($P_{\rm KS} = 0.090$ [barely inconsistency], $P_{\rm AD} = 0.039$) exponential models.

Table 4.4: Consistency of the Fr_g (or inner-truncated $\check{F}r_g$) distributions of SNe Ia with the surface brightness distribution of elliptical host galaxies.

SN subclass (Fr_g or $\check{F}r_g$)	$N_{\rm SN}$	$P_{\rm KS}$	$P_{\rm AD}$
all (Fr_g)	94	**0.021**	0.054
normal (Fr_g)	58	0.405	0.436
91bg-like (Fr_g)	34	**0.044**	0.056
all ($\check{F}r_g$)	79	0.482	0.404
normal ($\check{F}r_g$)	46	0.758	0.719
91bg-like ($\check{F}r_g$)	31	0.286	0.257

Notes. The $P_{\rm KS}$ and $P_{\rm AD}$ are the probabilities from one-sample KS and AD tests, respectively, that the distributions of Fr_g (or inner-truncated $\check{F}r_g$) are drawn from the surface brightness distribution of host galaxies. The statistically significant deviations (P-values ≤ 0.05) are highlighted in bold. Recall that 15 SNe, which are located far outside the elliptical apertures where fluxes are consistent with the sky background values, are removed from the fractional radial flux analysis (see Section 4.2).

and elongations [12]. If the SNe Ia are equally likely to arise from any part of the projected light distribution of the host galaxies, i.e. the surface brightness of galaxy I and the surface density of SNe Σ are related by $\Sigma = {\rm Const} \times I$, then one would expect that the Fr_g values are evenly distributed throughout the projected radii of hosts (a flat distribution, independent of radius) and the $\langle Fr_g \rangle = 0.5$ [262]. For the Fr_g values (from 0 to 1), the PDF and CDF are

$$p(Fr_g) = 1 \quad \text{and} \quad E(Fr_g) = Fr_g\,, \tag{4.5}$$

respectively.

From the P-values of one-sample KS and AD tests in Table 4.4, we see that the Fr_g distribution of Type Ia SNe is not consistent with the g-band light distribution of elliptical host galaxies (for the KS statistic but marginally so in the AD statistic), mainly due to the distribution of 91bg-like events. The upper panel of Fig. 4.6 illustrates that, as already stated above, the main inconsistency is due to the selection effect against the discovery of SNe Ia near the center of the host galaxies (also seen in the right-hand panels of fig. 2 in [12]). Therefore, we also use the inner-truncated fractional radial g-band fluxes of SNe ($\check{F}r_g$), excluding the central

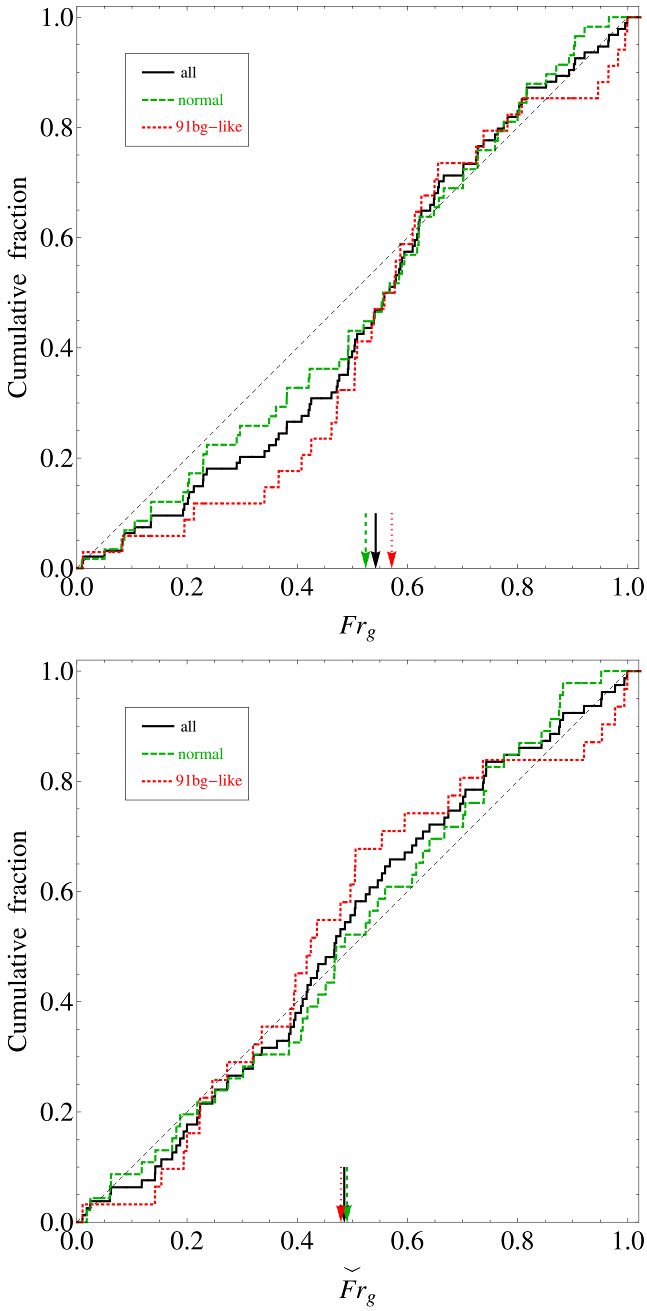

Figure 4.6: Upper panel: cumulative Fr_g distributions of SNe Ia (all – black solid, normal – green dashed, and 91bg-like – red dotted) with respect to the g-band surface brightness distribution of their elliptical host galaxies (black thin diagonal line). The mean values of the distributions are shown by arrows. Bottom panel: same as in upper panel but for the inner-truncated $\breve{Fr}_g$ distributions.

Table 4.5: Comparison of the distributions of $\widetilde{R}_{\rm SN}$, $\widehat{R}_{\rm SN}$, Fr_g and $\check{Fr}_g$ values between the subsamples of normal and 91bg-like SNe.

Parameter	normal		vs.	91bg-like		$P_{\rm KS}$	$P_{\rm AD}$
	$N_{\rm SN}$	$\langle$Parameter$\rangle$		$N_{\rm SN}$	$\langle$Parameter$\rangle$		
$\widetilde{R}_{\rm SN} \geq 0$	66	0.43 ± 0.05	vs.	41	0.50 ± 0.07	0.456	0.357
$\widetilde{R}_{\rm SN} \geq 0.1$	54	0.52 ± 0.06	vs.	38	0.53 ± 0.07	0.700	0.804
$\widehat{R}_{\rm SN} \geq 0$	66	1.77 ± 0.23	vs.	41	2.25 ± 0.32	0.502	0.232
$\widehat{R}_{\rm SN} \geq 0.4$	52	2.18 ± 0.26	vs.	38	2.41 ± 0.33	0.852	0.820
Fr_g	58	0.52 ± 0.03	vs.	34	0.57 ± 0.04	0.606	0.429
$\check{Fr}_g$	46	0.49 ± 0.04	vs.	31	0.48 ± 0.05	0.677	0.383

Notes. The explanations for the P-values are similar to those in Table 2.2. For the global distribution of all 109 SNe Ia, the mean values of $\widetilde{R}_{\rm SN} = 0.45 \pm 0.04$ and $\widehat{R}_{\rm SN} = 1.94 \pm 0.18$. For 94 SNe Ia, the mean value of $Fr_g = 0.54 \pm 0.03$. Recall that 15 SNe, which are located far outside the elliptical apertures where fluxes are consistent with the sky background values, are removed from the fractional radial flux analysis (see Section 4.2).

region of galaxies with one tenth of the optical radius ($0.1\,R_{25}$):

$$\check{Fr}_g = \frac{Fr_g - fr_g}{1 - fr_g}\,,$$

where fr_g is the fractional flux of $0.1\,R_{25}$ region. A similar definition of inner-truncated fractional flux for SNe in elliptical galaxies was first used by [270].

Simply replacing Fr_g with $\check{Fr}_g$ in Eqs. [4.5] and using one-sample KS and AD tests, we see that the $\check{Fr}_g$ distributions of all subclasses of Type Ia SNe are now consistent with the g-band light distribution of hosts, with mean values of $\check{Fr}_g$ near 0.5 as predicted (see Table 4.4 and the bottom panel of Fig. 4.6).

We now compare, in Table 4.5, the distributions of $\widetilde{R}_{\rm SN}$, $\widehat{R}_{\rm SN}$, Fr_g and $\check{Fr}_g$ values between the subsamples of normal and 91bg-like SNe, using the two-sample KS and AD tests. The mean values of the distributions are also listed. With the tests, we see no statistically significant differences between the global radial distributions of the SN subclasses. Similar results hold true for the inner-truncated distributions of SNe Ia.

Table 4.6: Comparison of the distributions of absolute magnitudes, colours, sizes, elongations, stellar masses, average metallicities and luminosity-weighted ages between the subsamples of host galaxies of normal and 91bg-like SNe.

Parameter	normal $\langle\text{Parameter}\rangle \pm \sigma$	vs.	91bg-like $\langle\text{Parameter}\rangle \pm \sigma$	$P_{\rm KS}$	$P_{\rm AD}$
	$\widetilde{R}_{\rm SN} \geq 0$ (66 vs. 41 hosts)				
M_u (mag)	-19.6 ± 1.0	vs.	-19.8 ± 0.9	0.218	0.276
M_g (mag)	-21.2 ± 1.1	vs.	-21.5 ± 0.9	0.112	0.137
M_r (mag)	-22.0 ± 1.1	vs.	-22.3 ± 0.9	0.113	0.134
M_i (mag)	-22.4 ± 1.1	vs.	-22.7 ± 0.9	0.188	0.153
M_z (mag)	-22.6 ± 1.1	vs.	-22.9 ± 0.9	0.260	0.156
$u-r$ (mag)	2.4 ± 0.1	vs.	2.5 ± 0.1	**0.013**	**0.007**
$g-i$ (mag)	1.2 ± 0.1	vs.	1.2 ± 0.1	0.101	0.255
$r-z$ (mag)	0.7 ± 0.05	vs.	0.7 ± 0.04	0.107	0.179
R_{25} (kpc)	23.0 ± 12.6	vs.	25.6 ± 11.3	0.096	0.142
$R_{\rm e}$ (kpc)	6.0 ± 3.8	vs.	6.0 ± 3.0	0.296	0.345
a/b	1.3 ± 0.2	vs.	1.3 ± 0.2	0.766	0.729
$\log(M_*/{\rm M}_\odot)$	$11.1^{+0.3}_{-1.3}$	vs.	$11.2^{+0.2}_{-0.6}$	0.107	0.175
$\log(Z_*/{\rm Z}_\odot)$	$0.09^{+0.07}_{-0.08}$	vs.	$0.11^{+0.06}_{-0.07}$	0.107	0.175
age (Gyr)	$11.7^{+2.3}_{-2.8}$	vs.	$12.8^{+1.2}_{-1.6}$	**0.017**	**0.012**
	$\widetilde{R}_{\rm SN} \geq 0.1$ (54 vs. 38 hosts)				
M_u (mag)	-19.6 ± 1.0	vs.	-19.8 ± 0.8	0.286	0.416
M_g (mag)	-21.2 ± 1.1	vs.	-21.4 ± 0.8	0.309	0.275
M_r (mag)	-22.0 ± 1.1	vs.	-22.2 ± 0.9	0.306	0.252
M_i (mag)	-22.4 ± 1.1	vs.	-22.6 ± 0.9	0.365	0.325
M_z (mag)	-22.7 ± 1.1	vs.	-22.9 ± 0.9	0.365	0.314
$u-r$ (mag)	2.4 ± 0.1	vs.	2.5 ± 0.1	**0.047**	**0.018**
$g-i$ (mag)	1.2 ± 0.1	vs.	1.2 ± 0.1	0.480	0.721
$r-z$ (mag)	0.7 ± 0.05	vs.	0.7 ± 0.04	0.274	0.462
R_{25} (kpc)	23.3 ± 12.7	vs.	24.2 ± 9.9	0.389	0.399
$R_{\rm e}$ (kpc)	6.1 ± 4.0	vs.	5.5 ± 2.3	0.450	0.390
a/b	1.2 ± 0.2	vs.	1.3 ± 0.2	0.706	0.559
$\log(M_*/{\rm M}_\odot)$	$11.2^{+0.3}_{-1.2}$	vs.	$11.2^{+0.2}_{-0.5}$	0.224	0.385
$\log(Z_*/{\rm Z}_\odot)$	$0.09^{+0.07}_{-0.08}$	vs.	$0.10^{+0.06}_{-0.06}$	0.224	0.385
age (Gyr)	$11.9^{+2.1}_{-2.7}$	vs.	$12.7^{+1.3}_{-1.7}$	**0.025**	**0.032**

Notes. The $P_{\rm KS}$ and $P_{\rm AD}$ are the probabilities from two-sample KS and AD tests, respectively, that the two distributions being compared (with respective mean values and standard deviations) are drawn from the same parent distribution. The statistically significant differences (P-values ≤ 0.05) between the distributions are highlighted in bold.

4.3.4 The global properties of SNe Ia elliptical host galaxies

In the SDSS DR15, different estimates of the parameters of galaxies (e.g. stellar mass, metallicity and age of stellar population) encompass calculations based on various stellar population models (e.g. Evolutionary Population Synthesis, [271]; Principal Component Analysis-based model, [272]; Flexible Stellar Population Synthesis, [273]), and different assumptions about galaxy extinction and star formation histories.[7] However, from 109 SNe Ia elliptical hosts of our study, only 43 SNe (29 normal, thirteen 91bg-like and one 06gz-like) have available SDSS spectra of hosts, thus reliable estimates of mass, age, and metallicity. Therefore, instead of using them we prefer to estimate the stellar masses (M_*) of all our elliptical hosts, using the empirical relation of [208] between $\log(M_*/\mathrm{M}_\odot)$, $g-i$ colour and i-band absolute magnitude (M_i) as determined from more than 10^5 galaxies with redshifts $z<0.65$:

$$\log\left(\frac{M_*}{\mathrm{M}_\odot}\right) = 1.15 + 0.70(g-i) - 0.4M_i\,, \tag{4.6}$$

where M_* has solar mass units. According to [208], this relation provides an estimate of the stellar mass-to-light ratio (M_*/L_i) to a 1σ accuracy of ~ 0.1 dex. In addition, to estimate average host galaxy stellar metallicities, we use the [274] correlation between stellar mass of E–S0 galaxy and $\log(Z_*/\mathrm{Z}_\odot)$ as determined from about 26000 SDSS galaxies (see also [275] for early-type/high mass galaxies):

$$\log\left(\frac{Z_*}{\mathrm{Z}_\odot}\right) = -1.757 + 0.168\log\left(\frac{M_*}{\mathrm{M}_\odot}\right), \tag{4.7}$$

where Z_* has solar metallicity units, with a scatter of ~ 0.1 dex. It should be noted that we use mass measurements coupled to a (monotonic) formula to convert it to host metallicity, which adds no original information to the statistical analysis, however, this gives a chance to qualitatively discuss our results in term of metallicities of SNe Ia hosts (see Section 4.4).

Finally, following the procedure outlined in [276], we use the fixed redshifts of SN hosts to

[7] For more detailed information with corresponding references, the reader is referred to https://www.sdss.org/dr15/spectro/galaxy/.

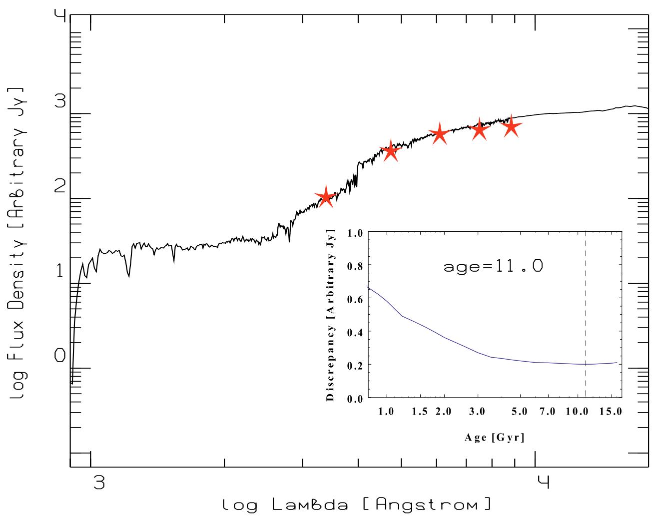

Figure 4.7: Photometric points (in the SDSS five bands, red asterisks) of SN 2018zs host elliptical galaxy with the best-SED, all in the rest-frame. The inset shows the curve of the dependence of the model rms deviations on age for the galaxy, with the best-age of 11 Gyr (minimum of the curve is shown by the vertical dashed line).

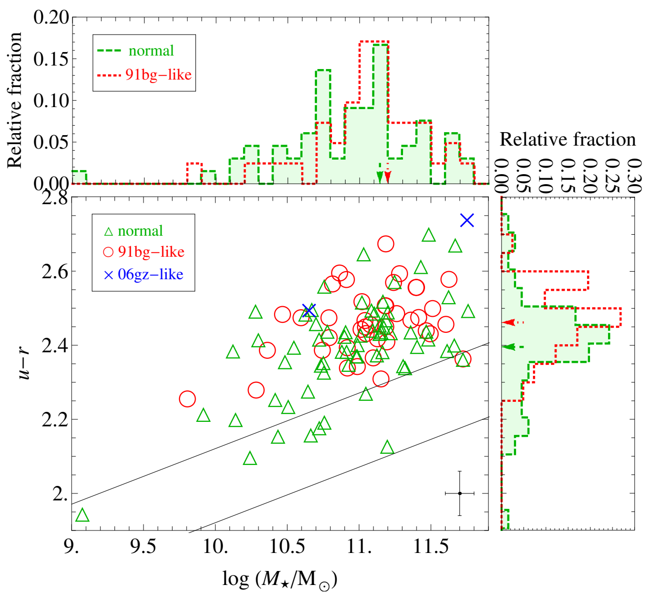

Figure 4.8: The $u - r$ colour–mass diagram for 109 SNe Ia elliptical host galaxies. Green triangles, red circles and blue crosses show normal, 91bg-like and 06gz-like SNe hosts, respectively. The region between two solid lines indicates the Green Valley (see the text for more details). The vertical and horizontal error bars, in the bottom-right corner, show the characteristic errors in the colour and mass estimations, respectively. For normal (green dashed and filled) and 91bg-like (red dotted) SNe hosts, the right and upper panels represent separately the histograms of the colours and masses, respectively. The mean values of the distributions are shown by arrows.

fit the PEGASE.2 [220,221] elliptical galaxy models to our u-, g-, r-, i- and z-band photometry to determine the luminosity-weighted ages of hosts.[8] In short, the measured five photometric points of a host galaxy in the SDSS bands with fixed redshift are used to select the best location of the points on the SED templates. Such a location can be found by shifting the points lengthwise and transverse the SED template at which the sum of the squares of the discrepancies is a minimum. From the PEGASE.2 model [220,221], the procedure uses already computed collection of synthetic SED templates for different ages (up to 19 Gyr) of elliptical galaxies. Fig. 4.7 presents an example of SN host galaxy photometric points (in the SDSS five bands) with the best-SED, all in the rest-frame. For more detailed information on the SED fitting procedure with filter smoothing option, the reader is referred to http://sed.sao.ru/.

To reveal possible differences in global properties of SNe Ia elliptical hosts, in Table 4.6, using the two-sample KS and AD tests, we compare absolute magnitudes, colours, sizes, elongations, stellar masses, average metallicities and luminosity-weighted ages between the subsamples of host galaxies of normal and 91bg-like SNe. The table shows that the distributions of absolute magnitudes, $g - i$ and $r - z$ colours (red part of the SEDs), sizes, elongations, stellar masses and average metallicities are not significantly different between host galaxies of normal and 91bg-like SNe. On the other hand, the distributions of $u - r$ colours (blue part of the SEDs) and luminosity-weighted ages of the hosts are significantly inconsistent between the subclasses of SNe Ia. In the histograms of Fig. 4.8, we show the distributions of host galaxy stellar masses and $u - r$ colours. The cumulative distributions of luminosity-weighted ages of the elliptical hosts are presented in Fig. 4.9. It is clear that, despite their comparable stellar masses, the elliptical host galaxies of normal SNe Ia are on average bluer and younger than those of 91bg-like SNe.

In Table 4.6, we also check the impact of the described bias in Subsection 4.3.2, i.e. the stronger central loss of 91bg-like SNe, on the comparison of the global properties of ellipticals by excluding the host galaxies with $\widetilde{R}_{\rm SN} < 0.1$. We obtain nearly identical results showing that the central bias has negligible impact on the comparison of the elliptical host galaxies in

[8] The luminosity-weighted ages of our 104 elliptical host galaxies are available online [264].

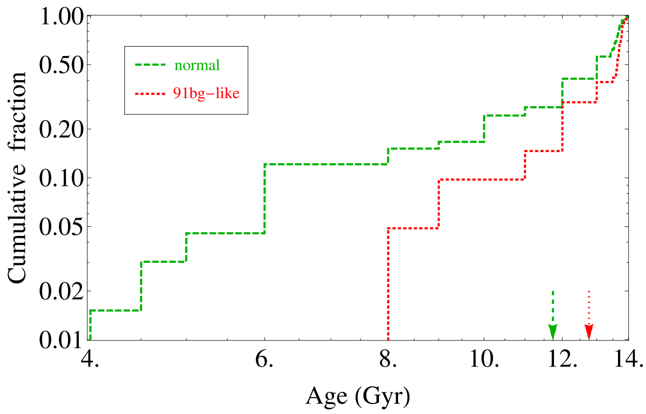

Figure 4.9: Cumulative distributions of luminosity-weighted ages of elliptical host galaxies of normal (green dashed) and 91bg-like (red dotted) SNe. The mean values of the distributions are shown by arrows.

Table 4.6.

4.4 Chapter discussion and summary

In this section, we discuss all the results obtained above and give summary within an evolutionary (interacting) scenario of SNe Ia elliptical host galaxies that can explain the similarity of the spatial distributions of normal and 91bg-like SNe in hosts and at the same time the differences of some global properties of elliptical hosts such as the $u - r$ colours and the ages of the stellar population.

In Subsection 4.3.2, we have shown that the distributions of projected galactocentric radii (with different normalizations) of normal and 91bg-like SNe in elliptical galaxies follow the de Vaucouleurs model, except in the central region of ellipticals where the different SN surveys are biased against the discovery of the events (Table 4.3 and Fig. 4.5). These results are in agreement with a more generalized result of [12], who showed that the projected surface density distribution of Type Ia SNe (without separating the subclasses) in morphologically selected early-type host galaxies is consistent with the de Vaucouleurs profile [243, 265]. Even without specifying the profile shape and excluding the bias against central SNe, the radial distributions of SN Ia subclasses are consistent with the radial light distribution of stellar populations of elliptical hosts in the SDSS g-band (Table 4.4 and Fig. 4.6). We have not seen any significant differences between the radial distributions of normal and 91bg-like SNe (Table 4.5).

These results are in agreement with those of [68], who studied the distribution of 57 local Type Ia SNe LC decline rates (Δm_{15}) in the B-band versus projected distances (in kpc) from the centers of spiral and E–S0 host galaxies. Despite their smaller statistics of E–S0 galaxies, they found that the Δm_{15} values are distributed evenly with projected galactocentric radii, showing no preference to the center of host galaxies for slowly declining (normal SNe Ia) or faster declining (91bg-like) SNe (see also [1] for projected and normalized galactocentric radii). Using a larger SN Ia sample at redshifts below 0.25 and output parameters from two LC fitters, MLCS2k2 [215] and SALT2 [216], [80] also studied the dependencies between SN properties and the projected galactocentric radii. For 64 SNe Ia in elliptical hosts, with determined morphology based on the concentration indices and Sérsic profiles, the authors found some indications that SNe tend to have faster declining LCs if they explode at larger galactocentric radii. However, this trend is visible when the LC parameters from MLCS2k2 were used, in contrast to the homologous parameters from SALT2. In addition, [80] noted that their finding might be due to the possible selection effects and explained by the difficulty in detecting faster declining/fainter SNe Ia near the galaxy center, which we demonstrated in Subsection 4.3.2, based on the surface density distributions of normal and 91bg-like events in elliptical hosts.

In Subsection 4.3.4, we have shown that the distributions of absolute magnitudes, stellar masses and average metallicities are not significantly different between host galaxies of normal and 91bg-like SNe (Table 4.6). Similar results were also obtained by [68], who found no correlation between the LC decline rates of SNe Ia and absolute B-band magnitudes (a sufficient tracer of galactic mass) of their E–S0 hosts. [81] also studied optical absorption-line spectra of 29 early-type (mostly E–S0) host galaxies of SNe Ia up to about 200 Mpc and found a mild correlation, if any, between host global metallicity and SN Ia peak luminosity.

Indeed, the variety of metallicities of the MS stars that become WDs could theoretically affect the mass of ^{56}Ni synthesized in SNe Ia [277], and cause a variety in the properties of SNe Ia (e.g. in luminosities and/or decline rates). These authors hypothesized that less luminous

SNe Ia arise from high-metallicity progenitors that produce less ^{56}Ni. However, [73] noted that the effect is dominant at metallicities significantly above solar, whereas early-type hosts of SNe Ia have only moderately above-solar metallicities (with no detectable star formation). In this respect, our elliptical host galaxies also span moderately above-solar metallicities (see Table 4.6), mostly within $0 \lesssim \log(Z_*/\mathrm{Z}_\odot) \lesssim 0.2$ range, and therefore the metallicity effect in our sample might be sufficient to vary the optical peak brightness of SN Ia by less than 0.2 mag [277], but not enough for the differences between peak magnitudes of normal and 91bg-like SNe (as already mentioned, the latter have peak luminosities that are 2 ± 0.5 mag lower in optical bands than do normal SNe, see [234]).

On the other hand, the radial metallicity gradient in elliptical galaxies [278] might be a useful tool to probe the differences between the properties of SN Ia subclasses. However, [159] recently studied nearby galaxies, including 41 ellipticals, with redshifts < 0.03, using the precise data of integral field spectroscopy, and found that the average radial metallicity profile of elliptical galaxies (with negative gradient) declines only moderately from 0.2 dex above solar to solar from the galactic center up to $3R_\mathrm{e}$, respectively. Therefore, most probably this small metallicity variation does not allow (according to [277]) to see the differences between the distributions of normal and 91bg-like SNe along the radius of their elliptical hosts (Table 4.5). Our results confirm that the masses as well as global and radial metallicity distributions of elliptical hosts are not decisive factors of the nature of normal and 91bg-like SN populations (see also discussions by [1, 68, 81]).

At the same time, in Subsection 4.3.4, we have shown that the distributions of $u-r$ colours and luminosity-weighted ages are inconsistent significantly between the elliptical host galaxies of different SN Ia subclasses (Table 4.6): the hosts of normal SNe Ia are on average bluer (the right histograms in Fig. 4.8) and younger (Fig. 4.9) than those of 91bg-like SNe. These results are in excellent agreement with those of [81], who found a strong correlation between SN peak luminosities and the luminosity-weighted ages of dominant population of E–S0 hosts. They suggested that SNe Ia in galaxies with a characteristic age greater than several Gyr are on average ~ 1 mag fainter at the peak in V-band than those in early-type hosts with younger populations (i.e. a fairly large number of subluminous/91bg-like SNe are discovered in older hosts). In addition, [81] noted about the difficulty to distinguish whether this effect is a smooth transition with age or the result of two distinct SN Ia populations. Recently, [162] analysed integral field observations of the apparent/underlying explosion sites of eleven spectroscopically identified 91bg-like SNe (redshifts ≤ 0.04) in hosts with different morphologies (including six E–S0 galaxies) and found that the majority of the stellar populations that host these events are dominated by old stars with a lack of evidence for recent star formation. [162] concluded that the 91bg-like SN progenitors are likely to have DTD weighted toward long delay times ($>$ 6 Gyr, see also [171]), much longer than the typical delay times of normal SNe Ia in star forming environments, whose delay times peak between several hundred Myr and $\sim$ 1 Gyr [19, 71]. These results are in good agreement with our findings in Table 4.6 and Fig. 4.9.

It is important to note that the global ages of elliptical galaxies are not significantly different, on average, from local ones at any radii, i.e. there is no clear age gradient in ellipticals, being only mildly negative up to $R_{\rm e}$ and flat beyond that radius [159]. For this reason, we see no difference between the radial distributions of the subclasses of SNe Ia (Table 4.5), meanwhile seeing the clear differences of the global ages of normal and 91bg-like hosts (Table 4.6 and Fig. 4.9). Thus, our results support the earlier suggestions [1, 68, 81, 279] that the age of SN Ia progenitor populations is a more important factor than metallicity or mass of elliptical host galaxies in determining the properties of normal and 91bg-like events.

We now interpret and summarise our results within an evolutionary (interacting) scenario of SNe Ia elliptical host galaxies. In Fig. 4.8, we show $u-r$ colour–mass diagram of elliptical host galaxies (the right and upper panels represent separately the histograms of the colours and masses, respectively). In Fig. 4.8, the region between two solid lines indicates the location of the Green Valley, i.e. the region between blue star-forming galaxies and the Red Sequence of quiescent E–S0 galaxies [87, 211]. For galaxies with elliptical morphology, this is a transitional state through which blue galaxies evolve into the Red Sequence via major merging processes with morphological transformation from disc to spheroidal shape [88, 280], and/or a state of galaxies demonstrating some residual star formation via minor merging processes with no global

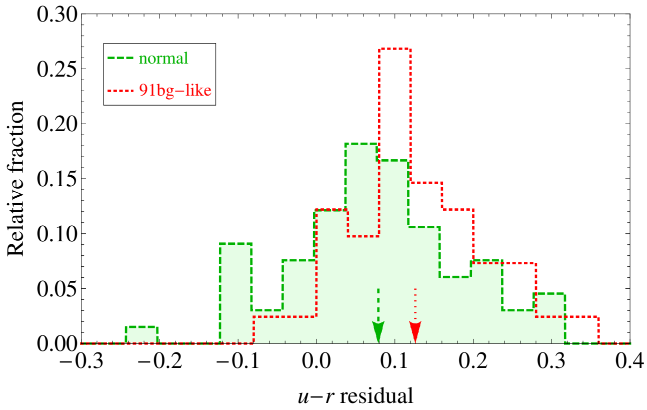

Figure 4.10: Distributions of colour residuals of elliptical hosts of normal (green dashed and filled) and 91bg-like (red dotted) SNe relative to the upper border of our Green Valley. The mean values of the distributions are shown by arrows.

changes in spheroidal structure [86].

It should be noted that we use the modification of the Green Valley defined by [87]. These authors used the SDSS `modelMag` values[9] of about 9000 early- and about 17000 late-type galaxies with redshifts $0.02 < z < 0.05$, while we use the magnitudes of host galaxies based on the g-band 25 mag arcsec^{-2} elliptical apertures (see Section 4.2). The comparison of SDSS DR15 `modelMag` measurements of our elliptical host galaxies with those obtained in Section 4.2, and the best-fit of our $u - r$ versus $\log(M_*/\mathrm{M}_\odot)$ bring a negative shift and a small change in slope for the modification of the Green Valley[10] in comparison with that in [87].

In Fig. 4.8, we see that the tail of the colour distribution of normal SN hosts stretches well into the Green Valley, while the same tail of 91bg-like SN hosts barely reaches the Green Valley border, and only at high stellar masses. To quantify this difference, we compare the distributions of colour residuals of elliptical hosts of the SN subclasses relative to the upper border of our Green Valley (see Fig. 4.10). The two-sample KS and AD tests show that the distributions are significantly different ($P_{\mathrm{KS}} = 0.049$, $P_{\mathrm{AD}} = 0.026$). Therefore, the bluer and younger elliptical hosts of normal SNe Ia should have more residual star formation [86, 87] that gives

[9] The `modelMag` values are first calculated using the best-fit parameters in the r-band, and then applied these parameters to all other SDSS bands, therefore, the light is measured consistently through the same aperture in all bands.

[10] The best-fit is $u - r = 0.721 + 0.155 \log(M_*/\mathrm{M}_\odot)$ for normal and 91bg-like SNe hosts. The upper and bottom borders of our Green Valley in Fig. 4.8 are simply negative shifts of the best-fit in 0.1 and 0.3 mag, respectively.

rise to younger SN Ia progenitors, resulting in normal SNe with shorter delay times [19,71,281]. Interestingly, the results of [204,282] reveal that in such galaxies the residual star formation is well mixed radially and distributed within entire stellar population.

As was recalled in the 4.1, the rate of SNe Ia can be represented as a linear combination of prompt and delayed components [244]. The prompt component is dependent on the rate of recent star formation, and the delayed component is dependent on the galaxy total stellar mass [245–248]. In this context, the normal SNe Ia with shorter delay times correspond to the prompt component. The bluer and younger ellipticals (with residual star formation) can also produce 91bg-like events with lower rate [81], because of long delay times of these SNe [162], i.e. a delayed component of SN Ia explosions [70,244]. However, the distribution of host ages (lower age limit of the delay times) of 91bg-like SNe does not extend down to the stellar ages that produce a significant excess of $u-r$ colour (i.e. u-band flux, see Figs. 4.8 and 4.9) – younger stars in elliptical hosts do not produce 91bg-like SNe, i.e. the 91bg-like events have no prompt component. The redder and older elliptical hosts that already exhausted nearly all star formation budget during the evolution [87] may produce significantly less normal SNe Ia with shorter delay times, outnumbered by 91bg-like SNe with long delay times.

Finally, we would like to note that our results favor SN Ia progenitor models such as helium-ignited violent mergers as a unified model for normal (CO WD primary with CO WD companion) and 91bg-like (CO WD primary with He WD companion) SNe [171,172] that have the potential to explain the different luminosities, delay times, and relative rates of the SN subclasses (see also [225,226], for discussions of binary WDs mergers in elliptical galaxies). In particular, the models predict shorter delay times for normal SNe Ia in agreement with our finding that normal SNe occur in younger stellar population of elliptical hosts. Moreover, the model prediction of very long delay times for 91bg-like SNe ($\gtrsim$ several Gyr, [171]) is in good qualitative agreement with our estimation of older ages of host galaxies of these events.

General Conclusions

This PhD thesis is mainly focused on investigating the diversity of Type Ia SNe progenitors. The main results obtained in all the Chapters of the thesis are summarized below.

1. For the first time, we show that in both early- and late-type edge-on spiral galaxies the vertical distribution of CC SNe is about twice more concentrated to the plane of host disc than the distribution of Type Ia SNe. The difference between the distributions of the SN types is statistically significant with only the exception in late-type hosts.

2. When considering early- and late-type spiral galaxies separately, the vertical distribution of Type Ia is consistent with both the sech^2 and exp profiles. In wider morphological bins (S0–Sd or Sa–Sd), the vertical distribution of Type Ia SNe is not consistent with sech^2 profile, most probably due to the earlier and wider morphological distribution of SNe Ia host galaxies and the systematically thinner vertical distribution of the host stellar population from early- to late-type discs.

3. By narrowing the host morphologies to the most populated Sb–Sc galaxies (close to the MW morphology) of our sample, we exclude the morphological biasing of host galaxies between the SN types and the dependence of scale height of host stellar population on the morphological type. In these galaxies, we find that the sech^2 scale height ($\tilde{z}_0^{\mathrm{SN}}$) of Type Ia SNe is 0.096 ± 0.016. The exp scale height ($\tilde{H}_{\mathrm{SN}}$) is 0.065 ± 0.012.

4. In Sb–Sc hosts, the exp scale height (also the $h_{\mathrm{SN}}/H_{\mathrm{SN}}$ ratio) of SNe Ia is consistent with that of the old population in the thick disc of the MW.

5. For the first time, we show that the ratio of scale lengths to scale heights ($h_{\rm SN}/z_0^{\rm SN}$) of the distribution of Type Ia SNe is consistent and located between the values of the same ratios of the two populations of resolved stars with ages from a few 100 Myr up to a few Gyr and from a few Gyr up to $\sim$ 10 Gyr, as well as with the unresolved population of the thick disc of nearby edge-on galaxies.

6. For the first time, we demonstrate that 91T- and 91bg-like subclasses of SNe Ia are distributed differently toward the plane of their host edge-on disc. On average, the SN heights are rising, beginning with 91T-like events and progressing through normal and 91bg-like SNe Ia.

7. We roughly estimate that 91T-like events originate from relatively younger progenitors with ages of about several 100 Myr, the ages of progenitors of normal SNe Ia are from about one up to $\sim$ 10 Gyr, and 91bg-like SNe Ia arise from progenitors with significantly older ages $\sim$ 10 Gyr.

8. We show that the SN Ia LC decline rates correlate with their heights from the host disc, after excluding the selection effects brought by dust extinction. The observed correlation is consistent with the explosion models of a sub-$M_{\rm Ch}$ mass WD and the vertical age gradient of stellar population in discs.

9. In general, the B-band Δm_{15} distribution of SNe Ia seems to be bimodal, with the second (weaker) mode mostly distributed within $\sim$ 1.5 to 2.1 mag. This faster declining range is generally occupied by 91bg-like (subluminous) events, while the Δm_{15} of 91T-like (overluminous) SNe are distributed only within the first mode at slower declining range ($\Delta m_{15} \lesssim 1.1$ mag). The decline rates of 02cx-like SNe are spread on the faster side of the Δm_{15} distribution of normal SNe Ia. Statistically, all these distributions are significantly different from one another.

10. The host galaxies of normal, 91T-, and 91bg-like SNe Ia have morphological type distributions that are significantly inconsistent between one another. Hosts of 91bg-like

SNe have, on average, earlier morphological types ($\langle t \rangle \approx 0$) with a large number of the events discovered in E–S0 galaxies. While hosts of 91T-like SNe have on average later morphological types ($\langle t \rangle \approx 4$) with a single 91T-like event in the E–S0 bin. The same distribution of hosts of normal SNe Ia occupies an intermediate position between the host morphologies of 91T- and 91bg-like events. The morphological distribution of 02cx-like SNe hosts is similar to that of 91T-like SNe hosts.

11. As for galaxies in general, the distribution of SNe Ia hosts in the $u - r$ colour–mass diagram is bimodal. The hosts of 91bg-like SNe are located in the Red Sequence of the diagram, most of them have $u - r$ colours $\gtrsim 2$ mag (i.e. above the Green Valley). In comparison with hosts of normal, 91T-, and 02cx-like SNe, the colour distribution of hosts of 91bg-like SNe are significantly redder. Importantly, the bulk of hosts of 91bg-like SNe are significantly massive ($\log(M_*/\mathrm{M}_\odot) > 10.5$) and old (more than 10 Gyr). The hosts' mass (age) distribution is significantly inconsistent with those of the other SN Ia subclasses. At the same time, the colour (mass, age) distributions are not statistically different between hosts of normal and 91T-like SNe. Finally, all the host galaxies of 02cx-like SNe are positioned in the Blue Cloud of the colour–mass diagram, mostly below the Green Valley. Their colour (mass, age) distribution is significantly bluer (lower, younger) in comparison with that of normal SNe Ia hosts, but closer to that of 91T-like SNe hosts.

12. As previously shown with smaller nearby SN Ia samples, there is a significant correlation between normal SNe Ia LC decline rates and global ages (morphologies, colours, and masses) of their host galaxies. On average, those normal SNe Ia that are in galaxies above the Green Valley, i.e. in early-type, red, massive, and old hosts, have faster declining LCs in comparison with those in galaxies below the Green Valley, i.e. in late-type, blue, less massive, and younger hosts.

13. For the first time we show that the LC decline rates of subluminous/91bg-like SNe and overluminous/91T-like events do not show dependencies on the host galaxy morphology and colour. The distribution of hosts on the colour–mass diagram confirms the known

tendency for 91bg-like SNe to occur in globally red/old galaxies (from halo/bulge and old disc components) while 91T-like events prefer blue/younger hosts (related to star-forming component). Probably, the decline rates of 02cx-like SNe also do not show dependencies on hosts' properties. On average, the youngest global ages of 02cx-like SNe hosts and their positions in the colour–mass diagram hint that these events likely originate from the young stellar component, but they differ from 91T-like events in the LC decline rate.

14. We show that the distributions of projected galactocentric radii (with different normalizations) of normal and 91bg-like SNe in elliptical galaxies follow the de Vaucouleurs model, except in the central region of ellipticals where the different SN surveys are biased against the discovery of the events.

15. We show that the distributions of absolute magnitudes, stellar masses and average metallicities are not significantly different between host galaxies of normal and 91bg-like SNe.

16. We show that the distributions of $u-r$ colours and luminosity-weighted ages are inconsistent significantly between the elliptical host galaxies of different SN Ia subclasses: the hosts of normal SNe Ia are on average bluer and younger than those of 91bg-like SNe.

17. The distribution of host ages (lower age limit of the delay times) of 91bg-like SNe does not extend down to the stellar ages that produce a significant excess of $u-r$ colour (i.e. u-band flux)– younger stars in elliptical hosts do not produce 91bg-like SNe, i.e. the 91bg-like events have no prompt component. The redder and older elliptical hosts that already exhausted nearly all star formation budget during the evolution may produce significantly less normal SNe Ia with shorter delay times, outnumbered by 91bg-like SNe with long delay times.

18. Our results favor SN Ia progenitor models such as helium-ignited violent mergers as a unified model for normal (CO WD primary with CO WD companion) and 91bg-like (CO WD primary with He WD companion) SNe that have the potential to explain the different luminosities, delay times, and relative rates of the SN subclasses.

Acknowledgement

I would like to extend my deep gratitude to Dr. Artur Hakobyan for his exceptional guidance, steadfast encouragement and invaluable assistance. I hold his support, concern, aid, and the motivation he provided me in high regard. I extend my heartfelt appreciation to my all coauthors, particularly to Drs. Daniel Kunth, Gary Mamon, Massimo Turatto, and Vardan Adibekyan, individuals with whom I collaborated closely during this scientific investigation. Their continuous conversations, support, and assistance produced highly positive results. My scientific trips to the Institut d'Astrophysique de Paris played a crucial role for my professional career. I would like to thank Vardan Adibekyan for hosting me during my research visit to Instituto de Astrofisica e Ciências do Espaço. I hold his support and assistance in high regard. I wish to sincerely thank all of my colleagues at the Center for Cosmology and Astrophysics of the Alikhanyan National Science Laboratory. Finally, I would like to express my sincere appreciation to my family and close friends who have offered both direct and indirect assistance during this demanding endeavor.

The work was supported by the Science Committee of RA, in the frames of the research project № 21T–1C236.

Bibliography

[1] Ivanov, V. D., Hamuy, M. and Pinto, P. A., *On the Relation between Peak Luminosity and Parent Population of Type Ia Supernovae: A New Tool for Probing the Ages of Distant Galaxies*, The Astrophysical Journal, 2000, **542**, 588-596.

[2] Hakobyan, A. A. and et al., *Early-type galaxies with core collapse supernovae*, Astronomy and Astrophysics, 2008, **488**, 523-531.

[3] Hakobyan, A. A. and et al., *The radial distribution of core-collapse supernovae in spiral host galaxies*, Astronomy and Astrophysics, 2009, **508**, 1259-1268.

[4] Hakobyan, A. A., *The statistical investigation of supernovae and their host galaxies*, Ph.D. thesis, Byurakan Astrophysical Observatory, 2009.

[5] Nazaryan, T. A. and et al., *Paired galaxies with different activity levels and their supernovae*, Astrophysics and Space Science, 2013, **347**, 365-374.

[6] Galbany, L. and et al., *Nearby supernova host galaxies from the CALIFA Survey. I. Sample, data analysis, and correlation to star-forming regions*, Astronomy and Astrophysics, 2014, **572**, A38/24.

[7] Aramyan, L. S. and et al., *Supernovae and their host galaxies - IV. The distribution of supernovae relative to spiral arms*, Monthly Notices of the Royal Astronomical Society, 2016, **459**, 3130-3143.

[8] Karapetyan, A. G., *Constraining Type Ia supernovae via their distances from spiral arms*, Monthly Notices of the Royal Astronomical Society, 2022, **517**, L132-L137.

[9] Anderson, J. P. and et al., *Progenitor mass constraints for core-collapse supernovae from correlations with host galaxy star formation*, Monthly Notices of the Royal Astronomical Society, 2012, **424**, 1372-1391.

[10] Kangas, T. and et al., *Core-collapse supernova progenitor constraints using the spatial distributions of massive stars in local galaxies*, Astronomy and Astrophysics, 2017, **597**, A92/19.

[11] McMillan, R. J. and Ciardullo, R., *Constraining the Ages of Supernova Progenitors. I. Supernovae and Spiral Arms*, The Astrophysical Journal, 1996, **473**, 707-712.

[12] Förster, F. and Schawinski, K., *The radial distribution of Type Ia supernovae in early-type galaxies: implications for progenitor scenarios*, Monthly Notices of the Royal Astronomical Society, 2008, **388**, L74-L78.

[13] Modjaz, M. and et al., *Progenitor Diagnostics for Stripped Core-collapse Supernovae: Measured Metallicities at Explosion Sites*, The Astrophysical Journal, 2011, **731**, L4/6.

[14] Galbany, L. and et al., *Nearby supernova host galaxies from the CALIFA survey. II. Supernova environmental metallicity*, Astronomy and Astrophysics, 2016, **591**, A48/25.

[15] Anderson, J. P. and et al., *Statistical Studies of Supernova Environments*, Publications of the Astronomical Society of Australia, 2015, **32**, id.e019/30.

[16] Turatto, M., *Classification of Supernovae*, Supernovae and Gamma-Ray Bursters. Edited by K. Weiler., Lecture Notes in Physics, 2003, **598**, 21-36.

[17] Smartt, S. J., *Progenitors of Core-Collapse Supernovae*, Annual Review of Astronomy and Astrophysics, 2009, **47**, 63-106.

[18] Smith, N. and et al., *Observed fractions of core-collapse supernova types and initial masses of their single and binary progenitor stars*, Monthly Notices of the Royal Astronomical Society, 2011, **412**, 1522-1538.

[19] Maoz, D., Mannucci, F. and Nelemans, G., *Observational Clues to the Progenitors of Type Ia Supernovae*, Annual Review of Astronomy and Astrophysics, 2014, **52**, 107-170.

[20] Maeda, K. and Terada, Y., *Progenitors of type Ia supernovae*, International Journal of Modern Physics D, 2016, **25**, id.1630024/22.

[21] Ruiter, A. J., Belczynski, K. and Fryer, C., *Rates and Delay Times of Type Ia Supernovae*, The Astrophysical Journal, 2009, **699**, 2026-2036.

[22] Matteucci, F. and Greggio, L., *Relative roles of type I and II supernovae in the chemical enrichment of the interstellar gas*, Astronomy and Astrophysics, 1986, **154**, 279-287.

[23] Riess, A. G. and et al., *Observational Evidence from Supernovae for an Accelerating Universe and a Cosmological Constant*, The Astronomical Journal, 1998, **116**, 1009-1038.

[24] Perlmutter, S. and et al., *Measurements of Ω and Λ from 42 High-Redshift Supernovae*, The Astrophysical Journal, 1999, **517**, 565-586.

[25] Taubenberger, S., *The Extremes of Thermonuclear Supernovae*, Handbook of Supernovae. Springer International Publishing AG, 2017, 317-373.

[26] Jha, S. W., *Type Iax Supernovae*, Handbook of Supernovae, Springer International Publishing AG, 2017, 375-401.

[27] Branch, D., Fisher, A. and Nugent, P., *On the Relative Frequencies of Spectroscopically Normal and Peculiar Type Ia Supernovae*, The Astronomical Journal, 1993, **106**, 2383-2391.

[28] Li, W. and et al., *Nearby supernova rates from the Lick Observatory Supernova Search - II. The observed luminosity functions and fractions of supernovae in a complete sample*, Monthly Notices of the Royal Astronomical Society, 2011, **412**, 1441-1472.

[29] Graur, O. and et al., *LOSS Revisited. II. The Relative Rates of Different Types of Supernovae Vary between Low- and High-mass Galaxies*, The Astrophysical Journal, 2017, **837**, id.121/11.

[30] Filippenko, A. V. and et al., *The Peculiar Type IA SN 1991T: Detonation of a White Dwarf?*, The Astrophysical Journal, 1992, **384**, L15-L18.

[31] Phillips, M. M. and et al., *SN 1991T: Further Evidence of the Heterogeneous Nature of Type Ia Supernovae*, The Astronomical Journal, 1992, **103**, 1632-1637.

[32] Filippenko, A. V., *Optical Spectra of Supernovae*, Annual Review of Astronomy and Astrophysics, 1997, **35**, 309-355.

[33] Filippenko, A. V. and et al., *The Subluminous, Spectroscopically Peculiar Type Ia Supernova 1991bg in the Elliptical Galaxy NGC 4374*, The Astronomical Journal, 1992, **104**, 1543-1556.

[34] Leibundgut, B. and et al., *SN 1991bg: A Type Ia Supernova With a Difference*, The Astronomical Journal, 1993, **105**, 301-313.

[35] Turatto, M. and et al., *The properties of the peculiar type Ia supernova 1991bg. I. Analysis and discussion of two years of observations*, Monthly Notices of the Royal Astronomical Society, 1996, **283**, 1-17.

[36] Li, W. and et al., *SN 2002cx: The Most Peculiar Known Type Ia Supernova*, Publications of the Astronomical Society of the Pacific, 2003, **115**, 453-473.

[37] Foley, R. J. and et al., *Type Iax Supernovae: A New Class of Stellar Explosion*, The Astrophysical Journal, 2013, **767**, id.57/28.

[38] Mazzali, P. A. and et al., *Hubble Space Telescope spectra of the Type Ia supernova SN 2011fe: a tail of low-density, high-velocity material with $Z < Z_{\odot}$*, Monthly Notices of the Royal Astronomical Society, 2014, **439**, 1959-1979.

[39] Filippenko, A. V., *Early-Time Spectra of Type Ic Supernovae: Further Evidence for the Presence of Hydrogen*, The Astrophysical Journal, 1992, **384**, L37-L40.

[40] Mazzali, P. A. and et al., *The properties of the peculiar type Ia supernova 1991bg - II. The amount of* ^{56}Ni *and the total ejecta mass determined from spectrum synthesis and energetics considerations*, Monthly Notices of the Royal Astronomical Society, 1997, **284**, 151-171.

[41] Ganeshalingam, M. and et al., *Results of the Lick Observatory Supernova Search Follow-up Photometry Program: BVRI Light Curves of 165 Type Ia Supernovae*, The Astrophysical Journal Supplement Series, 2010, **190**, 418-448.

[42] Lira, P. and et al., *Optical Light Curves of the Type Ia Supernovae SN 1990N and SN 1991T*, The Astronomical Journal, 1998, **115**, 234-246.

[43] Garnavich, P. M. and et al., *The Luminosity of SN 1999by in NGC 2841 and the Nature of "Peculiar" Type Ia Supernovae*, The Astrophysical Journal, 2004, **613**, 1120-1132.

[44] Gal-Yam, A., *Observational and Physical Classification of Supernovae*, Handbook of Supernovae, Springer International Publishing AG, 2017, 195-237.

[45] Arnett, W. D., *Type I supernovae. I - Analytic solutions for the early part of the light curve*, The Astrophysical Journal, 1982, **253**, 785-797.

[46] Mazzali, P. A. and et al., *A Common Explosion Mechanism for Type Ia Supernovae*, Science, 2007, **315**, 825-828.

[47] Phillips, M. M., *The Absolute Magnitudes of Type Ia Supernovae*, The Astrophysical Journal, 1993, **413**, L105-L108.

[48] Ashall, C. and et al., *Luminosity distributions of Type Ia supernovae*, Monthly Notices of the Royal Astronomical Society, 2016, **460**, 3529-3544.

[49] Phillips, M. M. and et al., *The Reddening-Free Decline Rate Versus Luminosity Relationship for Type Ia Supernovae*, The Astronomical Journal, 1997, **118**, 1766-1776.

[50] Livio, M. and Mazzali, P., *On the progenitors of Type Ia supernovae*, Physics Reports, 2018, **736**, 1-23.

[51] Ruiter, A. J., *Type Ia supernova sub-classes and progenitor origin*, IAU Symposium, 2020, **357**, 1-15.

[52] Hillebrandt, W. and et al., *Towards an understanding of Type Ia supernovae from a synthesis of theory and observations*, Frontiers of Physics, 2013, **8**, 116-143.

[53] Whelan, J. and Iben, I., *Binaries and Supernovae of Type I*, The Astrophysical Journal, 1973, **186**, 1007-1014.

[54] Nomoto, K., Iwamoto, K. and Kishimoto, N., *Type Ia supernovae: their origin and possible applications in cosmology*, Science, 1997, **276**, 1378-1382.

[55] Iben, I. and Tutukov, A. V., *Supernovae of type I as end products of the evolution of binaries with components of moderate initial mass*, The Astrophysical Journal Supplement Series, 1984, **54**, 335-372.

[56] Iben, I. and Tutukov, A. V., *On the evolution of close binaries with components of initial mass between 3 Msun and 12 Msun*, The Astrophysical Journal Supplement Series, 1985, **58**, 661-710.

[57] Blondin, S. and et al., *Evidence for sub-Chandrasekhar-mass progenitors of Type Ia supernovae at the faint end of the width-luminosity relation*, Monthly Notices of the Royal Astronomical Society, 2017, **470**, 157-165.

[58] Shen, K. J., Toonen, S. and Graur, O., *The Evolution of the Type Ia Supernova Luminosity Function*, The Astrophysical Journal, 2017, **851**, L50/5.

[59] Sim, S. A. and et al., *Detonations in Sub-Chandrasekhar-mass C+O White Dwarfs*, The Astrophysical Journal, 2010, **714**, L52-L57.

[60] Stritzinger, M. and et al., *Constraints on the progenitor systems of type Ia supernovae*, Astronomy and Astrophysics, 2006, **450**, 241-251.

[61] Piro, A. L., Thompson, T. A. and Kochanek, C. S., *Reconciling* ^{56}*Ni production in Type Ia supernovae with double degenerate scenarios*, Monthly Notices of the Royal Astronomical Society, 2014, **438**, 3456-3464.

[62] Shen, K. J. and et al., *Sub-Chandrasekhar-mass White Dwarf Detonations Revisited*, The Astrophysical Journal, 2018, **854**, id.52/15.

[63] Shen, K. J. and et al., *Non-local Thermodynamic Equilibrium Radiative Transfer Simulations of Sub-Chandrasekhar-mass White Dwarf Detonations*, The Astrophysical Journal, 2021, **909**, L18/11.

[64] Liu, Z.-W., Röpke, F. K. and Han, Z., *Type Ia Supernova Explosions in Binary Systems: A Review*, Research in Astronomy and Astrophysics, 2023, **23**, id.082001/43.

[65] González-Gaitán, S. and et al., *Defining Photometric Peculiar Type Ia Supernovae*, The Astrophysical Journal, 2014, **795**, id.142/23.

[66] Hamuy, M. and et al., *The Absolute Luminosities of the Calan/Tololo Type Ia Supernovae*, The Astronomical Journal, 1996, **112**, 2391-2397.

[67] Howell, D. A., *The Progenitors of Subluminous Type Ia Supernovae*, The Astrophysical Journal, 2001, **554**, L193-L196.

[68] Gallagher, J. S. and et al., *Chemistry and Star Formation in the Host Galaxies of Type Ia Supernovae*, The Astrophysical Journal, 2005, **634**, 210-226.

[69] Neill, J. D. and et al., *The Local Hosts of Type Ia Supernovae*, The Astrophysical Journal, 2009, **707**, 1449-1465.

[70] González-Gaitán, S. and et al., *Subluminous Type Ia Supernovae at High Redshift from the Supernova Legacy Survey*, The Astrophysical Journal, 2011, **727**, id.107/18.

[71] Childress, M. J., Wolf, C. and Zahid, H. J., *Ages of Type Ia supernovae over cosmic time*, Monthly Notices of the Royal Astronomical Society, 2014, **445**, 1898-1911.

[72] Hakobyan, A. A. and et al., *Study of the HII regions in the spiral galaxy NGC6384*, Astrophysics, 2007, **50**, 426-439.

[73] Howell, D. A. and et al., *The Effect of Progenitor Age and Metallicity on Luminosity and* ^{56}*Ni Yield in Type Ia Supernovae*, The Astrophysical Journal, 2009, **691**, 661-671.

[74] Gupta, R. R. and et al., *Improved Constraints on Type Ia Supernova Host Galaxy Properties Using Multi-wavelength Photometry and Their Correlations with Supernova Properties*, The Astrophysical Journal, 2011, **740**, id.92/12.

[75] Aramyan, L. S. and et al., *On the Nature of Unconfirmed Supernovae*, Astrophysics, 2013, **56**, 153-164.

[76] Pan, Y.-C. and et al., *The host galaxies of Type Ia supernovae discovered by the Palomar Transient Factory*, Monthly Notices of the Royal Astronomical Society, 2014, **438**, 1391-1416.

[77] Hamuy, M. and et al., *A Search for Environmental Effects on Type Ia Supernovae*, The Astronomical Journal, 2000, **120**, 1479-1486.

[78] Sullivan, M. and et al., *The dependence of Type Ia Supernovae luminosities on their host galaxies*, Monthly Notices of the Royal Astronomical Society, 2010, **406**, 782-802.

[79] Rose, B. M., Garnavich, P. M. and Berg, M. A., *Think Global, Act Local: The Influence of Environment Age and Host Mass on Type Ia Supernova Light Curves*, The Astrophysical Journal, 2019, **874**, id.32/18.

[80] Galbany, L. and et al., *Type Ia Supernova Properties as a Function of the Distance to the Host Galaxy in the SDSS-II SN Survey*, The Astrophysical Journal, 2012, **755**, id.125/14.

[81] Gallagher, J. S. and et al., *Supernovae in Early-Type Galaxies: Directly Connecting Age and Metallicity with Type Ia Luminosity*, The Astrophysical Journal, 2008, **685**, 752-766.

[82] Kang, Y. and et al., *Early-type Host Galaxies of Type Ia Supernovae. II. Evidence for Luminosity Evolution in Supernova Cosmology*, The Astrophysical Journal, 2020, **889**, id.8/23.

[83] Rigault, M. and et al., *Evidence of environmental dependencies of Type Ia supernovae from the Nearby Supernova Factory indicated by local Hα*, Astronomy and Astrophysics, 2013, **560**, A66/17.

[84] Hakobyan, A. A. and et al., *Supernovae and their host galaxies - III. The impact of bars and bulges on the radial distribution of supernovae in disc galaxies*, Monthly Notices of the Royal Astronomical Society, 2016, **456**, 2848-2860.

[85] Hakobyan, A. A. and et al., *Supernovae and their host galaxies - V. The vertical distribution of supernovae in disc galaxies*, Monthly Notices of the Royal Astronomical Society, 2017, **471**, 1390-1400.

[86] Kaviraj, S. and et al., *The role of minor mergers in the recent star formation history of early-type galaxies*, Monthly Notices of the Royal Astronomical Society, 2009, **394**, 1713-1720.

[87] Schawinski, K. and et al., *The green valley is a red herring: Galaxy Zoo reveals two evolutionary pathways towards quenching of star formation in early- and late-type galaxies*, Monthly Notices of the Royal Astronomical Society, 2014, **440**, 889-907.

[88] McIntosh, D. H. and et al., *A new population of recently quenched elliptical galaxies in the SDSS*, Monthly Notices of the Royal Astronomical Society, 2014, **442**, 533-557.

[89] Hakobyan, A. A., *The statistical investigation of type Ib/c and II supernovae and their host galaxies*, Astrophysics, 2008, **51**, 69-76.

[90] Wang, X. and et al., *Evidence for Two Distinct Populations of Type Ia Supernovae*, Science, 2013, **340**, 170-173.

[91] Hatano, K., Branch, D. and Deaton, J., *Extinction and Radial Distribution of Supernova Properties in Their Parent Galaxies*, The Astrophysical Journal, 1998, **502**, 177-181.

[92] Pavlyuk, N. N. and Tsvetkov, D. Y., *Distributions of supernovae of different types along the radius and in z coordinate of galaxies*, Astronomy Letters, 2016, **42**, 495-505.

[93] McMillan, R. J., *Constraining the Ages of Supernova Progenitors*, Ph.D. thesis, Pennsylvania State University, 1997.

[94] Molloy, M., *The distributions of stellar remnants in disk galaxies*, Masters thesis, Dublin City University, 2012.

[95] Bizyaev, D. V. and et al., *The Catalog of Edge-on Disk Galaxies from SDSS. I. The Catalog and the Structural Parameters of Stellar Disks*, The Astrophysical Journal, 2014, **787**, id.24/12.

[96] Yoachim, P. and Dalcanton, J. J., *Structural Parameters of Thin and Thick Disks in Edge-on Disk Galaxies*, The Astronomical Journal, 2006, **131**, 226-249.

[97] Seth, A. C., Dalcanton, J. J. and de Jong, R. S., *A Study of Edge-On Galaxies with the Hubble Space Telescope Advanced Camera for Surveys. II. Vertical Distribution of the Resolved Stellar Population*, The Astronomical Journal, 2005, **130**, 1574-1592.

[98] Chen, B. and et al., *Stellar Population Studies with the SDSS. I. The Vertical Distribution of Stars in the Milky Way*, The Astrophysical Journal, 2001, **553**, 184-197.

[99] Larsen, J. A. and Humphreys, R. M., *Fitting a Galactic Model to an All-Sky Survey*, The Astronomical Journal, 2003, **125**, 1958-1979.

[100] Jurić, M. and et al., *The Milky Way Tomography with SDSS. I. Stellar Number Density Distribution*, The Astrophysical Journal, 2008, **673**, 864-914.

[101] Alam, S. and et al., *The Eleventh and Twelfth Data Releases of the Sloan Digital Sky Survey: Final Data from SDSS-III*, The Astrophysical Journal Supplement Series, 2015, **219**, id.12/27.

[102] Hakobyan, A. A. and et al., *Supernovae and their host galaxies. I. The SDSS DR8 database and statistics*, Astronomy and Astrophysics, 2012, **544**, A81/19.

[103] Spergel, D. N. and et al., *Three-Year Wilkinson Microwave Anisotropy Probe (WMAP) Observations: Implications for Cosmology*, The Astrophysical Journal Supplement Series, 2007, **170**, 377-408.

[104] Barbon, R. and et al., *The Asiago Supernova Catalogue - 10 years after*, Astronomy and Astrophysics Supplement Series, 1999, **139**, 531-536.

[105] Hakobyan, A. A. and et al., *Supernovae and their host galaxies - II. The relative frequencies of supernovae types in spirals*, Monthly Notices of the Royal Astronomical Society, 2014, **444**, 2428-2441.

[106] Paturel, G. and et al., *Extragalactic database. VII. Reduction of astrophysical parameters*, Astronomy and Astrophysics Supplement Series, 1997, **124**, 109-122.

[107] Habergham, S. M. and et al., *Environments of interacting transients: impostors and Type IIn supernovae*, Monthly Notices of the Royal Astronomical Society, 2014, **441**, 2230-2252.

[108] Reshetnikov, V. P. and et al., *Galaxies with conspicuous optical warps*, Monthly Notices of the Royal Astronomical Society, 2016, **461**, 4233-4245.

[109] Perets, H. B. and et al., *A faint type of supernova from a white dwarf with a helium-rich companion*, Nature, 2010, **465**, 322-325.

[110] Hakobyan, A. A. and et al., *VizieR Online Data Catalog: Properties of 102 SNe and their 100 hosts (Hakobyan+, 2017)*, VizieR Online Data Catalog, 2017.

[111] de Grijs, R., Peletier, R. F. and van der Kruit, P. C., *The z-structure of disk galaxies towards the galaxy planes*, Astronomy and Astrophysics, 1997, **327**, 966-982.

[112] Bizyaev, D. and Mitronova, S., *Photometric parameters of edge-on galaxies from 2MASS observations*, Astronomy and Astrophysics, 2002, **389**, 795-801.

[113] de Grijs, R. and Peletier, R. F., *The shape of galaxy disks: how the scale height increases with galactocentric distance.*, Astronomy and Astrophysics, 1997, **320**, L21-L24.

[114] Mosenkov, A. V., Sotnikova, N. Y. and Reshetnikov, V. P., *2MASS photometry of edge-on spiral galaxies - I. Sample and general results*, Monthly Notices of the Royal Astronomical Society, 2010, **401**, 559-576.

[115] Bianchi, S., *The dust distribution in edge-on galaxies. Radiative transfer fits of V and K-band images*, Astronomy and Astrophysics, 2007, **471**, 765-773.

[116] Hatano, K. and et al., *On the spatial distribution and occurrence rate of Galactic classical novae*, Monthly Notices of the Royal Astronomical Society, 1997, **290**, 113-118.

[117] Dawson, P. C. and Johnson, R. G., *The visibility of galactic supernovae.*, Journal of the Royal Astronomical Society of Canada, 1994, **88**, 369-382.

[118] Hatano, K., Fisher, A. and Branch, D., *Extending the model of Dawson & Johnson for the observability of supernovae*, Monthly Notices of the Royal Astronomical Society, 1997, **290**, 360-366.

[119] Ilovaisky, S. A. and Lequeux, J., *A Study of Galactic Supernova Remnants. I. Distances, Radio Luminosity Function and Galactic Distribution*, Astronomy and Astrophysics, 1972, **18**, 169-185.

[120] Andreasyan, H. R., Andreasyan, R. R. and Paronyan, G. M., *Distribution of Pulsars in the Galaxy*, Astrophysics, 2016, **59**, 57-67.

[121] Spitzer, L., *The Dynamics of the Interstellar Medium. III. Galactic Distribution.*, The Astrophysical Journal, 1942, **95**, 329-344.

[122] Engmann, S. and Cousineau, D., *Comparing distributions: The Two-Sample Anderson-Darling Test as an Alternative to the Kolmogorov-Smirnoff Test*, Journal of Applied Quantitative Methods, 2011, **6**, 1-17.

[123] Massey, F. J., *The Kolmogorov-Smirnov Test for Goodness of Fit*, Journal of the American Statistical Association, 1951, **46**, 68-78.

[124] D'Agostino, R. B. and Stephens, M. A., *Goodness-of-fit techniques*, Statistics: Textbooks and Monographs, New York: Dekker, 1986.

[125] Pettitt, A. N., *A two-sample Anderson-Darling rank Statistic*, Biometrika, 1976, **63**, 161-168.

[126] Cappellaro, E. and Turatto, M., *The rate of supernovae: biases and uncertainties*, Thermonuclear Supernovae, NATO Advanced Study Institute (ASI) Series C, 1997, **486**, 77-86.

[127] Holwerda, B. W. and et al., *SN Ia host galaxy properties and the dust extinction distribution*, Monthly Notices of the Royal Astronomical Society, 2015, **446**, 3768-3775.

[128] della Valle, M. and Panagia, N., *Type Ia Supernovae in Late Type Galaxies: Reddening Correction, Scale Height, and Absolute Maximum Magnitude*, The Astronomical Journal, 1992, **104**, 696-703.

[129] De Geyter, G. and et al., *The distribution of interstellar dust in CALIFA edge-on galaxies via oligochromatic radiative transfer fitting*, Monthly Notices of the Royal Astronomical Society, 2014, **441**, 869-885.

[130] de Grijs, R., *The global structure of galactic discs*, Monthly Notices of the Royal Astronomical Society, 1998, **299**, 595-610.

[131] Tsvetkov, D. Y., *The Space Distribution of Type-I and Type-II Supernovae in Spiral Galaxies*, Soviet Astronomy Letters, 1981, **7**, 254-256.

[132] Tsvetkov, D. Y., *Frequency of Outbursts and Spatial Distribution of Type-I and Type-II Supernovae*, Soviet Astronomy, 1987, **31**, 39-44.

[133] Bizyaev, D. V. and et al., *Very thin disc galaxies in the SDSS catalogue of edge-on galaxies*, Monthly Notices of the Royal Astronomical Society, 2017, **465**, 3784-3792.

[134] Richardson, D. and et al., *A Comparative Study of the Absolute Magnitude Distributions of Supernovae*, The Astronomical Journal, 2002, **123**, 745-752.

[135] Barkhudaryan, L. V. and et al., *Supernovae and their host galaxies - VI. Normal Type Ia and 91bg-like supernovae in ellipticals*, Monthly Notices of the Royal Astronomical Society, 2019, **490**, 718-732.

[136] Gilmore, G. and Reid, N., *New light on faint stars - III. Galactic structure towards the South Pole and the Galactic thick disc.*, Monthly Notices of the Royal Astronomical Society, 1983, **202**, 1025-1047.

[137] Robin, A. C. and et al., *The thick disc of the Galaxy: sequel of a merging event.*, Astronomy and Astrophysics, 1996, **305**, 125-134.

[138] Ng, Y. K. and et al., *Probing the Galaxy. I. The galactic structure towards the galactic pole*, Astronomy and Astrophysics, 1997, **324**, 65-79.

[139] Buser, R., Rong, J. and Karaali, S., *The new Basel high-latitude field star survey of the Galaxy. II. The thick disk component: density structure, luminosity function, and metallicity distribution*, Astronomy and Astrophysics, 1999, **348**, 98-112.

[140] Ojha, D. K., *Radial scalelengths of the galactic thin and thick disc with 2MASS data*, Monthly Notices of the Royal Astronomical Society, 2001, **322**, 426-432.

[141] Chen, L., Hou, J. L. and Wang, J. J., *On the Galactic Disk Metallicity Distribution from Open Clusters. I. New Catalogs and Abundance Gradient*, The Astronomical Journal, 2003, **125**, 1397-1406.

[142] Bobylev, V. V. and Bajkova, A. T., *Analysis of the Z distribution of young objects in the Galactic thin disk*, Astronomy Letters, 2016, **42**, 1-9.

[143] Licquia, T. C., Newman, J. A. and Brinchmann, J., *Unveiling the Milky Way: A New Technique for Determining the Optical Color and Luminosity of Our Galaxy*, The Astrophysical Journal, 2015, **809**, id.96/19.

[144] Loebman, S. R., and et al., *The Genesis of the Milky Way's Thick Disk Via Stellar Migration*, The Astrophysical Journal, 2011, **737**, id.8/17.

[145] Bovy, J., and et al., *The Spatial Structure of Mono-abundance Sub-populations of the Milky Way Disk*, The Astrophysical Journal, 2012, **753**, id.148/25.

[146] Maoz, D. and Mannucci, F., *Type-Ia Supernova Rates and the Progenitor Problem: A Review*, Publications of the Astronomical Society of Australia, 2012, **29**, 447-465.

[147] Zapartas, E. and et al., *Delay-time distribution of core-collapse supernovae with late events resulting from binary interaction*, Astronomy and Astrophysics, 2017, **601**, A29/22.

[148] Ciucă, I. and et al., *The vertical metallicity gradients of mono-age stellar populations in the Milky Way with the RAVE and Gaia data*, Monthly Notices of the Royal Astronomical Society, 2018, **475**, 1203-1212.

[149] Hakobyan, A. A. and et al., *Supernovae and their host galaxies - VII. The diversity of Type Ia supernova progenitors*, Monthly Notices of the Royal Astronomical Society, 2020, **499**, 1424-1440.

[150] Guillochon, J. and et al., *An Open Catalog for Supernova Data*, The Astrophysical Journal, 2017, **835**, id.64/15.

[151] Yaron, O. and Gal-Yam, A., *WISeREP—An Interactive Supernova Data Repository*, Publications of the Astronomical Society of the Pacific, 2012, **124**, 668-681.

[152] Ahumada, R. and et al., *The 16th Data Release of the Sloan Digital Sky Surveys: First Release from the APOGEE-2 Southern Survey and Full Release of eBOSS Spectra*, The Astrophysical Journal Supplement Series, 2020, **249**, id.3/21.

[153] Onken, C. A. and et al., *SkyMapper Southern Survey: Second data release (DR2)*, Publications of the Astronomical Society of Australia, 2019, **36**, id.e033/19.

[154] Chambers, K. C. and et al., *The Pan-STARRS1 Surveys*, preprint (arXiv:1612.05560), 2016.

[155] Barkhudaryan, L. V., *VizieR Online Data Catalog: Data on 197 SNe Ia and their 196 hosts (Barkhudaryan, 2023)*, VizieR Online Data Catalog, 2023.

[156] Hakobyan, A. A. and et al., *Type Ia supernovae in the star formation deserts of spiral host galaxies*, Monthly Notices of the Royal Astronomical Society, 2021, **505**, L52-L57.

[157] Breda, I. and Papaderos, P., *The continuous rise of bulges out of galactic disks*, Astronomy and Astrophysics, 2018, **614**, A48/19.

[158] Graham, A. W. and Worley, C. C., *Inclination- and dust-corrected galaxy parameters: bulge-to-disc ratios and size-luminosity relations*, Monthly Notices of the Royal Astronomical Society, 2008, **388**, 1708-1728.

[159] González Delgado, R. M. and et al., *The CALIFA survey across the Hubble sequence. Spatially resolved stellar population properties in galaxies*, Astronomy and Astrophysics, 2015, **581**, A103/44.

[160] Raskin, C. and et al., *Prompt Ia Supernovae are Significantly Delayed*, The Astrophysical Journal, 2009, **707**, 74-78.

[161] Ruiter, A. J. and et al., *On the brightness distribution of Type Ia supernovae from violent white dwarf mergers*, Monthly Notices of the Royal Astronomical Society, 2013, **429**, 1425-1436.

[162] Panther, F. H. and et al., *SN1991bg-like supernovae are associated with old stellar populations*, Publications of the Astronomical Society of Australia, 2019, **36**, id.e031/9.

[163] Comerón, S., Salo, H. and Knapen, J. H., *The reports of thick discs' deaths are greatly exaggerated. Thick discs are NOT artefacts caused by diffuse scattered light*, Astronomy and Astrophysics, 2018, **610**, A5/169.

[164] Yoachim, P. and Dalcanton, J. J., *Lick Indices in the Thin and Thick Disks of Edge-On Disk Galaxies*, The Astrophysical Journal, 2008, **683**, 707-721.

[165] Comerón, S., *A prediction about the age of thick discs as a function of the stellar mass of the host galaxy*, Astronomy and Astrophysics, 2021, **645**, L13/4.

[166] Comerón, S. and et al., *Galactic archaeology of a thick disc: Excavating ESO 533-4 with VIMOS*, Astronomy and Astrophysics, 2015, **584**, A34/13.

[167] Kasparova, A. V. and et al., *The diversity of thick galactic discs*, Monthly Notices of the Royal Astronomical Society, 2016, **460**, L89-L93.

[168] Bensby, T. and et al., *Tracing the Galactic Thick Disk to Solar Metallicities*, The Astrophysical Journal, 2007, **663**, L13-L16.

[169] Roman, M. and et al., *Dependence of Type Ia supernova luminosities on their local environment*, Astronomy and Astrophysics, 2018, **615**, A68/24.

[170] Hacke, G., Schielicke, R. and Schmidt, K.-H., *On the widths of dust layers in galaxies*, Astronomische Nachrichten, 1982, **303**, 245-249.

[171] Crocker, R. M. and et al., *Diffuse Galactic antimatter from faint thermonuclear supernovae in old stellar populations*, Nature Astronomy, 2017, **1**, id.0135/6.

[172] Pakmor, R. and et al., *Helium-ignited Violent Mergers as a Unified Model for Normal and Rapidly Declining Type Ia Supernovae*, The Astrophysical Journal, 2013, **770**, L8/7.

[173] Hicken, M. and et al., *CfA3: 185 Type Ia Supernova Light Curves from the CfA*, The Astrophysical Journal, 2009, **700**, 331-357.

[174] Folatelli, G. and et al., *Spectroscopy of Type Ia Supernovae by the Carnegie Supernova Project*, The Astrophysical Journal, 2013, **773**, id.53/28.

[175] Stahl, B. E. and et al., *Lick Observatory Supernova Search follow-up program: photometry data release of 93 Type Ia supernovae*, Monthly Notices of the Royal Astronomical Society, 2019, **490**, 3882-3907.

[176] Uddin, S. A. and et al., *The Carnegie Supernova Project-I: Correlation between Type Ia Supernovae and Their Host Galaxies from Optical to Near-infrared Bands*, The Astrophysical Journal, 2020, **901**, id.143/18.

[177] Cameron, E., *On the Estimation of Confidence Intervals for Binomial Population Proportions in Astronomy: The Simplicity and Superiority of the Bayesian Approach*, Publications of the Astronomical Society of Australia, 2011, **28**, 128-139.

[178] White, C. J. and et al., *Slow-speed Supernovae from the Palomar Transient Factory: Two Channels*, The Astrophysical Journal, 2015, **799**, id.52/21.

[179] Siebert, M. R. and et al., *Investigating the diversity of Type Ia supernova spectra with the open-source relational data base KAEPORA*, Monthly Notices of the Royal Astronomical Society, 2019, **486**, 5785-5808.

[180] Silverman, J. M. and et al., *Berkeley Supernova Ia Program - I. Observations, data reduction and spectroscopic sample of 582 low-redshift Type Ia supernovae*, Monthly Notices of the Royal Astronomical Society, 2012, **425**, 1789-1818.

[181] Könyves-Tóth, R. and et al., *Constraints on the Physical Properties of SNe Ia from Photometry*, The Astrophysical Journal, 2020, **892**, id.121/20.

[182] Coelho, R. C. V. and et al., *Standardization of type Ia supernovae*, European Journal of Physics, 2015, **36**, id.015007/23.

[183] Feigelson E. D. and Babu G. J., *Modern Statistical Methods for Astronomy*, Cambridge Univ. Press, Cambridge, UK, 2012.

[184] Karapetyan, A. G. and et al., *The impact of spiral density waves on the distribution of supernovae*, Monthly Notices of the Royal Astronomical Society, 2018, **481**, 566-577.

[185] Wolf, C. and et al., *SkyMapper Southern Survey: First Data Release (DR1)*, Publications of the Astronomical Society of Australia, 2018, **35**, id.e010/29.

[186] Finkbeiner, D. P. and et al., *Hypercalibration: A Pan-STARRS1-based Recalibration of the Sloan Digital Sky Survey Photometry*, The Astrophysical Journal, 2016, **822**, id.66/12.

[187] Schlafly, E. F. and Finkbeiner, D. P., *Measuring Reddening with Sloan Digital Sky Survey Stellar Spectra and Recalibrating SFD*, The Astrophysical Journal, 2011, **737**, id.103/13.

[188] Schlegel, D. J., Finkbeiner, D. P. and Davis, M., *Maps of Dust Infrared Emission for Use in Estimation of Reddening and Cosmic Microwave Background Radiation Foregrounds*, The Astrophysical Journal, 1998, **500**, 525-553.

[189] Bottinelli, L.and et al., *Extragalactic database. VI. Inclination corrections for spiral galaxies and disk opaqueness in the B-band.*, Astronomy and Astrophysics, 1995, **296**, 64-72.

[190] Chilingarian, I. V., Melchior, A.-L. and Zolotukhin, I. Y., *Analytical approximations of K-corrections in optical and near-infrared bands*, Monthly Notices of the Royal Astronomical Society, 2010, **405**, 1409-1420.

[191] Hakobyan, A. A. and et al., *VizieR Online Data Catalog: Properties of 407 SNe and their 394 hosts (Hakobyan+, 2020)*, VizieR Online Data Catalog, 2020.

[192] Stritzinger, M. D. and et al., *Comprehensive observations of the bright and energetic Type Iax SN 2012Z: Interpretation as a Chandrasekhar mass white dwarf explosion*, Astronomy and Astrophysics 2015, **573**, A2/24.

[193] Foley, R. J. and et al., *SN 2008ha: An Extremely Low Luminosity and Exceptionally Low Energy Supernova*, The Astronomical Journal, 2009, **138**, 376-391.

[194] Valenti, S. and et al., *A low-energy core-collapse supernova without a hydrogen envelope*, Nature, 2009, **459**, 674-677.

[195] Taubenberger, S. and et al., *High luminosity, slow ejecta and persistent carbon lines: SN 2009dc challenges thermonuclear explosion scenarios*, Monthly Notices of the Royal Astronomical Society, 2011, **412**, 2735-2762.

[196] Altavilla, G. and et al., *Cepheid calibration of Type Ia supernovae and the Hubble constant*, Monthly Notices of the Royal Astronomical Society, 2004, **349**, 1344-1352.

[197] Pruzhinskaya, M. V. and et al., *The dependence of Type Ia Supernovae SALT2 light-curve parameters on host galaxy morphology*, Monthly Notices of the Royal Astronomical Society, 2020, **499**, 5121-5135.

[198] Oohama, N. and et al., *Properties of Disks and Bulges of Spiral and Lenticular Galaxies in the Sloan Digital Sky Survey*, The Astrophysical Journal, 2009, **705**, 245-254.

[199] de Lapparent, V., Baillard, A. and Bertin, E., *The EFIGI catalogue of 4458 nearby galaxies with morphology. II. Statistical properties along the Hubble sequence*, Astronomy and Astrophysics, 2011, **532**, A75/19.

[200] Graham, J. and Foley, R. J., *Supernova 2004br in NGC 4493*, International Astronomical Union Circular, 2004, **8340**, 1.

[201] Wild, P., *Supernova 1994M in NGC 4493*, International Astronomical Union Circular, 1994, **5982**, 2.

[202] Blondin, S. and et al., *The Spectroscopic Diversity of Type Ia Supernovae*, The Astronomical Journal, 2012, **143**, id.126/33.

[203] Schawinski, K., *How old are SN Ia progenitor systems? New observational constraints on the distribution of time delays from GALEX*, Monthly Notices of the Royal Astronomical Society, 2009, **397**, 717-725.

[204] Gomes, J. M. and et al., *Warm ionized gas in CALIFA early-type galaxies. 2D emission-line patterns and kinematics for 32 galaxies*, Astronomy and Astrophysics, 2016, **588**, A68/58.

[205] Ge, X. and et al., *The Physical Properties of S0 Galaxy PGC 26218: The Origin of Starburst and Star Formation*, The Astrophysical Journal, 2020, **889**, id.132/12.

[206] Suh, H. and et al., *Early-type Host Galaxies of Type II and Ib Supernovae*, The Astrophysical Journal, 2011, **730**, id.110/5.

[207] Lee, M. G., Jang, I. S. and Kang, J., *Star Clusters in the Elliptical Galaxy NGC 4589 Hosting a Calcium-rich SN Ib (SN 2005cz)*, The Astrophysical Journal, 2019, **871**, id.33/16.

[208] Taylor, E. N. and et al., *Galaxy And Mass Assembly (GAMA): stellar mass estimates*, Monthly Notices of the Royal Astronomical Society, 2011, **418**, 1587-1620.

[209] Perley, D. A. and et al., *The Zwicky Transient Facility Bright Transient Survey. II. A Public Statistical Sample for Exploring Supernova Demographics*, The Astrophysical Journal, 2020, **904**, id.35/24.

[210] Baldry, I. K. and et al., *Galaxy bimodality versus stellar mass and environment*, Monthly Notices of the Royal Astronomical Society, 2006, **373**, 469-483.

[211] Mendez, A. J. and et al., *AEGIS: The Morphologies of Green Galaxies at $0.4 < z < 1.2$*, The Astrophysical Journal, 2011, **736**, id.110/21.

[212] Campbell, H., Fraser, M. and Gilmore, G., *How SN Ia host-galaxy properties affect cosmological parameters*, Monthly Notices of the Royal Astronomical Society, 2016, **457**, 3470-3491.

[213] Uddin, S. A. and et al., *The Influence of Host Galaxies in Type Ia Supernova Cosmology*, The Astrophysical Journal, 2017, **848**, id.56/14.

[214] Kelsey, L. and et al., *The effect of environment on Type Ia supernovae in the Dark Energy Survey three-year cosmological sample*, Monthly Notices of the Royal Astronomical Society, 2021, **501**, 4861-4876.

[215] Jha, S., Riess, A. G. and Kirshner, R. P., *Improved Distances to Type Ia Supernovae with Multicolor Light-Curve Shapes: MLCS2k2*, The Astrophysical Journal, 2007, **659**, 122-148.

[216] Guy, J. and et al., *SALT2: using distant supernovae to improve the use of type Ia supernovae as distance indicators*, Astronomy and Astrophysics, 2007, **466**, 11-21.

[217] Burns, C. R. and et al., *The Carnegie Supernova Project: Absolute Calibration and the Hubble Constant*, The Astrophysical Journal, 2018, **869**, id.56/23.

[218] Brout, D. and Scolnic, D., *It's Dust: Solving the Mysteries of the Intrinsic Scatter and Host-galaxy Dependence of Standardized Type Ia Supernova Brightnesses*, The Astrophysical Journal, 2021, **909**, id.26/17.

[219] Ponder, K. A. and et al., *Are Type Ia Supernovae in Rest-frame H Brighter in More Massive Galaxies?*, The Astrophysical Journal, 2021, **923**, id.197/34.

[220] Fioc, M. and Rocca-Volmerange, B., *PEGASE: a UV to NIR spectral evolution model of galaxies. Application to the calibration of bright galaxy counts*, Astronomy and Astrophysics, 1997, **326**, 950-962.

[221] Fioc, M. and Rocca-Volmerange, B., *PEGASE.2, a metallicity-consistent spectral evolution model of galaxies: the documentation and the code*, preprint (arXiv:astro-ph/9912179), 1999.

[222] Johansson, J. and et al., *SN Ia host galaxy properties from Sloan Digital Sky Survey-II spectroscopy*, Monthly Notices of the Royal Astronomical Society, 2013, **435**, 1680-1700.

[223] Yungelson, L. R. and Livio, M., *Supernova Rates: A Cosmic History*, The Astrophysical Journal, 2000, **528**, 108-117.

[224] Greggio, L., *The rates of type Ia supernovae. I. Analytical formulations*, Astronomy and Astrophysics, 2005, **441**, 1055-1078.

[225] Gilfanov, M. and Bogdán, Á., *An upper limit on the contribution of accreting white dwarfs to the type Ia supernova rate*, Nature, 2010, **463**, 924-925.

[226] Lipunov, V. M., Panchenko, I. E. and Pruzhinskaya, M. V., *The mechanism of supernova Ia explosion in elliptical galaxies*, New Astronomy, 2011, **16**, 250-252.

[227] Perets, H. B. and et al., *Normal type Ia supernovae from disruptions of hybrid He-CO white-dwarfs by CO white-dwarfs*, preprint (arXiv:1910.07532), 2019.

[228] Zenati, Y., Toonen, S. and Perets, H. B., *Formation and evolution of hybrid He-CO white dwarfs and their properties*, Monthly Notices of the Royal Astronomical Society, 2019, **482**, 1135-1142.

[229] Fisher, R. and Jumper, K., *Single-degenerate Type Ia Supernovae Are Preferentially Overluminous*, The Astrophysical Journal, 2015, **805**, id.150/10.

[230] Han, Z. and Podsiadlowski, P., *The single-degenerate channel for the progenitors of Type Ia supernovae*, Monthly Notices of the Royal Astronomical Society, 2004, **350**, 1301-1309.

[231] Postnov, K. A. and Yungelson, L. R., *The Evolution of Compact Binary Star Systems*, Living Reviews in Relativity, 2014, **17**, id.3/166.

[232] Claeys, J. S. W. and et al., *Theoretical uncertainties of the Type Ia supernova rate*, Astronomy and Astrophysics, 2014, **563**, A83/24.

[233] Kormendy, J. and et al., *Structure and Formation of Elliptical and Spheroidal Galaxies*, The Astrophysical Journal Supplement Series, 2009, **182**, 216-309.

[234] Taubenberger, S. and et al., *The underluminous Type Ia supernova 2005bl and the class of objects similar to SN 1991bg*, Monthly Notices of the Royal Astronomical Society, 2008, **385**, 75-96.

[235] Benetti, S. and et al., *The Diversity of Type Ia Supernovae: Evidence for Systematics?*, The Astrophysical Journal, 2005, **623**, 1011-1016.

[236] Kollmeier, J. A. and et al., *H α emission in the nebular spectrum of the Type Ia supernova ASASSN-18tb*, Monthly Notices of the Royal Astronomical Society, 2019, **486**, 3041-3046.

[237] Sand, D. J. and et al., *Nebular Hα Limits for Fast Declining SNe Ia*, The Astrophysical Journal, 2019, **877**, L4/9.

[238] Hillebrandt, W. and Niemeyer, J. C., *Type Ia Supernova Explosion Models*, Annual Review of Astronomy and Astrophysics, 2000, **38**, 191-230.

[239] Mazzali, P. A. and Hachinger, S., *The nebular spectra of the Type Ia supernova 1991bg: further evidence of a non-standard explosion*, Monthly Notices of the Royal Astronomical Society, 2012, **424**, 2926-2935.

[240] Dong, S. and et al., *Type Ia supernovae with bimodal explosions are common - possible smoking gun for direct collisions of white dwarfs.*, Monthly Notices of the Royal Astronomical Society, 2015, **454**, L61-L65.

[241] Guseinov, O. H., Kasumov, F. K. and Kalinin, E. V., *Radial Distribution of Type-I and Type-II Supernovae in Spiral and Elliptical Galaxies*, Astrophysics and Space Science, 1980, **68**, 385-392.

[242] Bartunov, O. S., Makarova, I. N. and Tsvetkov, D. I., *The radial distribution of supernovae in galaxies*, Astronomy and Astrophysics, 1992, **264**, 428-432.

[243] Tsvetkov, D. Y., Pavlyuk, N. N. and Bartunov, O. S., *The SAI Catalog of Supernovae and Radial Distributions of Supernovae of Various Types in Galaxies*, Astronomy Letters, 2004, **30**, 729-736.

[244] Scannapieco, E. and Bildsten, L., *The Type Ia Supernova Rate*, The Astrophysical Journal, 2005, **629**, L85-L88.

[245] Mannucci, F. and et al., *The supernova rate per unit mass*, Astronomy and Astrophysics, 2005, **433**, 807-814.

[246] Hakobyan, A. A. and et al., *Five supernova survey galaxies in the southern hemisphere. I. Optical and near-infrared database*, Astrophysics, 2009, **52**, 40-53.

[247] Li, W. and et al., *Nearby supernova rates from the Lick Observatory Supernova Search - III. The rate-size relation, and the rates as a function of galaxy Hubble type and colour*, Monthly Notices of the Royal Astronomical Society, 2011, **412**, 1473-1507.

[248] Hakobyan, A. A. and et al., *Five supernova survey galaxies in the southern hemisphere. II. The supernova rates*, Astrophysics, 2011, **54**, 301-314.

[249] Aguado, D. S. and et al., *The Fifteenth Data Release of the Sloan Digital Sky Surveys: First Release of MaNGA-derived Quantities, Data Visualization Tools, and Stellar Library*, The Astrophysical Journal Supplement Series, 2019, **240**, id.23/25.

[250] Yahil, A., Tammann, G. A. and Sandage, A., *The Local Group: the solar motion relative to its centroid.*, The Astrophysical Journal, 1977, **217**, 903-915.

[251] Theureau, G. and et al., *Kinematics of the local universe. VIII. Normalized distances as a tool for Malmquist bias corrections and application to the study of peculiar velocities in the direction of the Perseus-Pisces and the Great Attractor regions*, Astronomy and Astrophysics, 1998, **340**, 21-34.

[252] Terry, J. N., Paturel, G. and Ekholm, T., *Local velocity field from sosie galaxies. I. The Peebles' model*, Astronomy and Astrophysics, 2002, **393**, 57-68.

[253] Tomasella , L. and et al., *Asiago Supernova classification program: Blowing out the first two hundred candles*, Astronomische Nachrichten, 2014, **335**, 841-849.

[254] Sérsic, J. L., *Influence of the atmospheric and instrumental dispersion on the brightness distribution in a galaxy*, Boletin de la Asociacion Argentina de Astronomia La Plata Argentina, 1963, **6**, 41-43.

[255] Capaccioli, M., *Photometry of early-type galaxies and the* $r^{1/4}$ *law*, In: Corwin, H.G., Bottinelli, L. (eds), The World of Galaxies (Le Monde des Galaxies), Springer, New York, 1989, 208-228.

[256] de Vaucouleurs, G., *Recherches sur les Nebuleuses Extragalactiques*, Annales d'Astrophysique, 1948, **11**, 247-289.

[257] Lupton, R. and et al., *The SDSS Imaging Pipelines*, Astronomical Data Analysis Software and Systems X, 2001, **238**, 269-278.

[258] Freeman, K. C., *On the Disks of Spiral and S0 Galaxies*, The Astrophysical Journal, 1970, **160**, 811-830.

[259] Bernardi, M. and et al., *Evolution and Environment of Early-Type Galaxies*, The Astronomical Journal, 2006, **131**, 1288-1317.

[260] Nair, P. B. and Abraham, R. G., *A Catalog of Detailed Visual Morphological Classifications for 14,034 Galaxies in the Sloan Digital Sky Survey*, The Astrophysical Journal Supplement Series, 2010, **186**, 427-456.

[261] Vika, M. and et al., *MegaMorph - multiwavelength measurement of galaxy structure. Sérsic profile fits to galaxies near and far*, Monthly Notices of the Royal Astronomical Society, 2013, **435**, 623-649.

[262] James, P. A. and Anderson, J. P., *The Hα Galaxy Survey . III. Constraints on supernova progenitors from spatial correlations with Hα emission*, Astronomy and Astrophysics, 2006, **453**, 57-65.

[263] Anderson, J. P. and James, P. A., *Comparisons of the radial distributions of core-collapse supernovae with those of young and old stellar populations*, Monthly Notices of the Royal Astronomical Society, 2009, **399**, 559-573.

[264] Barkhudaryan, L. V. and et al., *VizieR Online Data Catalog: Properties of 109 SNe and their 104 hosts (Barkhudaryan+, 2019)*, VizieR Online Data Catalog, 2019.

[265] Dilday, B. and et al., *A Measurement of the Rate of Type Ia Supernovae in Galaxy Clusters from the SDSS-II Supernova Survey*, The Astrophysical Journal, 2010, **715**, 1021-1035.

[266] Leaman, J. and et al., *Nearby supernova rates from the Lick Observatory Supernova Search - I. The methods and data base*, Monthly Notices of the Royal Astronomical Society, 2011, **412**, 1419-1440.

[267] Hamuy, M. and Pinto, P. A., *Selection Effects, Biases, and Constraints in the CalÁn/Tololo Supernova Survey*, The Astronomical Journal, 1999, **117**, 1185-1205.

[268] Shaw, R. L., *Supernovae: a new selection effect.*, Astronomy and Astrophysics, 1979, **76**, 188-191.

[269] Howell, D. A., Wang, L. and Wheeler, J. C., *The Distribution of High- and Low-Redshift Type Ia Supernovae*, The Astrophysical Journal, 2000, **530**, 166-171.

[270] Maza, J. and van den Bergh, S., *Statistics of extragalactic supernovae*, The Astrophysical Journal, 1976, **204**, 519-529.

[271] Maraston, C., *Evolutionary population synthesis: models, analysis of the ingredients and application to high-z galaxies*, Monthly Notices of the Royal Astronomical Society, 2005, **362**, 799-825.

[272] Chen, Y.-M. and et al., *Evolution of the most massive galaxies to z= 0.6 - I. A new method for physical parameter estimation*, Monthly Notices of the Royal Astronomical Society, 2012, **421**, 314-332.

[273] Conroy, C., Gunn, J. E. and White, M., *The Propagation of Uncertainties in Stellar Population Synthesis Modeling. I. The Relevance of Uncertain Aspects of Stellar Evolution and the Initial Mass Function to the Derived Physical Properties of Galaxies*, The Astrophysical Journal, 2009, **699**, 486-506.

[274] Gallazzi, A. and et al., *Ages and metallicities of early-type galaxies in the Sloan Digital Sky Survey: new insight into the physical origin of the colour-magnitude and the* Mg_2-σ_V *relations*, Monthly Notices of the Royal Astronomical Society, 2006, **370**, 1106-1124.

[275] Scott, N. and et al., *The SAMI Galaxy Survey: global stellar populations on the size-mass plane*, Monthly Notices of the Royal Astronomical Society, 2017, **472**, 2833-2855.

[276] Verkhodanov, O. V. and et al., *The software system "Evolution of radio galaxies"*, Astronomical and Astrophysical Transactions, 2000, **19**, 663-667.

[277] Timmes, F. X., Brown, E. F. and Truran, J. W., *On Variations in the Peak Luminosity of Type Ia Supernovae*, The Astrophysical Journal, 2003, **590**, L83-L86.

[278] Henry, R. B. C. and Worthey, G., *The Distribution of Heavy Elements in Spiral and Elliptical Galaxies*, Publications of the Astronomical Society of the Pacific, 1999, **111**, 919-945.

[279] Kang, Y. and et al., *Early-type Host Galaxies of Type Ia Supernovae. I. Evidence for Downsizing*, The Astrophysical Journal Supplement Series, 2016, **223**, id.7/14.

[280] Schawinski, K. and et al., *The Role of Mergers in Early-type Galaxy Evolution and Black Hole Growth*, The Astrophysical Journal, 2010, **714**, L108-L112.

[281] Uddin, S. A., Mould, J. and Wang, L., *Average Spectral Properties of Type Ia Supernova Host Galaxies*, The Astrophysical Journal, 2017, **850**, id.135/6.

[282] Gomes, J. M. and et al., *Spiral-like star-forming patterns in CALIFA early-type galaxies*, Astronomy and Astrophysics, 2016, **585**, A92/6.